Article:

Aad, G., Abbott, B., Abeling, K. et al. (2929 more authors) (2024) Measurement and interpretation of same-sign W boson pair production in association with two jets in pp collisions at √s = 13 TeV with the ATLAS detector. Journal of High Energy Physics, 2024 (4). 26. ISSN 1029-8479

https://doi.org/10.1007/jhep04(2024)026

Published for SISSA by Springer

Received: *December 4, 2023*
Accepted: *March 4, 2024*
Published: *April 4, 2024*

Measurement and interpretation of same-sign W boson pair production in association with two jets in pp collisions at $\sqrt{s} = 13$ TeV with the ATLAS detector

The ATLAS collaboration

E-mail: atlas.publications@cern.ch

Abstract: This paper presents the measurement of fiducial and differential cross sections for both the inclusive and electroweak production of a same-sign W-boson pair in association with two jets ($W^{\pm}W^{\pm}jj$) using 139 fb^{-1} of proton-proton collision data recorded at a centre-of-mass energy of $\sqrt{s} = 13$ TeV by the ATLAS detector at the Large Hadron Collider. The analysis is performed by selecting two same-charge leptons, electron or muon, and at least two jets with large invariant mass and a large rapidity difference. The measured fiducial cross sections for electroweak and inclusive $W^{\pm}W^{\pm}jj$ production are $2.92 \pm 0.22\,(\text{stat.}) \pm 0.19\,(\text{syst.})$ fb and $3.38 \pm 0.22\,(\text{stat.}) \pm 0.19\,(\text{syst.})$ fb, respectively, in agreement with Standard Model predictions. The measurements are used to constrain anomalous quartic gauge couplings by extracting 95% confidence level intervals on dimension-8 operators. A search for doubly charged Higgs bosons $H^{\pm\pm}$ that are produced in vector-boson fusion processes and decay into a same-sign W boson pair is performed. The largest deviation from the Standard Model occurs for an $H^{\pm\pm}$ mass near 450 GeV, with a global significance of 2.5 standard deviations.

Keywords: Hadron-Hadron Scattering, Vector Boson Production

ArXiv ePrint: 2312.00420

https://doi.org/10.1007/JHEP04(2024)026

Contents

1 Introduction

The study of massive vector boson scattering (VBS), $VV \to VV$ ($V = W, Z$), at the Large Hadron Collider (LHC) probes the mechanism of electroweak (EW) symmetry breaking (EWSB) in the Standard Model (SM), and provides unique sensitivity for new physics phenomena that affect the gauge sector [1–3]. In the SM, couplings to the Higgs boson prevent the divergence of longitudinally polarised VBS amplitudes at high energies and unitarity violation at the TeV scale [4–7].

In proton−proton (pp) collisions, VBS at leading order (LO) involves two initial quarks, each of which radiates a vector boson. The two bosons subsequently interact and then

JHEP04(2024)026

decay. The two outgoing quarks fragment usually close to the beam direction. The final state consists of two vector bosons and two jets (j), $VVjj$, and can also be produced from non-VBS processes.

The production of $VVjj$ at LO has contributions both from modes that involve only the EW-interaction vertices (EW $VVjj$) and from modes that involve the strong interaction (quantum chromodynamics, QCD) vertices (QCD $VVjj$). Representative LO Feynman diagrams for EW $VVjj$ are shown in figures 1 and 2. The leading QCD $VVjj$ diagrams are shown in figure 3, where the two diagrams with gluons in the initial state are forbidden when there are two W bosons with the same electric charge produced, $W^{\pm}W^{\pm}jj$. The EW production is further categorised into two components. The first component is EW VBS production (see figure 1), which involves the actual scattering of the two vector bosons. The scattering occurs via triple or quartic gauge vertices, the s- or t-channel exchange of a Higgs boson or a $W/Z/\gamma$ boson. The diagrams with bosons in the s-channel, shown in figures 1(a) and 1(d), are forbidden in the SM for $W^{\pm}W^{\pm}jj$ final states. The diagram in figure 1(d) is possible in extensions of the SM with a doubly charged Higgs boson. The second component is EW non-VBS production (see figure 2) with EW vertices only, where the two bosons do not interact. The EW non-VBS component cannot be separated from the EW VBS component in a gauge-invariant way and is therefore considered as a contribution to the signal. Triboson production where one boson decays hadronically also results in the $VVjj$ final state. These processes only contain EW interactions and are separable in a gauge-invariant manner [8]. The resonant decay of a boson into two quarks can be suppressed by applying a requirement on the invariant dijet mass m_{jj} arising from the two quarks. As a consequence, triboson processes are suppressed in the EW VBS phase-space region.

The $W^{\pm}W^{\pm}jj$ final state has the largest ratio of electroweak to strong production cross sections among final states sensitive to VBS diboson processes [3]; this is because quark-gluon and gluon-gluon initiated diagrams are absent at LO accuracy in perturbative QCD and contributions from quark and (anti-)quark annihilation diagrams are suppressed. This production ratio is of order five in the fiducial phase-space region of the analysis. The s-channel VBS diagrams with trilinear interactions are absent in the $W^{\pm}W^{\pm}jj$ final state. In addition, electroweak diagrams not involving self interactions are suppressed [9], which enhances the sensitivity of this final state to gauge-boson self couplings.

$W^{\pm}W^{\pm}jj$ scattering where both W bosons decay leptonically (into $e\nu$ or $\mu\nu$, collectively denoted by $\ell\nu$) is a sensitive process for studying VBS, since the electric charges of W bosons can be determined directly from leptons. The final state consists of two leptons with the same electric charge, two neutrinos, and two jets with a large rapidity separation. The requirement of the presence of two leptons with the same electric charge significantly reduces SM backgrounds coming from top-anti-top quark pair production ($t\bar{t}$) and Z + jets events.

The first studies of the EW $W^{\pm}W^{\pm}jj$ production were performed by the ATLAS and CMS experiments using Run 1 LHC pp dataset with the centre-of-mass energy of $\sqrt{s} = 8$ TeV [10–12]. They were followed by an observation of this process by both experiments using partial LHC Run 2 data at $\sqrt{s} = 13$ TeV [13, 14]. More recently, the CMS Collaboration published an updated measurement using full Run 2 data, corresponding to an integrated luminosity of 137 fb^{-1} [15].

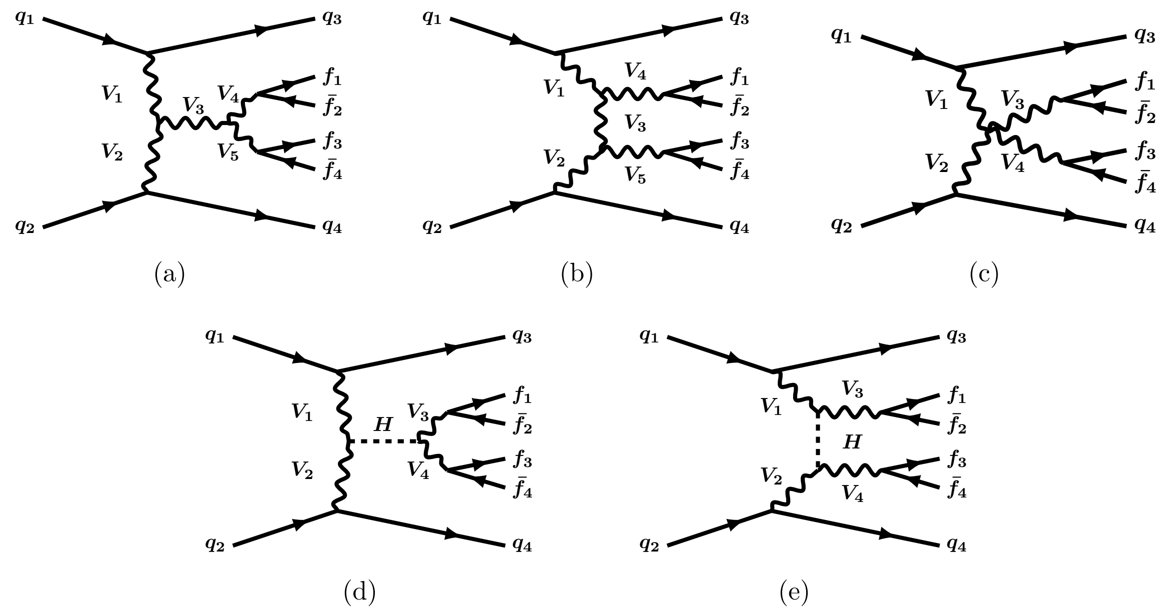

(a) (b) (c)

(d) (e)

Figure 1. Representative Feynman diagrams for EW $VVjj$ production with a scattering topology that includes either a triple-gauge-boson vertex with an internal electroweak gauge boson in the (a) s-channel or the (b) t-channel, (c) a quartic gauge boson vertex, or the exchange of a Higgs boson in the (d) s-channel or the (e) t-channel. The lines are labelled by quarks (q), vector bosons ($V = W/Z/\gamma$), the Higgs boson (H) and fermions (f). The s-channel diagrams, (a) and (d), are forbidden in the SM for $W^{\pm}W^{\pm}jj$ final states. The diagram (d) is possible in extensions of the SM with a doubly charged Higgs boson. In these and following Feynman diagrams, not all boson combinations are allowed by the Standard Model.

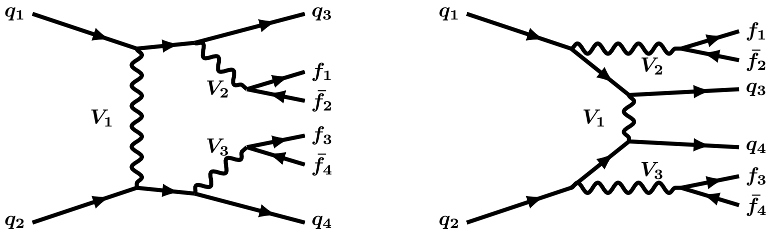

Figure 2. Representative Feynman diagrams for EW $VVjj$ production without vector-boson scattering. The lines are labelled by quarks (q), vector bosons ($V = W/Z/\gamma$), and fermions (f).

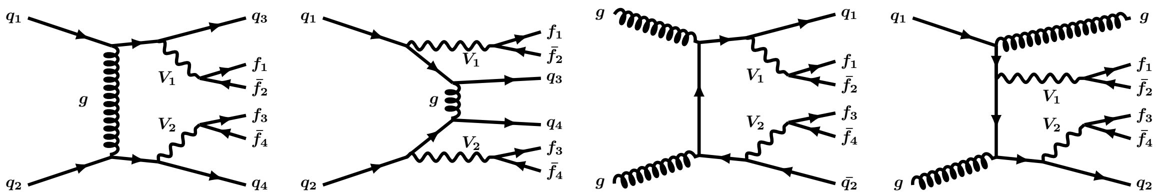

Figure 3. Representative Feynman diagrams for QCD $VVjj$ production with strong interaction vertices. The lines are labelled by quarks (q), vector bosons ($V = W/Z/\gamma$), fermions (f), and gluons (g). The two diagrams on the right with gluons in the initial state are forbidden for $W^{\pm}W^{\pm}jj$ production.

This paper presents fiducial and differential EW and inclusive $W^{\pm}W^{\pm}jj$ production cross section measurements at $\sqrt{s} = 13\,\text{TeV}$ using $139\,\text{fb}^{-1}$ of data recorded by the ATLAS detector at the LHC. There are several changes with respect to the previous result [14]. The current measurement uses improved baseline signal modelling, implements a tighter veto on additional leptons, includes a charge selector tool based on boosted decision trees for rejecting electron candidates where the charge is likely misidentified, employs a data-driven extraction of the m_{jj} shape of the WZ background, and incorporates updates to the estimation of non-prompt lepton background.

The distribution of reconstructed dilepton invariant mass $m_{\ell\ell}$ for $W^{\pm}W^{\pm}jj$ event candidates is used in an Effective Field Theory (EFT) interpretation to constrain dimension-8 (D-8) operators [16], to extract one-dimensional limits on these operators and to simultaneously constrain two operators (two-dimensional limits). Using the distribution of the transverse mass of the dilepton system and the missing transverse momentum (m_{T}), a search for doubly charged Higgs bosons produced in vector-boson fusion (VBF) processes and decaying into a pair of same-sign W bosons is performed in the context of the Georgi-Machacek (GM) model [17], and 95% Confidence Level (CL) limits are extracted on the model parameter describing contributions of the isotriplet scalar fields to the masses of the W and Z bosons, and on the corresponding cross section times branching ratio.

The data corresponding to many plots presented in this paper and a Rivet [18] routine are available on HEPData [19].

2 Experimental setup

The ATLAS detector [20] at the LHC covers nearly the entire solid angle around the collision point.[1] It consists of an inner tracking detector surrounded by a thin superconducting solenoid, electromagnetic and hadron calorimeters, and a muon spectrometer that incorporates three large superconducting air-core toroidal magnets.

The inner-detector system (ID) is immersed in a 2 T axial magnetic field and provides charged-particle tracking in the region $|\eta| < 2.5$. The high-granularity silicon pixel detector covers the vertex region and typically provides four measurements (hits) per track, the first hit normally being in the insertable B-layer (IBL) installed before Run 2 [21, 22]. It is followed by the silicon microstrip tracker (SCT), which usually provides eight measurements per track. These silicon detectors are complemented by the transition radiation tracker (TRT), which enables radially extended track reconstruction up to $|\eta| = 2.0$. The TRT also provides electron identification information based on the fraction of hits (typically 30 in total) above a higher energy-deposit threshold corresponding to transition radiation.

The calorimeter system covers the pseudorapidity range $|\eta| < 4.9$. Within the region $|\eta| < 3.2$, electromagnetic calorimetry is provided by barrel and endcap high-granularity lead/liquid-argon (LAr) calorimeters, with an additional thin LAr presampler covering

---

[1] ATLAS uses a right-handed coordinate system with its origin at the nominal interaction point (IP) in the centre of the detector and the z-axis along the beam pipe. The x-axis points from the IP to the centre of the LHC ring, and the y-axis points upwards. Cylindrical coordinates (r, ϕ) are used in the transverse plane, ϕ being the azimuthal angle around the z-axis. The pseudorapidity is defined in terms of the polar angle θ as $\eta = -\ln\tan(\theta/2)$. Angular distance is measured in units of $\Delta R \equiv \sqrt{(\Delta\eta)^2 + (\Delta\phi)^2}$.

$|\eta| < 1.8$ to correct for energy loss in material upstream of the calorimeters. Hadron calorimetry is provided by the steel/scintillator-tile calorimeter, segmented into three barrel structures within $|\eta| < 1.7$, and two copper/LAr hadron endcap calorimeters. The solid angle coverage is completed with forward copper/LAr and tungsten/LAr calorimeter modules optimised for electromagnetic and hadronic energy measurements, respectively.

The muon spectrometer (MS) comprises separate trigger and high-precision tracking chambers to measure the deflection of muons in the magnetic field generated by the superconducting air-core toroidal magnets. The field integral of the toroids ranges between 2.0 and 6.0 T m across most of the detector. Three layers of precision chambers, each consisting of layers of monitored drift tubes, cover the region $|\eta| < 2.7$, complemented by cathode-strip chambers in the forward region, where the background is highest. The muon trigger system covers the range $|\eta| < 2.4$ with resistive-plate chambers in the barrel, and thin-gap chambers in the endcap regions.

Interesting events are selected by the first-level trigger system implemented in custom hardware, followed by selections made by algorithms implemented in software in the high-level trigger [23]. The first-level trigger accepts events from the 40 MHz bunch crossings at a rate below 100 kHz, which the high-level trigger further reduces in order to record events to disk at about 1 kHz.

An extensive software suite [24] is used in data simulation, in the reconstruction and analysis of real and simulated data, in detector operations, and in the trigger and data acquisition systems of the experiment.

3 Data and simulation

The results presented in this paper are based on data from pp collisions at a centre-of-mass energy of $\sqrt{s} = 13$ TeV. The data were collected between 2015 and 2018 (LHC Run-2) with the ATLAS detector and correspond to an integrated luminosity of 139 fb^{-1}, with an uncertainty of 1.7% [25], obtained using the LUCID-2 detector [26] for the primary luminosity measurements. The number of pp interactions per bunch crossing ranged between around 8 and 70, with the mean value of 33.7.

A set of single-electron[2] [27] and single-muon triggers [28] were used, with transverse momentum (p_{T}) thresholds in the range 20–26 GeV depending on the lepton flavour and data-taking period. All detector subsystems were required to be operational during data taking and to satisfy data quality requirements [29].

Signal kinematic distributions were modelled using Monte Carlo (MC) simulation, while background processes were modelled using a mixture of MC and data-driven techniques. All samples were produced using the ATLAS simulation infrastructure [30] and GEANT4 [31]. The effect of additional pp interactions per bunch crossing (pile-up) is accounted for by overlaying the hard-scattering process with minimum-bias events generated with PYTHIA 8.186 [32] using the NNPDF2.3LO set of parton distribution functions (PDF) [33] and the A3 set of tuned parameters [34]. Different pile-up conditions between data and simulation are taken into account by reweighting the mean number of interactions per bunch crossing in simulation

---

[2] Throughout this paper, the term “electron” indicates both electrons and positrons.

Process, short description	ME Generator + parton shower	Order	Tune	PDF set in ME
EW, Int, QCD $W^{\pm}W^{\pm}jj$, nominal signal	MadGraph5_aMC@NLO2.6.7 + Herwig7.2	LO	Herwig	NNPDF3.0nlo
EW, Int, QCD $W^{\pm}W^{\pm}jj$, alternative shower	MadGraph5_aMC@NLO2.6.7 + Pythia8.244	LO	A14	NNPDF3.0nlo
EW $W^{\pm}W^{\pm}jj$, NLO pQCD approx.	Sherpa2.2.11 & Sherpa2.2.2(WWW) & Powheg Box2+Pythia8.235 (WH)	+0,1j@LO NLO	Sherpa A14	NNPDF3.0nnlo
EW $W^{\pm}W^{\pm}jj$, NLO pQCD approx.	Powheg Boxv2 + Pythia8.230	NLO (VBS approx.)	AZNLO	NNPDF3.0nlo
QCD $W^{\pm}W^{\pm}jj$, NLO pQCD approx.	Sherpa2.2.2	+0,1j@LO	Sherpa	NNPDF3.0nnlo
QCD $VVjj$	Sherpa2.2.2	+0,1j@NLO; +2,3j@LO	Sherpa	NNPDF3.0nnlo
EW $W^{\pm}Z/\gamma^{*}jj$	MadGraph5_aMC@NLO2.6.2+Pythia8.235	LO	A14	NNPDF3.0nlo
EW $Z/\gamma^{*}Z/\gamma^{*}jj$	Sherpa2.2.2	LO	Sherpa	NNPDF3.0nnlo
QCD $V\gamma jj$	Sherpa2.2.11	+0,1j@NLO; +2,3j@LO	A14	NNPDF3.0nnlo
EW $V\gamma jj$	MadGraph5_aMC@NLO2.6.5+Pythia8.240	LO	A14	NNPDF3.0nlo
VVV	Sherpa2.2.1 (leptonic) & Sherpa2.2.2 (one $V \to jj$)	+0,1j@LO	Sherpa	NNPDF3.0nnlo
$t\bar{t}V$	MadGraph5_aMC@NLO2.3.3.p0 + Pythia8.210	NLO	A14	NNPDF3.0nlo
tZq	MadGraph5_aMC@NLO2.3.3.p1 + Pythia8.212	LO	A14	NNPDF2.3lo
$W^{\pm}W^{\pm}jj$ EFT	MadGraph5_aMC@NLO 2.6.5 + Pythia8.235	LO	A14	NNPDF3.0nlo
$\mathrm{H}_5^{\pm\pm}$	MadGraph5_aMC@NLO 2.9.5 + Pythia8.245	LO	A14	NNPDF3.0nlo

Table 1. Summary of the MC samples used to simulate signal (upper part of the table) and background (lower part of the table) processes in the signal region. The notation V is used to represent either W or Z/γ^{*}.

to the number observed in data. The samples generated with MadGraph5_aMC@NLO or Powheg Box described below used the EvtGen 1.2.0 or 1.6.0 program [35] for the properties of b- and c-hadron decays.

A detailed description of the MC samples is given below. A summary of the generators used for modelling signal and background SM processes in the signal region is given in table 1.

3.1 $W^{\pm}W^{\pm}jj$ samples

The $W^{\pm}W^{\pm}jj$ processes, $pp \to \ell^{\pm}\nu\ell^{\pm}\nu jj$, are simulated at LO accuracy in perturbative QCD (pQCD) with MadGraph5_aMC@NLO2.6.7 [36] separately for the QCD ($\mathcal{O}(\alpha^4\alpha_{\mathrm{s}}^2)$), interference (Int, $\mathcal{O}(\alpha^5\alpha_{\mathrm{s}})$) and EW ($\mathcal{O}(\alpha^6)$) production modes, where α and α_{s} are the electroweak and strong coupling constants, respectively. For the modelling of the parton shower, hadronisation and underlying event, Herwig7.2.1 [37, 38] (nominal sample) or Pythia8.244 [39] (alternative sample) are used. In the following, these samples are referred to as "MG5_aMC+Herwig7" and "MG5_aMC+Pythia8". The PDF set used was NNPDF3.0nlo [40] implemented at next-to-leading-order (NLO) in pQCD and with a strong coupling constant $\alpha_{\mathrm{s}}(M_Z) = 0.118$. For the nominal MG5_aMC+Herwig7 sample, the *dipole parton shower* mode [41] was used instead of the default angular-ordered mode. The alternative MG5_aMC+Pythia8 sample is produced using the *dipole recoil* scheme [42], since the default p_{T}-ordered shower used in Pythia8 for initial state radiation (ISR) emission, where the recoil of an ISR emission is taken by the whole final state, produces VBS samples with too much radiation in the central region of rapidity [8]. The dipole recoil scheme mitigates this behaviour by having only one final-state parton take the recoil of an emission. A dedicated study of the effect of these settings can be found in ref. [43]. The renormalisation and factorisation scales are chosen to be $\mu_{\mathrm{R}} = \mu_{\mathrm{F}} = \sqrt{p_{\mathrm{T}}^{\mathrm{j}_1} p_{\mathrm{T}}^{\mathrm{j}_2}}$, where $p_{\mathrm{T}}^{\mathrm{j}_1}$ and $p_{\mathrm{T}}^{\mathrm{j}_2}$ are the transverse momenta of the jets with the highest (leading) and second highest (subleading) transverse momentum, respectively.

A combination of MC samples is used to assess partial NLO pQCD corrections to the EW $W^{\pm}W^{\pm}jj$ production. This combination is based on a Sherpa2.2.11 EW $W^{\pm}W^{\pm}jj$ sample, which excludes triboson contributions, and is simulated with up to one additional parton at LO. The non-overlapping triboson WWW and WH ($H \to W^+W^-$) final states (in the decay mode $\ell^\pm\nu\ell^\pm\nu jj$) are modelled with SHERPA2.2.2 at NLO with up to two additional partons at LO, and POWHEG BOXv2 + PYTHIA8.235 samples [44], respectively. This combination is referred to as "SHERPA EW" in the following. Partial NLO pQCD corrections to the QCD $W^\pm W^\pm jj$ process are checked using a separate SHERPA2.2.2 sample, referred to as "SHERPA QCD", which also models $W^\pm W^\pm jj$ final states with up to one extra parton at LO. The μ_R and μ_F of both SHERPA models are set equal to the invariant mass of W boson pair. These and the following background SHERPA samples use dedicated parton shower tuning developed by the SHERPA authors [45].

An additional alternative EW $W^\pm W^\pm jj$ sample, simulated with the POWHEG BOXv2 event generator interfaced to the PYTHIA8.230 parton shower model without deploying the dipole recoil scheme, was used for comparisons. This POWHEG +PYTHIA EW $W^\pm W^\pm jj$ sample was generated at NLO in pQCD in the VBS approximation [46], using the NNPDF3.0NLO PDF set in the matrix element. The μ_R and μ_F are fixed to the W boson mass. The AZNLO set of tuned parameters [47] is used, with the CTEQ6L1 [48] PDF set, for the modelling of non-perturbative effects. The PHOTOS++ 3.61 program [49, 50] is used to simulate quantum electrodynamic emissions, including lepton pair emissions.

3.2 Background samples

Diboson QCD $VVjj$ processes $Z/\gamma^*(\ell^\pm\ell^\mp)Z/\gamma^*(\ell^\pm\ell^\mp)$ and $W(\ell^\pm\nu)Z/\gamma^*(\ell^\pm\ell^\mp)$ are simulated with the SHERPA2.2.2 event generator [51] using matrix elements that contain all diagrams with four EW vertices. These processes are calculated for up to one additional parton at NLO and up to three additional partons at LO using COMIX [52] and OPENLOOPS [53], and merged with the SHERPA parton shower based on Catani-Seymour dipole factorisation [54] according to the MEPS@NLO prescription [55–58]. The NNPDF3.0NNLO PDF set is used. The EW production of $W^\pm Z/\gamma^*jj$ is simulated using MADGRAPH5_AMC@NLO2.6.2 [36] at LO in pQCD, using the NNPDF3.0NLO PDF set, and interfaced to PYTHIA8.235 for modelling the parton shower in the dipole recoil scheme. The EW production of $Z/\gamma^*Z/\gamma^*jj$ is modelled using SHERPA2.2.2 at LO.

Samples for $V\gamma$ ($V = W, Z/\gamma^*$) processes are produced using SHERPA2.2.11. All off-shell contributions are taken into account. The NLO matrix elements with up to one additional parton and LO matrix elements with up to three partons are merged with the parton shower using an MEPS@NLO merging scale of $Q = 20\,\mathrm{GeV}$. The NNPDF3.0NNLO PDF set is used. The photon is required to have $p_\mathrm{T} > 7\,\mathrm{GeV}$ and be isolated from leptons [59]. The EW production of $V\gamma$ is modelled using MADGRAPH5_AMC@NLO2.6.5+PYTHIA8.240 at LO in pQCD.

Triboson processes VVV ($V = W, Z$), which lead to two-jets plus four-lepton (charged or neutrinos) final states, and do not contain W boson pairs with the same charge, are considered background and are simulated at LO with up to one extra parton in SHERPA2.2.2 using the NNPDF3.0NNLO PDF set.

The $t\bar{t}V$ ($V = W, Z$) samples are generated at NLO in pQCD using MADGRAPH5_AMC@NLO2.3.3.p0 [36] and showered by PYTHIA8.210, with the cross section normalised to the prediction including NLO EW and NLO QCD corrections [60]. The NNPDF3.0NLO PDF is used in the matrix element. The tZq contributions were modelled at LO accuracy in pQCD using MadGraph5_aMC@NLO2.3.3.p1 interfaced to Pythia8.212 for parton showering.

Several MC samples are used to subtract prompt lepton contributions in the region used to derive scale factors for the data-driven non-prompt lepton background estimate described in section 5.2. Events containing a W or Z boson with associated jets are simulated using MadGraph5_aMC@NLO2.3.2.p1 [36] at LO with up to four extra partons, interfaced to the Pythia8.210 [39] parton shower model. The W/Z samples are normalised using next-to-next-to-leading-order (NNLO) cross sections [61, 62].

The Powheg Boxv2 [44] program is used with the NNPDF3.0NLO PDF set to generate $t\bar{t}$ and single top-quark events in both the Wt- and s-channels. The parton shower, hadronisation, and the underlying event are simulated using Pythia8.230 with the NNPDF2.3LO PDF set [48] and the corresponding A14 [63] set of tuned parameters. The top quark mass is set to 172.5 GeV. Single-top events in the t-channel are generated with Powheg Boxv2 using the 4-flavour scheme for the NLO matrix element calculations together with the fixed four-flavour PDF set NNPDF3.0NLO4F. Pythia8 with the A14 set of tuned parameters is used for the parton shower. For all top processes, top-quark spin correlations are preserved (for t-channel, top quarks are decayed using MadSpin [64]). The cross sections of these processes involving top quarks are normalised to the NLO (NNLO for $t\bar{t}$) pQCD predictions including next-to-next-to-leading logarithmic soft gluon terms [65–72].

Contributions from prompt photon + jet production, where the converted photon is misreconstructed as an electron, are subtracted with other prompt electron contributions, and are simulated using Sherpa2.2.2 with up to two additional jets at NLO and with up to four jets at LO in pQCD, using the NNPDF3.0NNLO PDF set.

3.3 $W^{\pm}W^{\pm}jj$ EFT samples

For the EFT interpretation presented in section 8, individual samples that vary only one term at a time (SM, interference, quadratic or cross, see [73] for details) are generated. This amplitude decomposition technique is used to avoid generating multiple samples with different Wilson coefficient values or relying on an event-by-event matrix element reweighting. The $W^{\pm}W^{\pm}jj$ EFT samples are simulated using MadGraph5_aMC@NLO 2.6.5 [36] at LO interfaced to Pythia8.235 [32] for the modelling of the parton shower (using the dipole recoil scheme), hadronisation and underlying event. The PDF set used was NNPDF3.0NLO [40], with a strong coupling constant $\alpha_{\mathrm{s}}(M_Z) = 0.118$. Contrary to the samples described in section 3.1, where a custom scale was used as described, the samples that include the effect of EFT operators use half of the sum of the transverse masses of all objects in the event [74].

3.4 $\mathrm{H}_5^{\pm\pm}$ samples

The signal samples used to set limits on doubly-charged Higgs boson production (see section 9) are simulated with MadGraph5_aMC@NLO 2.9.5 [36] at LO interfaced to Pythia8.245 [32] for the modelling of the parton shower in the dipole recoil scheme, hadronisation and underlying event. The PDF set used was NNPDF3.0NLO [40], implemented at NLO in pQCD and with a strong coupling constant $\alpha_s(M_Z) = 0.118$. The signal simulation is produced for 23 mass points from 200 GeV to 3 TeV using the `H5plane` benchmark [75] assuming a narrow-width signal with the width-to-mass ratio of $H5$ states below 5%. The $\sin\theta_H$ values are set to 0.5 for masses up to 800 GeV and 0.25 for higher-mass samples to be compatible with present constraints.

4 Event reconstruction and selection

The signature of $W^{\pm}W^{\pm}jj$ events is the presence of two high-energy forward jets (tagging jets) in opposite hemispheres and the presence of a same-sign charged-lepton pair (e or μ) and missing transverse momentum (E_T^{miss}). Due to the emission of a vector boson from each initial quark line, the final-state quarks tend to be at high absolute values of rapidity, and have rather large momenta. The two jets therefore have a large absolute rapidity difference, $\Delta y_{jj} = |y_{j1} - y_{j2}|$, and a large invariant mass m_{jj}. In addition, the leptons from the decays of the two W bosons tend to lie between the tagging jets in rapidity.

Lepton candidates are first preselected using baseline criteria. Electron candidates are reconstructed [76] from electromagnetic calorimeter energy clusters and matched to a track reconstructed in the ID. Baseline electrons are required to have $|\eta| < 2.47$ and transverse momentum $p_T > 4.5$ GeV. They must be outside the barrel/endcap transition region ($1.37 < |\eta| < 1.52$) of the calorimeter. Muons are reconstructed [77] from tracks in the MS, matched to a corresponding track in the ID where possible. Baseline muons are required to have $p_T > 3$ GeV and $|\eta| < 2.7$. Electron and muon tracks are required to originate from the primary vertex.[3] The transverse impact parameter significance[4] is required to be less than 5 for electrons and 15 for muons. The longitudinal impact parameter[5] must be less than 0.5 (1.5) mm for electrons (muons). Baseline electrons and muons are required to satisfy respective loose identification criteria [76, 77].

Jets are reconstructed using the anti-k_t algorithm [78], with a radius parameter of $R = 0.4$, using particle-flow objects [79] as input. The jets are required to have $p_T > 25$ GeV and $|\eta| \leq 4.5$. Contamination from jets originating in pile-up collisions is reduced by using the jet-vertex-tagger algorithm [80]. Jets with $p_T > 20$ GeV and $|\eta| < 2.5$ that contain a b-hadron are identified using the 85% efficiency working point of the DL1r heavy-flavour tagger [81].

To avoid the double counting of physics objects, an overlap removal procedure is applied to baseline leptons and jets. First, non-b-jets are removed if they overlap with an electron or muon within $\Delta R < 0.2$ and have less than three associated tracks with $p_T > 500$ MeV. At the next step, electrons or muons that overlap with jets, including b-jets, within $\Delta R < 0.4$ are removed. Finally, electrons that share an ID track with a muon are removed.

---

[3] The primary vertex is identified as the vertex in the event with the highest scalar sum of the squared transverse momenta of its associated tracks.

[4] The transverse impact parameter significance is defined as $|d_0|/\sigma(d_0)$, where d_0 is the distance of closest approach of e or μ to the primary vertex in the transverse plane and $\sigma(d_0)$ is its uncertainty.

[5] The longitudinal impact parameter is equal to $|z_0 \cdot \sin\theta|$, where z_0 is the difference between the value of the z coordinate of the point on the track at which d_0 is defined and the longitudinal position of the primary vertex.

Two further categories of leptons are defined, which are mutually exclusive subsets of baseline leptons: signal leptons for the signal extraction and background leptons for the estimate of the non-prompt lepton background.

Signal electrons must satisfy the Tight likelihood-based identification criteria [82], and signal muons the Medium identification criteria [77]. Electrons (muons) are required to satisfy the Gradient [76] (PflowTight [77]) isolation criteria. The longitudinal impact parameter of muons is required to be less than 0.5 mm, while the transverse impact parameter significance must be less than 3. A charge selector tool based on boosted decision trees uses shower shape and track-to-cluster matching variables [76] to reject electron candidates where the charge is likely misidentified. The efficiency of the charge selector tool for selecting signal electrons with correctly identified charge is reaching 99.4% (95%), in the same time achieving a rejection of 83% (92%) of electrons with wrongly identified charge in the barrel (endcap) region.

Background lepton candidates are used to estimate the non-prompt lepton background. Background electrons are required to satisfy the Medium likelihood identification [82], while an isolation requirement is dropped. The isolation requirement for background muons is changed to PflowLoose [77] and the transverse impact parameter significance is required to be less than 10. All background leptons are required to fail the signal lepton selection to ensure that the samples of signal and background leptons are statistically independent.

Two signal leptons with the same charge are required in each event. Each lepton must have transverse momentum $p_{\mathrm{T}} > 27$ GeV. Muon pseudorapidity is restricted to the range $|\eta| < 2.5$, where a matching to the ID track is possible. One of the leptons must be matched to the lepton that fired a single lepton trigger mentioned in section 3. The dilepton invariant mass $m_{\ell\ell}$ is required to be above 20 GeV.

Due to a non-negligible charge misidentification rate for electrons (see section 5.3), $Z/\gamma* \to ee$ events can pass the same-sign selection. To reduce the Drell-Yan background, the pseudorapidities η of each electron must satisfy $|\eta| < 1.37$. This requirement restricts electrons to the detector region with a lower material budget, where the production of secondary particles (photons and electron-positron pairs) is less probable and allows a more accurate charge identification. In addition, events with two signal electrons must survive a Z veto, $|m_{ee} - m_Z| > 15$ GeV, where m_Z is the mass of the Z boson and m_{ee} is the dielectron invariant mass.

To suppress background from processes with more than two leptons in the final state (e.g., WZ and ZZ background), a third lepton veto is applied in the following way: events in which a third baseline lepton survives the overlap removal are rejected. If a third baseline lepton does not survive the overlap removal, but the dilepton invariant mass of a same-flavour opposite-charge signal lepton and the third lepton is compatible with the Z boson mass, $|m_{\ell\ell} - m_Z| < 15$ GeV, the event is also rejected.

Due to the presence of two neutrinos in the final state, signal events usually have a large $E_{\mathrm{T}}^{\mathrm{miss}}$. The latter is reconstructed from the p_{T} imbalance of baseline objects that survive the overlap removal and the soft track term [83], and must satisfy $E_{\mathrm{T}}^{\mathrm{miss}} > 30$ GeV.

At least two jets are required to be present in each event, with transverse momentum p_{T} that exceeds 65 GeV for the leading jet and 35 GeV for the subleading jet. The two jets with the highest p_{T} in the event are selected as tagging jets, i.e. they are used to calculate

Requirement	SR	Low-m_{jj} CR	WZ CR
Leading and subleading lepton p_{T}	> 27 GeV		
Electron $\|\eta\|$	< 2.47 (1.37 in ee), excluding $1.37 \leq \|\eta\| \leq 1.52$		
Muon $\|\eta\|$	< 2.5		
Leading (subleading) jet p_{T}	$> 65\,(35)$ GeV		
Additional jet p_{T}	> 25 GeV		
Jet $\|\eta\|$	< 4.5		
$m_{\ell\ell}$	> 20 GeV		
$E_{\text{T}}^{\text{miss}}$	> 30 GeV		
Charge misid. $Z \rightarrow ee$ veto	$\|m_{ee} - m_Z\| > 15$ GeV		–
b-jet veto	$N_{b\text{-jet}} = 0$, $p_{\text{T}}^{b\text{-jet}} > 20$ GeV, $\|\eta^{b\text{-jet}}\| < 2.5$		
$N_{\text{veto leptons}}$	$= 0$	$= 0$	$= 1\,, p_{\text{T}} > 15$ GeV
$m_{\ell\ell\ell}$	–	–	> 106 GeV
m_{jj}	> 500 GeV	$200 < m_{\text{jj}} < 500$ GeV	> 200 GeV
$\|\Delta y_{\text{jj}}\|$	> 2		

Table 2. Summary of the event selection for the signal and control regions.

m_{jj} and $|\Delta y_{\text{jj}}|$ used in the further selection. To suppress background contributions from top processes, events are vetoed if any jet with $p_{\text{T}} > 20$ GeV and $|\eta| < 2.5$ is identified as a b-jet.

The VBS signature of two jets with high invariant mass and large angular separation is used to further purify the events and in particular to separate the signal from QCD-induced processes that lead to the same final state. The dijet invariant mass and the difference in jet rapidities must satisfy $m_{\text{jj}} \geq 500$ GeV and $|\Delta y_{\text{jj}}| > 2$, respectively. The expected purity of the EW (QCD, Int) $W^{\pm}W^{\pm}jj$ process in the signal region (SR) is 52% (5.4%, 1.7%).

In addition to the SR, the measurement makes use of two control regions (CR), referred to in the following as the "WZ CR" and "low-m_{jj} CR". The WZ CR follows closely the SR selection with the exception that the third-lepton veto requirement is dropped, and exactly one more signal lepton with $p_{\text{T}} > 15$ GeV is required. In addition, the m_{jj} condition is loosened to $m_{\text{jj}} > 200$ GeV and the trilepton invariant mass is required to satisfy $m_{\ell\ell\ell} > 106$ GeV to suppress contamination from radiative Z boson decays. The WZ CR is used to improve the modelling of the dominant background coming from QCD-induced $W^{\pm}Zjj$ events.

The low-m_{jj} CR and the SR use the same selection criteria except on the dijet invariant mass, where the CR selection requires $200 < m_{\text{jj}} < 500$ GeV. As a result, this CR has a similar background composition to the SR but the contribution from signal events is reduced to 11%. The low-m_{jj} CR is used in the signal extraction fit to control the uncertainties of major background contributions, described in sections 5.1–5.3.

The SR and CR event selections are summarised in table 2.

5 Background estimation

The dominant background, which comes from $WZ/\gamma^{*}jj$, is estimated using MC and includes a data-driven correction to the shape of the m_{jj} distribution and an adjustment to the normalisation based on a dedicated CR. The non-prompt lepton and electron charge misidentification backgrounds are estimated using data-driven methods. The remaining background sources are modelled using MC simulations. The contributions from the hard double parton scattering process, where two W bosons are produced in two separate partonic interactions from the same pp collision, was checked using MC and found to be negligible. The fraction of signal events where at least one of the two signal jets originates from pile-up pp interactions was estimated using MC simulations to be about 0.5%.

5.1 WZ/γ^* background

The WZ/γ^* production, dubbed WZ in the following, where both the W and Z/γ^* bosons decay leptonically, comprises the dominant background in this measurement and contributes 22% of the overall expected event yield in the SR. It contributes when one lepton escapes the third lepton veto requirement, typically because it was outside of the geometrical acceptance of the detector.

The $W^\pm Zjj$ final states are modelled using MC simulations and are dominated by the QCD-induced production mode. The cross section extraction of the $W^\pm W^\pm jj$ signal relies on the proper modelling of m_{jj} templates, and to avoid a bias in the signal extraction induced by a possible m_{jj} mismodelling in background, the shape of this variable given by the QCD $W^\pm Zjj$ model is reweighted to data [84] in a dedicated region. First, the selection of the WZ CR described in section 4 is applied. In addition, to reduce the contamination from EW $W^\pm Zjj$ events, a requirement on the WZ system centrality, $\xi_{WZ} > 0.4$, is imposed, which suppresses events where the WZ system is located between the two tagging jets in rapidity — a characteristic topology for EW production mode. The centrality is defined as $\xi_{WZ} = \left|\frac{y_{WZ}-(y_{\mathrm{j1}}+y_{\mathrm{j2}})/2}{y_{\mathrm{j1}}-y_{\mathrm{j2}}}\right|$, where $y_{WZ} = (y_{\ell(W)} + y_{\ell\ell(Z)})/2$ is the average of the rapidity $y_{\ell(W)}$ of the charged lepton coming from the W and the rapidity $y_{\ell\ell(Z)}$ of the dilepton coming from the Z boson, and y_{j1} (y_{j2}) is the rapidity of the leading (subleading) jet. This requirement reduces the contribution of EW $W^\pm Zjj$ events to the total $W^\pm Zjj$ yield from 13% to 5%. The m_{jj} reweighting, which was derived in this special data region, is applied to the $W^\pm Zjj$ model in the SR and all CRs and is constructed to preserve the MC normalisation of the QCD $W^\pm Zjj$ background for $m_{\mathrm{jj}} > 200$ GeV. To test the impact of the selection on the reweighting function, the function was also derived in the WZ CR without applying the WZ centrality selection, and the result was found to be consistent with the nominal reweighting function within the uncertainty. The weight values range from 1.2 at $m_{\mathrm{jj}} = 200$ GeV to approximately 0.3 at $m_{\mathrm{jj}} = 3$ TeV. The uncertainty in the reweighting function, dominated by the limited data in the derivation region, is m_{jj} dependent, ranging between 10% at $m_{\mathrm{jj}} = 200$ GeV and 70% at $m_{\mathrm{jj}} = 3$ TeV. Additional sources of uncertainty in the reweighting function include renormalisation and factorisation scale variations, as well as PDF and α_{s} variations, are negligible compared with the statistical component.

5.2 Non-prompt lepton background

Leptons from hadron decays and jets misidentified as leptons are referred to as non-prompt leptons. They constitute the second-largest background source, corresponding to 12% of the expected event yield in the signal region, and arise mainly from W+jets and semileptonic $t\bar{t}$

processes. This background is estimated using a data-driven method involving the computation of scale factors defined as the ratio of the probability for a non-prompt lepton to pass the signal lepton requirements to the probability for it to pass the background lepton selection, as defined in section 4. This method is similar to the one used in ref. [14].

The scale factors are derived from a data sample containing events with a single non-prompt lepton candidate balanced by a jet. Jets with transverse momenta $p_{\mathrm{T}} > 25\,(30)$ GeV in the pseudorapidity range $|\eta| < 2.5$ ($2.5 < |\eta| < 4.5$) are selected if the jet and lepton candidates are opposite in azimuthal angle and satisfy $|\Delta\phi(\ell, j)| > 2.8$. The prompt lepton contributions are reduced by adding a requirement on the sum of $E_{\mathrm{T}}^{\mathrm{miss}}$ and the transverse mass m_{T} (see definition in section 7.2) of the lepton + $E_{\mathrm{T}}^{\mathrm{miss}}$ system, $E_{\mathrm{T}}^{\mathrm{miss}} + m_{\mathrm{T}} < 50$ GeV. Residual prompt lepton and prompt photon conversion contributions are modelled using MC. The scale factors are computed in bins of lepton p_{T} and, for electrons, in two bins of η corresponding to the barrel and endcap LAr calorimeters. The events in this sample are triggered by single-electron or single-muon triggers with low-p_{T} thresholds of 12 and 14 GeV, respectively, which require loosely identified leptons without any isolation requirement.

The uncertainty in the scale factors ranges from 10% to 40%. The dominant contributions to the uncertainty come from varying the prompt lepton contributions by ±5% and from the variation of the b-tagged jet selection (b-veto versus at least one b-jet), which is done to vary the amount of non-prompt leptons from light-flavour hadrons versus heavy-flavour hadrons. Additional uncertainties in the scale factors are estimated by varying the $E_{\mathrm{T}}^{\mathrm{miss}} + m_{\mathrm{T}}$ requirement, and by varying the level of prompt electron and muon contributions, related to a potential mismodelling of the identification and isolation efficiencies for background leptons (see section 4) that satisfy corresponding looser requirements but fail tighter requirements. Statistical uncertainties arising from the limited number of data and MC events in the region used to derive the scale factors are also included.

The estimate of the non-prompt background in the signal region is obtained by applying these scale factors to data events in the kinematic region defined by the SR selection, with the exception that instead of having two signal leptons, events are required to have one signal and one background lepton. In this region, contributions from processes with two prompt leptons or one prompt lepton plus a prompt photon, where the latter converts and is misreconstructed as an electron, are subtracted using MC. If a signal lepton plus background lepton event is triggered by the background lepton, a dedicated set of scale factors is applied, derived with the analysis triggers mentioned in section 3 instead of low-p_{T} triggers. This helps to avoid a bias due to having the lepton identification and isolation requirements of the analysis triggers be tighter than the selection of background leptons. Systematic uncertainties in these dedicated scale factors are obtained, considering the same sources used for the scale factors obtained using low-p_{T} single-lepton triggers.

5.3 Electron charge misidentification and photon conversion background

Background from Z and dileptonic $t\bar{t}$ events involving electrons, where the charge of an electron is misidentified in the detector, is estimated by weighting opposite-charge dilepton data events with charge misidentification probabilities obtained from MC. After applying the electron charge-selector tool [76] described in section 4, the residual contribution of the

Process	ee	$e\mu$	μe	$\mu\mu$	Combined
$W^{\pm}W^{\pm}jj$ EW	27.6 ± 0.9	68.2 ± 1.6	61.3 ± 1.5	77.8 ± 1.7	235 ± 5
$W^{\pm}W^{\pm}jj$ QCD	1.6 ± 0.5	7.3 ± 2.2	6.4 ± 1.9	8.8 ± 2.5	24 ± 7
$W^{\pm}W^{\pm}jj$ Int	0.93 ± 0.20	2.2 ± 0.5	2.0 ± 0.4	2.5 ± 0.5	7.6 ± 1.6
$W^{\pm}Zjj$ QCD	8.4 ± 1.0	26.8 ± 3.0	26.7 ± 3.0	20.9 ± 2.2	83 ± 9
$W^{\pm}Zjj$ EW	1.71 ± 0.14	4.9 ± 0.4	4.1 ± 0.4	4.2 ± 0.4	14.9 ± 1.2
Non-prompt	8.9 ± 2.6	15 ± 4	10.2 ± 3.2	21 ± 7	56 ± 12
$V\gamma$	1.3 ± 0.8	5.1 ± 2.2	4.6 ± 2.6	—	11 ± 5
Charge misid.	3.8 ± 2.0	5.0 ± 1.3	1.2 ± 0.4	—	10 ± 4
Other prompt	1.02 ± 0.29	2.5 ± 0.6	1.8 ± 0.5	1.7 ± 2.2	7.1 ± 2.8
Total expected	55 ± 4	137 ± 7	118 ± 6	137 ± 8	448 ± 20
Data	52	149	127	147	475

Table 3. Expected signal and background yields in the SR. The yields are shown for different dilepton final states where the first lepton has the highest p_{T}. The "Other prompt" category combines ZZ, VVV, $t\bar{t}V$, and tZq background processes. The sum of all contributions may differ from the total value due to rounding. The uncertainty includes both the statistical and systematic components.

overall dilepton background in the signal region is 2.3%, and is 1.4% for events with one signal electron and one signal muon. The uncertainty in this background contribution reaches 40% and is dominated by the uncertainties in the scale factors that calibrate the charge-selector tool, which were obtained using $Z \to e^+e^-$ events [76].

The background contribution from $\ell\gamma jj$ events, where the prompt photon γ is misreconstructed as an electron, is simulated using $V\gamma$ MC (see table 1). An overall normalisation uncertainty of 40% is assigned to this background, motivated by the scale factor uncertainties of the electron charge-selector tool. The expected contribution of this process to the SR event yield is 2.4%.

5.4 Other background

The rest of the prompt-lepton background arises from ZZ, triboson VVV (excluding triboson final states involving two same-sign W bosons), $t\bar{t}V$, and tZq processes, which together correspond to 1.6% of the expected total SR yield, and are modelled using MC (see table 1). A normalisation uncertainty of 20% [85] (30% [85, 86]) is applied on the cross section of the ZZ (VVV and top quark processes) production.

The expected signal and background yields in the SR are given in table 3.

6 Systematic uncertainties

Systematic uncertainties affecting the measurement arise from experimental sources and signal and background modelling uncertainties.

Experimental uncertainties. Experimental sources include uncertainty in the calibration of the objects and algorithms used in the measurement. In particular, uncertainties in the lepton reconstruction, identification, and isolation efficiencies [76, 77] and in the lepton trigger efficiency [27, 28] are taken into account. Uncertainties in the calibration of jet energy scale and resolution [79], the jet vertex tagger [80], and in the calibration of the b-tagger [81] used for applying a b-jet veto are included. The uncertainties in the $E_{\mathrm{T}}^{\mathrm{miss}}$ calibration [83] and MC pile-up reweighting are considered as well. A luminosity uncertainty of 1.7% [25] is assigned to all MC based predictions.

One of the dominant systematic uncertainty sources in this measurement is related to the non-prompt background estimate. The uncertainty estimates are obtained by varying p_{T}-dependent (and η-dependent for electrons) scale factors associated with the data-driven method used. More details about the types of systematic variations can be found in section 5.2.

Uncertainties in the data-driven electron charge misidentification background arise from the calibration uncertainties in the charge-selector tool [76], as described in section 5.3.

Signal and background modelling uncertainties. Theoretical signal modelling uncertainties are dominated by the effects of missing higher-order pQCD contributions in the nominal LO MG5_aMC+Herwig7 signal model. To account for them, two separate variations are studied. First, the μ_{R} and μ_{F} are varied up and down by a factor two, excluding variations in opposite directions [87], and applied to EW, Int, and QCD $W^{\pm}W^{\pm}jj$ samples coherently. It is important to note that the μ_{R} variation is zero for the EW $W^{\pm}W^{\pm}jj$ LO model. Therefore, as a second variation, the difference with respect to the Sherpa EW (Sherpa QCD) calculation is included as an uncertainty in the EW (QCD) $W^{\pm}W^{\pm}jj$ prediction. The NLO EW effects on the EW $W^{\pm}W^{\pm}jj$ prediction were derived by the authors of ref. [88] for the fiducial region of this measurement and are taken as an uncertainty in the nominal model as well, using an m_{jj}-dependent correction factor. The parton shower uncertainty is included by considering a difference between the nominal prediction using Pythia and an alternative prediction using the Herwig parton shower model. Additionally, PDF and α_{s} variations are included, using standard prescriptions from ref. [89]. For the cross section extraction, the theory variations of the respective signal process (which can be EW $W^{\pm}W^{\pm}jj$ or inclusive $W^{\pm}W^{\pm}jj$ production) are normalised to the nominal prediction in the fiducial region, defined in section 7.1.

The QCD-induced $W^{\pm}Zjj$ background MC model suffers from m_{jj} mismodelling, which is corrected for by reweighting the m_{jj} distribution to data with other processes subtracted. The uncertainty of the reweighting function is dominated by limited data in the reweighting region and is represented by corresponding parameter variations of the exponential reweighting fit function. Further details about the systematic uncertainties from the m_{jj} reweighting can be found in section 5.1. Additionally, uncertainties in the theoretical modelling of the QCD- and EW-induced $W^{\pm}Zjj$ processes are taken into account, including μ_{R} and μ_{F} variations [87], PDF, and α_{s} [89] variations.

Normalisation uncertainties of minor prompt lepton background sources are included, as quantified in section 5.4.

Statistical uncertainties of all signal and background predictions are considered and are subdominant.

Source	Impact [%]
Experimental	4.6
Electron calibration	0.4
Muon calibration	0.5
Jet energy scale and resolution	1.9
$E_{\mathrm{T}}^{\mathrm{miss}}$ scale and resolution	0.2
b-tagging inefficiency	0.7
Background, misid. leptons	3.4
Background, charge misrec.	1.0
Pile-up modelling	0.1
Luminosity	1.9
Modelling	4.5
EW $W^{\pm}W^{\pm}jj$, shower, scale, PDF & α_s	0.7
EW $W^{\pm}W^{\pm}jj$, QCD corrections	1.9
EW $W^{\pm}W^{\pm}jj$, EW corrections	0.9
Int $W^{\pm}W^{\pm}jj$, shower, scale, PDF & α_s	0.6
QCD $W^{\pm}W^{\pm}jj$, shower, scale, PDF & α_s	2.6
QCD $W^{\pm}W^{\pm}jj$, QCD corrections	0.8
Background, WZ scale, PDF & α_s	0.3
Background, WZ reweighting	1.5
Background, other	1.3
Model statistical	1.8
Experimental and modelling	6.4
Data statistical	7.4
Total	9.8

Table 4. Impact of the uncertainty on the EW $W^{\pm}W^{\pm}jj$ cross section measurement. The contribution of a systematic uncertainty (uncertainty group) to the total uncertainty is evaluated by fixing the respective NP (NPs) to its (their) best-fit value(s), redoing the fit, and subtracting the uncertainties of the cross section in quadrature. The procedure is implemented incrementally such that the grouped systematic and statistical uncertainties added in quadrature correspond to the total cross section uncertainty by construction. Lepton calibration uncertainties encompass the effects of calibration of lepton energy or momentum scale and resolution, as well as lepton trigger, reconstruction, identification, and isolation efficiencies. "Background, other" includes normalisation uncertainties of background samples modelled with MC where their normalisation is not obtained in a dedicated CR. The "Model statistical" category is related to the finite number of MC events and data events used for data-driven background estimates.

Systematic uncertainties are included in the cross section extraction fits, described in section 7.1, as nuisance parameters (NP) constrained by Gaussian functions. The statistical uncertainties in the model are included as NPs constrained by Poisson distributions. Table 4 shows the impact of these uncertainties on the fitted signal strength of the EW $W^{\pm}W^{\pm}jj$ production.

7 Cross section extraction

7.1 Fiducial cross section extraction

The fiducial phase space is chosen to conform as closely as possible to the detector acceptance and to the analysis selection, described in section 4. The analysis fiducial region is defined at the particle level using the collection of stable[6] particles from matrix-element plus parton-shower generators. Events are required to have two prompt leptons (e or μ) with $p_{\mathrm{T}} > 27$ GeV and $|\eta| < 2.5$ dressed with prompt photons that lie within $\Delta R < 0.1$. Events with τ-leptons from W decays in the matrix element calculation are vetoed. The two leptons must have the same sign of electric charge and have an invariant mass $m_{\ell\ell} > 20$ GeV. At least two jets reconstructed with the anti-k_t algorithm with a radius parameter of $R = 0.4$ are required, with $|\eta| < 4.5$ and $p_{\mathrm{T}} > 65$ GeV (35 GeV) for the leading (sub-leading) jet. In cases where a third jet is required, its p_{T} requirement is lowered to 25 GeV. The jets are clustered including electrons among the clustering inputs, but excluding muons and neutrinos, so an overlap removal step between electrons and jets is applied. If an electron and a jet overlap with $\Delta R(e, \mathrm{jet}) < 0.4$, and the ratio $p_{\mathrm{T,e}}/p_{\mathrm{T,jet}} < 0.5$, the electron is removed, otherwise the jet is removed. No overlap removal between muons and jets is applied. Events with b-jets within $|\eta| < 2.5$ and $p_{\mathrm{T}} > 20$ GeV, that are identified via ghost matching [78] to weakly decaying b-hadrons, are vetoed. Also events are vetoed when there is a third prompt lepton with $p_{\mathrm{T}} > 3$ GeV and within $|\eta| < 2.5$. Events with the dielectron invariant mass in the range $|m_{ee} - m_Z| < 15$ GeV are rejected. The particle-level $E_{\mathrm{T}}^{\mathrm{miss}}$ is reconstructed from the visible final-state objects that meet these criteria and must satisfy the condition $E_{\mathrm{T}}^{\mathrm{miss}} > 30$ GeV. Finally, the invariant mass of the two highest-p_{T} jets must satisfy $m_{\mathrm{jj}} > 500$ GeV and their separation in rapidity, $|\Delta y_{\mathrm{jj}}|$, must exceed 2.

Fiducial cross sections of the EW and inclusive $W^{\pm}W^{\pm}jj$ production are measured by performing separate maximum likelihood fits. The EW (inclusive) $W^{\pm}W^{\pm}jj$ signal strength, $\mu_{\mathrm{sig}}^{\mathrm{EW}}$ ($\mu_{\mathrm{sig}}^{\mathrm{EW+Int+QCD}}$), defined as the ratio of the observed to expected signal cross section, is a free parameter in the fit. The second free parameter in the fit is the normalisation coefficient of the dominant background, QCD $W^{\pm}Zjj$, $\mu^{\mathrm{QCD\ WZ}}$. To constrain the latter parameter, the WZ CR, as defined in section 4, is included in the fit as a single bin. Systematic uncertainties are included as NPs with Gaussian priors, correlated across all fit regions. Event yields in the low-m_{jj} CR, described in section 4, are also included in the fit. The SR and low-m_{jj} CR are each split into four subregions depending on the flavours of the leading- and subleading-p_{T} leptons: ee, $e\mu$, μe, $\mu\mu$, to enable a better constraint on p_{T} and flavour-dependent non-prompt and charge misidentification background uncertainties. The m_{jj} distribution, which provides good discrimination between the $W^{\pm}W^{\pm}jj$ signal and backgrounds, is used for the fit in the SR, with the binning optimised to maximise the expected signal sensitivity. In the fit for extracting the EW $W^{\pm}W^{\pm}jj$ cross section, the histogram corresponding to the interference term between the EW and QCD $W^{\pm}W^{\pm}jj$ production modes is scaled by $\sqrt{\mu_{\mathrm{sig}}^{\mathrm{EW}}}$.

The measured fiducial cross section, $\sigma_{\mathrm{fid,meas}}^{\mathrm{EW(+Int+QCD)}}$, is obtained by multiplying the fiducial cross section predicted by MC, $\sigma_{\mathrm{fid,pred}}^{\mathrm{EW(+Int+QCD)}}$ with the fitted signal strength $\mu_{\mathrm{sig}}^{\mathrm{EW(+Int+QCD)}}$, $\sigma_{\mathrm{fid,meas}}^{\mathrm{EW(+Int+QCD)}} = \mu_{\mathrm{sig}}^{\mathrm{EW(+Int+QCD)}} \cdot \sigma_{\mathrm{fid,pred}}^{\mathrm{EW(+Int+QCD)}}$.

---

[6] A particle is considered stable if its lifetime is greater than 3×10^{-11} s.

Even though the contributions from W bosons that decay to τ-leptons with a subsequent decay into electrons or muons are excluded in the fiducial region definition, they are treated as signal in the fit, assuming lepton universality in W decays, and correspond to around 11% of the total signal yield in the SR. The fraction of EW $W^{\pm}W^{\pm}jj$ signal events in the SR which do not pass the fiducial region selection corresponds to 31%. Such events are also treated as signal events in the fit, i.e. are scaled by the same signal strength parameter.

7.2 Differential cross section extraction

A fit procedure similar to the one described in section 7.1 is used for extracting single-differential cross sections, with the exception that two-dimensional distributions are used in the SR and low-m_{jj} CR. The variables of interest include the dilepton, $m_{\ell\ell}$, and dijet, m_{jj}, invariant masses, and the transverse mass, m_{T}, of the dilepton–$E_{\mathrm{T}}^{\mathrm{miss}}$ system, defined as

$$m_{\mathrm{T}} = \sqrt{\left(E_{\mathrm{T}}^{\ell\ell} + E_{\mathrm{T}}^{\mathrm{miss}}\right)^2 - \left|\vec{p}_{\mathrm{T}}^{\,\ell\ell} + \vec{E}_{\mathrm{T}}^{\mathrm{miss}}\right|^2},$$

where $E_{\mathrm{T}}^{\ell\ell}$ is the transverse energy of the dilepton system, $\vec{p}_{\mathrm{T}}^{\,\ell\ell}$ is the vectorial sum of the lepton transverse momenta, and $\vec{E}_{\mathrm{T}}^{\mathrm{miss}}$ is the missing transverse momentum vector. In addition, the cross sections are measured as a function of the number of jets between the two signal jets in rapidity, $N_{\text{gap jets}}$, and the Zeppenfeld variable of the third jet, $\xi_{\mathrm{j}3}$ [8]:

$$\xi_{\mathrm{j}3} = \left|\frac{\eta_{\mathrm{j}3} - \frac{1}{2}(\eta_{\mathrm{j}1} + \eta_{\mathrm{j}2})}{\eta_{\mathrm{j}2} - \eta_{\mathrm{j}1}}\right|.$$

The latter cross section is measured in the subset of the SR where a third jet is present.

One fit per variable of interest is performed to obtain the respective differential cross section. Separate fits are made to extract the EW $W^{\pm}W^{\pm}jj$ and inclusive $W^{\pm}W^{\pm}jj$ cross sections.

In every bin of the variable of interest, the m_{jj} distribution is fitted to obtain a better constraint on the signal strength. For the differential cross section extraction as a function of m_{jj}, the $m_{\ell\ell}$ shape is used for the signal fit in every m_{jj} bin, and the low-m_{jj} CR is dropped. No division according to lepton flavour is performed in the SR and the low-m_{jj} CR in these m_{jj} fits to simplify the fit model.

The cross section unfolding is based on a maximum-likelihood fit following the method of ref. [90]. The unfolding procedure is applied to the SR and CR distributions at the detector level. The detector-level signal distribution consists of a sum of subsamples, where each subsample contains signal events with the particle level value of the variable of interest in a specified range (“cross section bin”). The binning of the variable of interest in the SR and low-m_{jj} CR detector-level distributions used in the fit matches the cross section binning. Signal strength parameters associated with the particle-level signal predictions in the respective cross section bin are determined in the fit. The normalisation of the QCD $W^{\pm}Zjj$ background is also a free parameter. No regularisation is applied in the unfolding. Signal events that fail the fiducial region selection but pass the SR selection are scaled by the same signal strength parameter as the events that pass the fiducial region selection in the respective cross section bin. The signal strength parameters obtained in the fit are directly used to scale the MC particle-level cross sections, bin-wise, to obtain the unfolded measured cross sections.

Process	ee	$e\mu$	μe	$\mu\mu$	Combined
$W^{\pm}W^{\pm}jj$ EW	32.9 ± 3.4	81 ± 8	73 ± 7	90 ± 9	277 ± 26
$W^{\pm}W^{\pm}jj$ QCD	1.7 ± 0.5	8.0 ± 2.4	7.1 ± 2.1	9.7 ± 2.9	27 ± 8
$W^{\pm}W^{\pm}jj$ Int	1.00 ± 0.22	2.4 ± 0.5	2.1 ± 0.4	2.7 ± 0.6	8.2 ± 1.7
$W^{\pm}Zjj$ QCD	5.5 ± 0.7	18.2 ± 2.1	18.2 ± 2.2	14.0 ± 1.7	56 ± 6
$W^{\pm}Zjj$ EW	1.69 ± 0.14	4.9 ± 0.4	4.1 ± 0.4	4.2 ± 0.4	14.9 ± 1.2
Non-prompt	8.4 ± 1.6	14.9 ± 2.4	10.2 ± 1.6	21 ± 5	55 ± 9
$V\gamma$	1.5 ± 0.7	6.1 ± 2.4	5.5 ± 2.8	—	13 ± 5
Charge misid.	4.3 ± 2.0	5.4 ± 1.2	1.4 ± 0.4	—	11 ± 4
Other prompt	0.99 ± 0.25	2.5 ± 0.5	1.9 ± 0.5	1.4 ± 1.4	6.8 ± 2.1
Total	58 ± 4	143 ± 7	123 ± 6	143 ± 8	468 ± 21
Data	52	149	127	147	475

Table 5. Signal and background yields in the SR after the fit for the EW $W^{\pm}W^{\pm}jj$ fiducial cross section. The yields are shown for different dilepton final states where the first lepton has the highest p_{T}. The "Other prompt" category combines ZZ, VVV, $t\bar{t}V$, and tZq background processes. The sum of all contributions may differ from the total value due to rounding. The uncertainty includes both the statistical and systematic components.

The differential cross section binning for the $m_{\ell\ell}$, m_{T}, and m_{jj} variables is optimised to have similar expected EW $W^{\pm}W^{\pm}jj$ signal significances per bin. For the $N_{\text{gap jets}}$ variable, only two bins are possible due to the small number of events at high gap jet multiplicities. The binning of ξ_{j_3} is chosen to display a specific feature of the EW $W^{\pm}W^{\pm}jj$ cross section — the suppressed third jet production in the central region, $0 < \xi_{\mathrm{j}_3} < 0.5$.

7.3 Results

Post-fit yields for signal and background processes in the SR are shown in table 5, corresponding to the fit used for the EW $W^{\pm}W^{\pm}jj$ fiducial cross section extraction. The fitted value of the QCD $W^{\pm}Zjj$ background normalisation coefficient is found to be $\mu_{WZ}^{\mathrm{QCD}} = 0.67 \pm 0.03\,(\mathrm{stat.}) \pm 0.03\,(\mathrm{mod.\ syst.}) \pm 0.05\,(\mathrm{exp.\ syst.}) \pm 0.01\,(\mathrm{lumi.})$, where the uncertainties correspond to statistical, modelling systematic, experimental systematic, and luminosity uncertainties, respectively. The value well below unity is in agreement with the one found in the ATLAS observation of electroweak $W^{\pm}Zjj$ production [91], and with the inclusive WZ cross section measurement in the two-jet bin at high m_{jj} values [92]. The EW $W^{\pm}W^{\pm}jj$ signal strength is found to be $\mu_{\mathrm{sig}}^{\mathrm{EW}} = 1.15 \pm 0.09\,(\mathrm{stat.}) \pm 0.05\,(\mathrm{mod.\ syst.}) \pm 0.05\,(\mathrm{exp.\ syst.}) \pm 0.02\,(\mathrm{lumi.})$ and corresponds to the measured value of the fiducial cross section of EW $W^{\pm}W^{\pm}jj$ production of $\sigma_{\mathrm{fid}}^{\mathrm{EW}} = 2.92 \pm 0.22\,(\mathrm{stat.}) \pm 0.13\,(\mathrm{mod.\ syst.}) \pm 0.12\,(\mathrm{exp.\ syst.}) \pm 0.06\,(\mathrm{lumi.})$ fb.

The fitted value of the signal strength scaling the total $W^{\pm}W^{\pm}jj$ production, as obtained in a dedicated fit, is $\mu_{\mathrm{sig}}^{\mathrm{EW+Int+QCD}} = 1.16 \pm 0.08\,(\mathrm{stat.}) \pm 0.04\,(\mathrm{mod.\ syst.}) \pm 0.05\,(\mathrm{exp.\ syst.}) \pm 0.02\,(\mathrm{lumi.})$ and corresponds to the measured value of the fiducial cross section of the $W^{\pm}W^{\pm}jj$ production of $\sigma_{\mathrm{fid}}^{\mathrm{EW+Int+QCD}} = 3.38 \pm 0.22\,(\mathrm{stat.}) \pm 0.11\,(\mathrm{mod.\ syst.}) \pm 0.14\,(\mathrm{exp.\ syst.}) \pm 0.06\,(\mathrm{lumi.})$ fb. A summary of the measured and predicted EW and inclusive $W^{\pm}W^{\pm}jj$ fiducial cross sections is presented in table 6. The MC predictions generally agree with the measurement within the experimental and theoretical uncertainty, although all of the

Description	$\sigma_{\text{fid}}^{\text{EW}}$ [fb]	$\sigma_{\text{fid}}^{\text{EW+Int+QCD}}$ [fb]
Measured cross section	$2.92 \pm 0.22\,(\text{stat.}) \pm 0.19\,(\text{syst.})$	$3.38 \pm 0.22\,(\text{stat.}) \pm 0.19\,(\text{syst.})$
MG5_aMC+Herwig7	$2.53 \pm 0.04\,(\text{PDF})\ ^{+0.22}_{-0.19}\,(\text{scale})$	$2.92 \pm 0.05\,(\text{PDF})\ ^{+0.34}_{-0.27}\,(\text{scale})$
MG5_aMC+Pythia8	$2.53 \pm 0.04\,(\text{PDF})\ ^{+0.22}_{-0.19}\,(\text{scale})$	$2.90 \pm 0.05\,(\text{PDF})\ ^{+0.33}_{-0.26}\,(\text{scale})$
Sherpa	$2.48 \pm 0.04\,(\text{PDF})\ ^{+0.40}_{-0.27}\,(\text{scale})$	$2.92 \pm 0.03\,(\text{PDF})\ ^{+0.60}_{-0.40}\,(\text{scale})$
Sherpa ⊗ NLO EW	$2.10 \pm 0.03\,(\text{PDF})\ ^{+0.34}_{-0.23}\,(\text{scale})$	$2.54 \pm 0.03\,(\text{PDF})\ ^{+0.50}_{-0.33}\,(\text{scale})$
Powheg Box+Pythia	2.64	–

Table 6. Measured and predicted fiducial cross sections of the EW and inclusive $W^{\pm}W^{\pm}jj$ production, quoted with their respective uncertainties. For Powheg Box+Pythia only the central value is provided.

predictions underestimate the measured cross section values. The Sherpa MC models partial NLO QCD corrections by including real emissions of up to one extra parton and gives a 2% lower cross section of the EW $W^{\pm}W^{\pm}jj$ production than the LO MG5_aMC+Herwig7 and MG5_aMC+Pythia8 models. The NLO EW corrections [88] reduce the Sherpa prediction by around 15%. Both these observations are consistent with the effects of NLO corrections described in ref. [88]. The scale uncertainties are lower for MG5_aMC+Herwig7 and MG5_aMC+Pythia8 than for Sherpa, because renormalisation-scale variation of the LO EW $W^{\pm}W^{\pm}jj$ prediction is exactly zero due to the absence of QCD interactions at the matrix element level. The prediction from Powheg Box+Pythia MC, made at NLO in the VBS approximation, gives a 5% higher cross section than the LO models. This might be related to the renormalisation and factorisation scales of Powheg Box+Pythia being fixed to a constant value of $\mu_{\text{R}} = \mu_{\text{F}} = m_W$.

Post-fit distributions of m_{jj} and $m_{\ell\ell}$ as obtained in the fit for extracting the differential cross section as a function of $m_{\ell\ell}$ are presented in figure 4. Also shown in figure 4 are the corresponding post-fit $m_{\ell\ell}$ distribution in the low-m_{jj} CR and the WZ CR yield. The EW $W^{\pm}W^{\pm}jj$ signal from different particle-level $m_{\ell\ell}$ slices is shown in different shades of blue and denoted by “bin N” in the legend, where $N = 1, \ldots, 6$ gives the number of the $m_{\ell\ell}$ bin. Overall, a very good agreement between the data and post-fit model is seen, the agreement is nearly perfect in the $m_{\ell\ell}$ distribution in SR and in the WZ CR, where by construction the free-floating fit parameters compensate for the differences between the pre-fit model and the data.

Differential cross sections for the EW $W^{\pm}W^{\pm}jj$ production as a function of $m_{\ell\ell}$, m_{T}, m_{jj}, $N_{\text{gap jets}}$, and ξ_{j3} are shown in figure 5 and compared with SM predictions from MG5_aMC+Herwig7, MG5_aMC+Pythia8, Sherpa-EW, and Powheg Box+Pythia. A variant of the Sherpa-EW prediction with the NLO EW corrections applied via m_{jj}-dependent factors [88] is also shown. The NLO EW corrections move the prediction to lower values, especially at high m_{jj}. The uncertainties of the measured cross sections are dominated by the statistical component in all bins. In general, the SM predictions agree well with the measured cross sections within the quoted uncertainties, although all of the predictions tend to underestimate the data. The agreement is worse for m_{T} where an overprediction of the data in the region $170 < m_{\text{T}} < 210$ GeV and underprediction in the region $310 < m_{\text{T}} < 410$ GeV

Variable	EW $W^{\pm}W^{\pm}jj$		Inclusive $W^{\pm}W^{\pm}jj$		Max. value in data
	χ^2/N_{dof}	p-value	χ^2/N_{dof}	p-value	
$m_{\ell\ell}$	4.5/6	0.605	7.34/6	0.291	1081 GeV
m_{T}	13.0/6	0.043	16.33/6	0.012	1270 GeV
m_{jj}	7.6/6	0.266	8.67/6	0.193	6328 GeV
$N_{\mathrm{gap\ jets}}$	2.5/2	0.282	2.53/2	0.282	5
ξ_{j3}	4.2/5	0.517	4.93/5	0.424	1.74

Table 7. χ^2 and p-values obtained from the measured differential cross sections and the nominal MG5_aMC+Herwig7 prediction, computed using the covariance matrix of the measured differential cross section and the difference between data and model. The number of degrees of freedom N_{dof} is equal to the number of the cross section bins. The uncertainties in the MC prediction are ignored when computing χ^2 and p-values. The values are provided for both EW and inclusive differential $W^{\pm}W^{\pm}jj$ cross sections. The last column shows the maximum value of the respective variable observed in data.

are observed, which follow the behaviour at the reconstructed level. This is reflected in table 7 which summarises the compatibility between the nominal predicted and measured differential cross sections in the form of χ^2 and p-values. With the exception of m_{T}, the p-values for the EW $W^{\pm}W^{\pm}jj$ differential cross sections range from 0.27 to 0.61, while for the differential cross section as a function of m_{T} the p-value is only 0.043.

Differential cross sections of the inclusive $W^{\pm}W^{\pm}jj$ production as a function of $m_{\ell\ell}$, m_{T}, m_{jj}, $N_{\mathrm{gap\ jets}}$, and ξ_{j3} are shown in figure 6 and compared with SM predictions from MG5_aMC+Herwig7 and MG5_aMC+Pythia8, the sum of the predictions by Sherpa-EW and Sherpa-QCD, and the sum of predictions from Powheg Box+Pythia and Sherpa-QCD. In all cases the interference term between EW and QCD production modes is included. A similar or slightly worse level of agreement between data and SM is observed, compared with the case of EW $W^{\pm}W^{\pm}jj$ cross sections (see table 7).

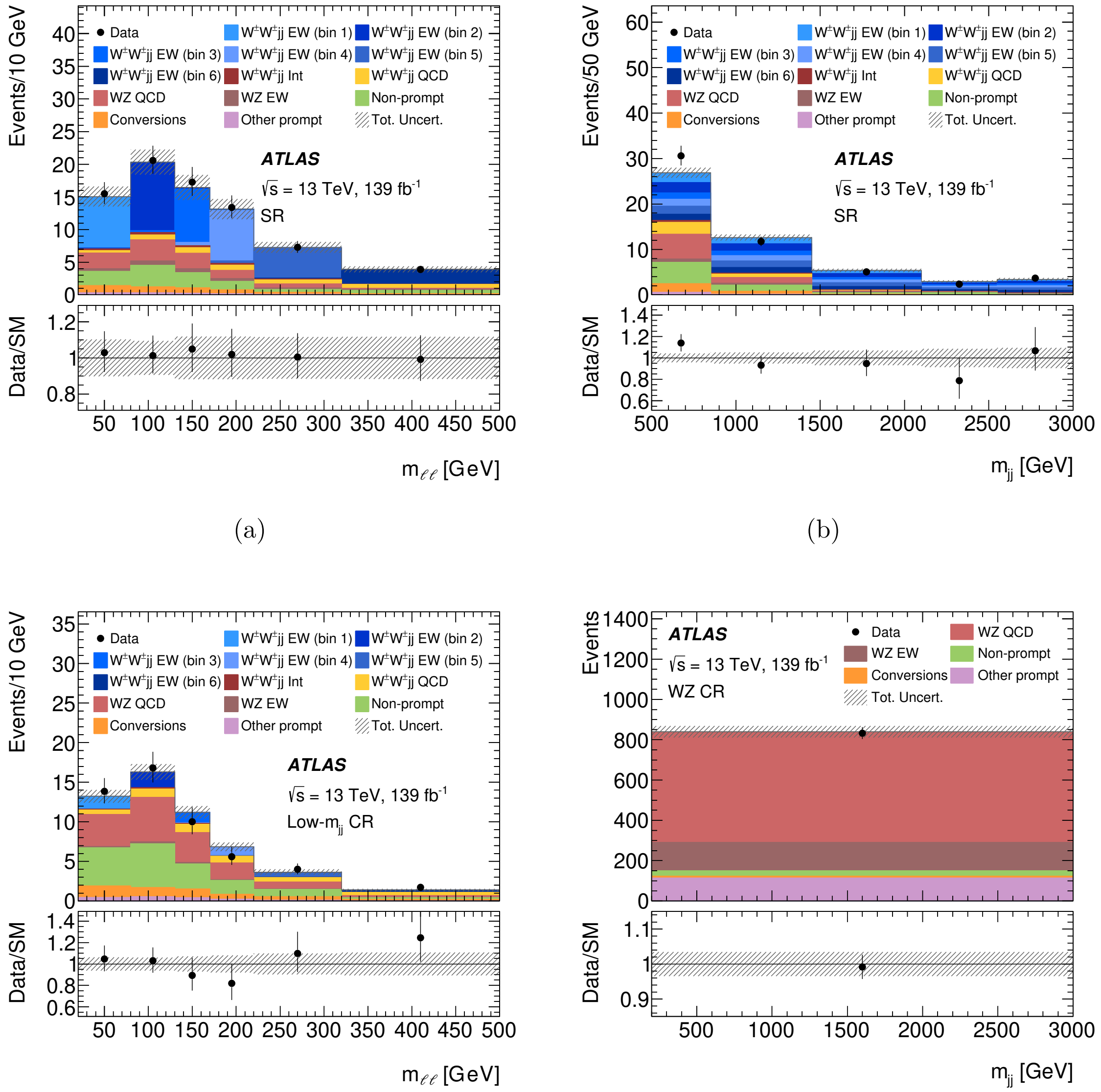

(a) (b)

(c) (d)

Figure 4. Post-fit distributions of (a) $m_{\ell\ell}$ in SR, (b) m_{jj} in SR, (c) $m_{\ell\ell}$ in low-m_{jj} CR, and (d) event yield in the WZ CR, as obtained in the extraction of the differential cross section of EW $W^{\pm}W^{\pm}jj$ production as a function of $m_{\ell\ell}$. Data are shown as black markers with vertical error bars representing the statistical uncertainty. Contributions of EW $W^{\pm}W^{\pm}jj$ events in SR and low-m_{jj} CR from different particle level $m_{\ell\ell}$ bins are presented in different shades of blue, denoted with "bin N" ($N = 1, 2, \ldots, 6$) in the legend. The last bin of each distribution includes overflow events. The hatched error band on the prediction corresponds to the total uncertainty. The lower panel of each plot shows the ratio of data to prediction.

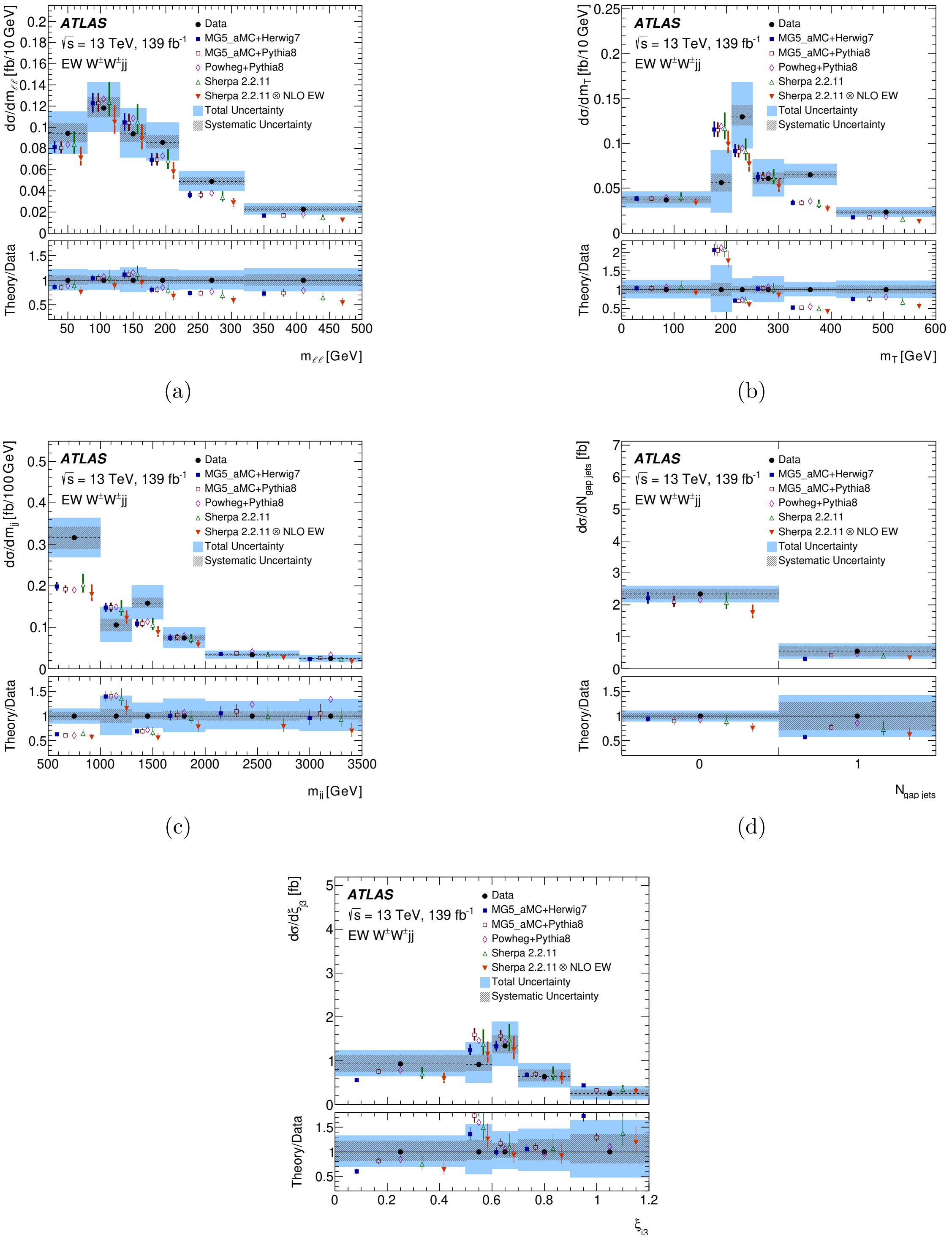

(a)

(b)

(c)

(d)

(e)

Figure 5. Fiducial differential cross sections for the EW $W^{\pm}W^{\pm}jj$ production as a function of (a) $m_{\ell\ell}$, (b) m_{T}, (c) m_{jj}, (d) $N_{\text{gap jets}}$, and (e) ξ_{j3}. The measured data are shown as black points with horizontal bars indicating the bin range and hatched (filled) boxes representing the systematic (total) uncertainty. Different SM predictions as described in the text are compared to the data. The vertical error bars shown on the predictions correspond to the uncertainty coming from the variations of the renormalisation and factorisation scales, PDF and α_{s}. Overflow events are included in the last bin. The lower panel of each plot shows the ratio of the predicted to measured cross sections.

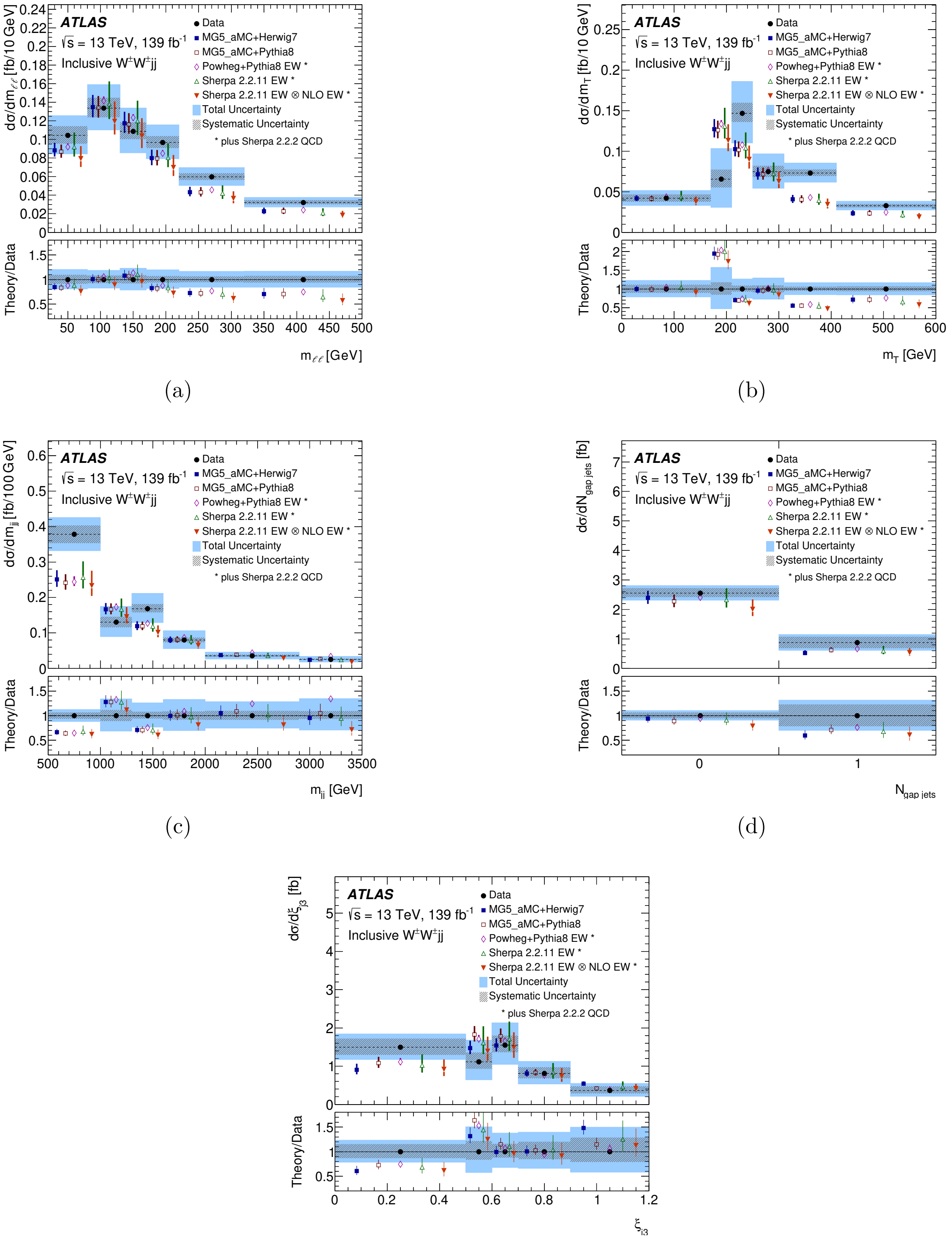

(a) (b) (c) (d) (e)

Figure 6. Measured fiducial cross sections for inclusive $W^{\pm}W^{\pm}jj$ production as a function of (a) $m_{\ell\ell}$, (b) m_{T}, (c) m_{jj}, (d) $N_{\text{gap jets}}$, and (e) ξ_{j3}. The measured data are shown as black points with horizontal bars indicating the bin range and hatched (filled) boxes representing the systematic (total) uncertainty. Different SM predictions as described in the text are compared to the data. The vertical error bars shown on the predictions correspond to the uncertainty coming from the variations of the renormalisation and factorisation scales, PDF and α_{s}. Overflow events are included in the last bin. The lower panel of each plot shows the ratio of predicted to measured cross sections.

8 Limits on anomalous quartic gauge couplings

Contributions from models beyond the SM can modify the quartic interactions of weak bosons (figure 1 (c)). The EW production of $W^{\pm}W^{\pm}jj$ in particular is sensitive to the interaction of four W bosons. This measurement can therefore be used to search for new physics that affects the $WWWW$ coupling. The sensitivity is quantified by setting limits on relevant D-8 EFT operators. The operators are expressed using a model [16, 93] that provides nine independent charge-conjugate and parity conserving D-8 effective operators relevant to the $WWWW$ quartic couplings. The interpretation uses the reconstructed dilepton invariant mass $m_{\ell\ell}$ obtained in the current measurement. The approach used is similar to that of the re-interpretation of the $W^{\pm}W^{\pm}jj$ and $W^{\pm}Zjj$ measurements based on the 36 fb^{-1} data set made by the ATLAS Collaboration [73].

The EFT Lagrangian can be written as an expansion in inverse energy where the first terms that conserve baryon and lepton numbers have coefficients quadratic in energy. As a consequence, the corresponding field operators relevant for the LHC are dimension-6 (D-6) and D-8 operators. Therefore, the effective Lagrangian can be written in terms of higher dimension operators and their respective Wilson coefficients as:

$$\mathcal{L}_{\text{eff}} = \mathcal{L}_{\text{SM}} + \sum_i \frac{f_i^{(6)}}{\Lambda^2} O_i^{(6)} + \sum_j \frac{f_j^{(8)}}{\Lambda^4} O_j^{(8)} + \ldots$$

where $O_{i,j}^{(6),(8)}$ are the D-6 and D-8 operators and involve SM fields with respective dimensionless couplings $f_i^{(6)}$ and $f_j^{(8)}$, and Λ is the energy scale of the new processes.

The basic units needed to construct the effective Lagrangian for VBS are genuine Quartic Gauge Coupling (QGC) vertices, which appear in lowest order as D-8 operators[7] and can be classified into three groups [93]: operators that contain four covariant derivatives of the Higgs field ($O_{\text{S0,1,2}}$ of scalar type); those that contain two Higgs boson covariant derivatives and two field-strength tensors ($O_{\text{M0,1,2,3,4,5,7}}$ of mixed — scalar and tensor — type); and those with four field-strength tensors ($O_{\text{T0,1,2,5,6,7,8,9}}$ of tensor type). Among these, the operators that affect $W^{\pm}W^{\pm}jj$ are $O_{\text{S0,1,2}}$, $O_{\text{M0,1,7}}$ and $O_{\text{T0,1,2}}$. Consequently, the respective coefficients that are constrained from these measurements are: $f_{\text{S02,1}}/\Lambda^4$, $f_{\text{M0,1,7}}/\Lambda^4$ and $f_{\text{T0,1,2}}/\Lambda^4$. Because the operators O_{S0} and O_{S2} are Hermitian conjugates of each other, they are varied simultaneously, with equal coefficient values $f_{\text{S0}} = f_{\text{S2}} = f_{\text{S02}}$. For simplicity, the parameters $c_i = c_i^{(8)} = f_i^{(8)}/\Lambda^4$ are used in the following.

An individual sample for every term (SM, interference, quadratic or cross, see ref. [73] for details) is generated as described in section 3.3. To generate events corresponding to a given value of the EFT coefficient c_i (or c_i and c_j for cross terms), the respective sample is multiplied by the appropriate parameter(s) (c_i, $|c_i|^2$, $c_i c_j$).

The interpretation of the data is performed using a likelihood modelled as a Poisson distribution, with systematic uncertainties implemented via Gaussian constraints. It uses the m_{ll} distribution in the SR and the low-m_{jj} CR, including also the WZ CR as previously

---

[7] D-8 operators are the lowest-dimension operators that affect QGC but do not affect triple gauge coupling vertices. The effect of D-6 operators in VBS processes and in QCD diboson production accompanied by jets is of interest on its own [94–96], but is not studied here.

defined. The SM normalisation of EW $W^{\pm}W^{\pm}jj$ is assumed, while the EFT signal strength parameter is parameterised in terms of real Wilson coefficients c_i, with a separate signal strength parameter for each c_i. A profile-likelihood ratio test statistic is constructed to estimate the confidence intervals for a given c_i. For each individual c_i (or a pair c_i, c_j for two-dimensional limits), maximum likelihood fits are performed by setting other coefficients to zero and maximising the likelihood with respect to the NPs.

Confidence intervals are derived using Wilks' theorem [97], namely, assuming that the profile likelihood test statistic is χ^2 distributed [98] (asymptotic formula). A cross-check is performed where the distribution of the profile likelihood test statistic was calculated in a set of pseudo-experiments that were generated by sampling in the neighbourhood of each scanned parameter point. This confirmed the result obtained using the asymptotic formula.

In the EFT framework, the presence of non-zero anomalous QGCs will violate tree-level unitarity at sufficiently large energy. More physical limits are obtained by removing the EFT contributions above the unitarity limit and keeping the SM predictions for all VV invariant masses, even above the unitarity limit. The unitarity limits from ref. [99] are used with only one non-zero Wilson coefficient. For two-dimensional limits the eigenvalues from ref. [99] are used to calculate unitarity bounds where only two Wilson coefficients are non-zero. In this paper, individual limits for the coefficients corresponding to the EFT operators are extracted by removing the EFT contributions that exceed a scale M_{cut}. The removal is performed using boson kinematics at parton level (i.e., before the parton shower) and applied on the invariant mass of the VV system. This clipping (unitarisation) technique is described in ref. [15].

The systematic uncertainties are listed in section 6. Theory uncertainties affecting the EFT model include the variation of μ_{R} and μ_{F} and the choice of functional form for these scales, along with PDF and α_S uncertainties. The SM EW $W^{\pm}W^{\pm}jj$ MC sample used in the EFT interpretation corresponds to around 20% lower yield in the SR, compared to the SM EW $W^{\pm}W^{\pm}jj$ MC sample used for the cross section extraction in section 7, with the difference reaching 40% in the highest-$m_{\ell\ell}$ bin. This difference stems from different choices of μ_{R} and μ_{F} for these two samples, as described in section 3.3. The difference was assigned as an uncertainty during limit setting. Systematic uncertainties weaken the derived limits by up to 10%.

Using the samples described above, limits at 95% CL for the parameters corresponding to the operators with label S02, S1, M0, M1, M7, T0, T1 and T2 are extracted, based on their impact on both EW $W^{\pm}W^{\pm}jj$ and EW $W^{\pm}Zjj$. When including the effect of the EFT operators on EW $W^{\pm}Zjj$ production, the limits typically improve by 1% to 4%.

The pre-fit $m_{\ell\ell}$ distribution overlaid with the EFT M0 operator prediction are shown in figure 7(a) for cases when no unitarisation cut-off is applied, and for an EFT unitarisation cut-off of 700 GeV. The boundaries of the last $m_{\ell\ell}$ bin are optimised to have best expected limits with no unitarisation cut-off, while other bins in the tail of the distribution are defined to improve the limits when a unitarisation cut-off is applied. Figure 7(b) shows the $m_{\ell\ell}$ distribution after the fit of the sum of SM and M0 contributions to data, in case when no EFT unitarisation cut-off is applied.

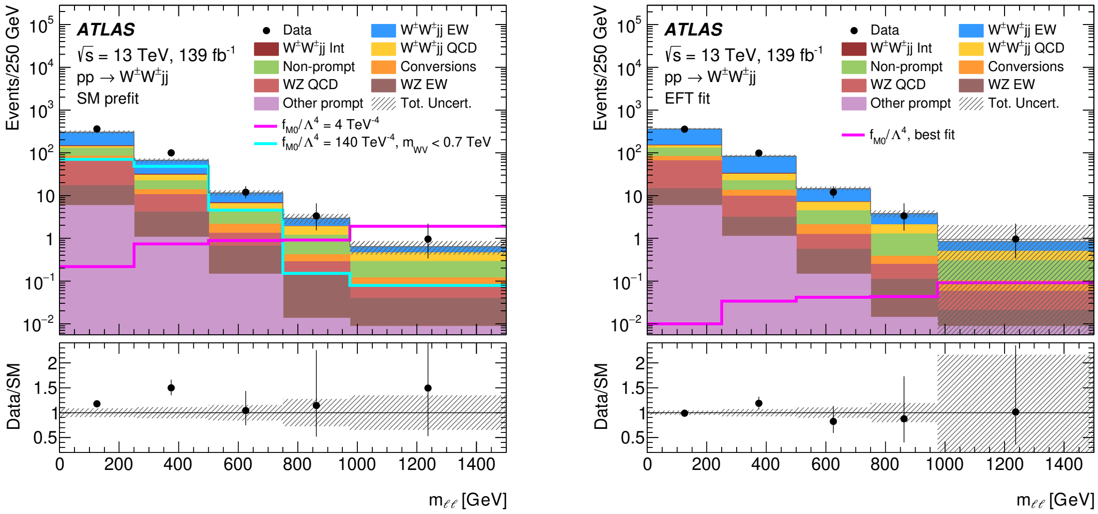

(a) (b)

Figure 7. The observed $m_{\ell\ell}$ distribution and the SM distribution before (a) and after (b) the EFT fit. Data are shown as black markers with vertical error bars representing the statistical uncertainty. Filled histograms show contributions of SM processes, with the hatched error band corresponding to the total uncertainty. In (a), the sums of $W^{\pm}W^{\pm}jj$ and $W^{\pm}Zjj$ EFT contributions that correspond to the M0 operator with its Wilson coefficient set to its observed upper limit are shown as continuous lines for two cases, one where no unitarisation cut-off is applied, and another where the EFT contributions above $m_{WV} > 0.7$ TeV are removed. In (b), the continuous line presents the best-fit contribution of the M0 operator without the unitarisation cut-off. Overflow events are included in the last bin. The lower panel shows the ratio of data to SM prediction.

Table 8 shows the expected and observed limits at 95% CL obtained without using any unitarisation procedure and with a unitarisation cut-off at the unitarity bound. The unitarity bounds for each operator as a function of the cut-off scale are defined for one non-zero Wilson coefficient following ref. [99]. Figure 8 presents the evolution of these limits as a function of the cut-off scale of the unitarisation procedure. For clipping scales below approximately 1 TeV, zero values of the coefficients f_{M0}, f_{S1}, f_{S02}, and f_{T0} are excluded at 95% CL as seen from figure 8. This is explained by the shape of the clipped EFT prediction, which exhibits a peak at $m_{\ell\ell}$ values around 400 GeV, where an upward fluctuation is also present in data, as seen in figure 7, and leads to a double-minimum shape for the test statistic. The limits obtained are competitive with those from the CMS measurement of ref. [15], which is also based on the full Run 2 data set.

The expected and observed two-dimensional limits at 95% CL on operator pairs belonging to the same group are presented in figure 9 where no unitarisation cut-off has been imposed. Figure 10 shows two-dimensional expected and observed limits at 95% CL obtained with a unitarisation cut-off scale of 1.5 TeV for all combinations of the operators studied. The predicted differential yields of nearly all operator pairs are positively correlated, except for the pairs with labels M0-M1 and M1-M7, which are anti-correlated. In the phase space studied, the predicted yields for O_{S02} and O_{S1} are nearly 100% correlated, and thus a band

Coefficient	Type	No unitarisation cut-off [TeV^{-4}]	Lower, upper limit at the respective unitarity bound [TeV^{-4}]
$f_{\mathrm{M0}}/\Lambda^4$	Exp.	[-3.9, 3.8]	-64 at 0.9 TeV, 40 at 1.0 TeV
	Obs.	[-4.1, 4.1]	-140 at 0.7 TeV, 117 at 0.8 TeV
$f_{\mathrm{M1}}/\Lambda^4$	Exp.	[-6.3, 6.6]	-25.5 at 1.6 TeV, 31 at 1.5 TeV
	Obs.	[-6.8, 7.0]	-45 at 1.4 TeV, 54 at 1.3 TeV
$f_{\mathrm{M7}}/\Lambda^4$	Exp.	[-9.3, 8.8]	-33 at 1.8 TeV, 29.1 at 1.8 TeV
	Obs.	[-9.8, 9.5]	-39 at 1.7 TeV, 42 at 1.7 TeV
$f_{\mathrm{S02}}/\Lambda^4$	Exp.	[-5.5, 5.7]	-94 at 0.8 TeV, 122 at 0.7 TeV
	Obs.	[-5.9, 5.9]	–
$f_{\mathrm{S1}}/\Lambda^4$	Exp.	[-22.0, 22.5]	–
	Obs.	[-23.5, 23.6]	–
$f_{\mathrm{T0}}/\Lambda^4$	Exp.	[-0.34, 0.34]	-3.2 at 1.2 TeV, 4.9 at 1.1 TeV
	Obs.	[-0.36, 0.36]	-7.4 at 1.0 TeV, 12.4 at 0.9 TeV
$f_{\mathrm{T1}}/\Lambda^4$	Exp.	[-0.158, 0.174]	-0.32 at 2.6 TeV, 0.44 at 2.4 TeV
	Obs.	[-0.174, 0.186]	-0.38 at 2.5 TeV, 0.49 at 2.4 TeV
$f_{\mathrm{T2}}/\Lambda^4$	Exp.	[-0.56, 0.70]	-2.60 at 1.7 TeV, 10.3 at 1.2 TeV
	Obs.	[-0.63, 0.74]	–

Table 8. Expected and observed limits on the Wilson coefficients for various operators without any unitarisation procedure and with a unitarisation cut-off at the unitarity bound. The last column represents lower and upper limits at the respective cut-off value, where the unitarity bound and experimental bound cross. Cases where no crossing with the unitarity bound was found in the scanned region above 600 GeV are labelled by "–". The notation S02 is used to indicate that the coefficients corresponding to the operators O_{S0} and O_{S2} are assigned the same value. The limits on M7 are obtained without taking into account the SM-EFT interference for the EW $W^{\pm}Zjj$ final state.

cannot be excluded. These two-dimensional limits improve upon the combined ATLAS interpretation of $W^{\pm}W^{\pm}jj$ and $W^{\pm}Zjj$ measurements based on 36 fb^{-1} data [73], except for the M1-M7 combination, which is likely explained by the missing cross-term for the $W^{\pm}Zjj$ final state in the present study.

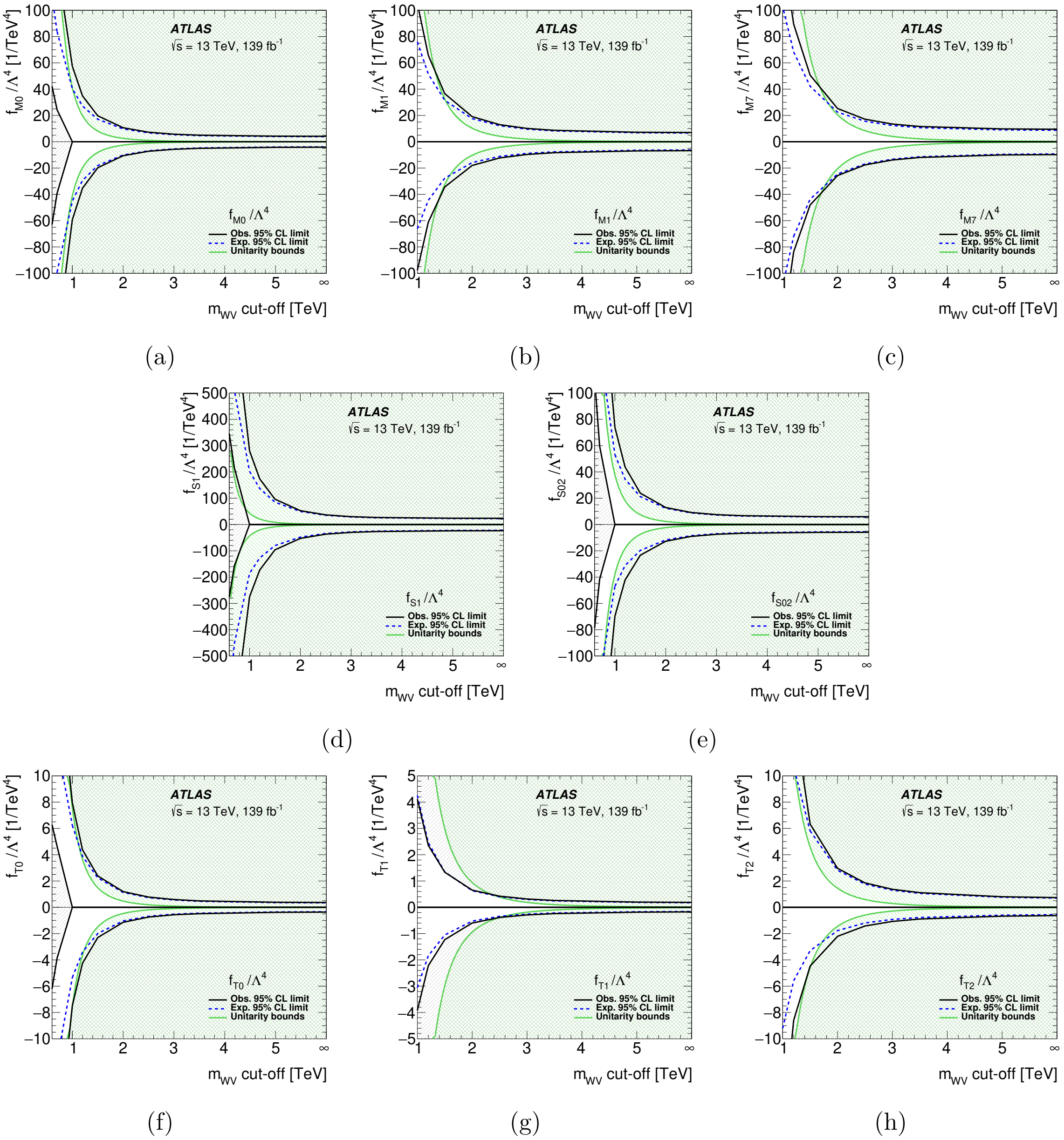

(a) (b) (c)

(d) (e)

(f) (g) (h)

Figure 8. Evolution of the one-dimensional expected (blue dashed line) and observed (black line) limits at 95% CL on the parameters corresponding to the quartic operators with label (a) M0, (b) M1, (c) M7, (d) S1, (e) S02, (f) T0, (g) T1, and (h) T2 as a function of the cut-off scale. The unitarity bounds (green line) for each operator as a function of the cut-off scale are defined for one non-zero Wilson coefficient following ref. [99]. The filled area corresponds to parameter values excluded either by the data at 95% CL or by the unitarity condition of the theory. The limits on M7 are obtained without taking into account the SM-EFT interference for the EW $W^{\pm}Zjj$ final state.

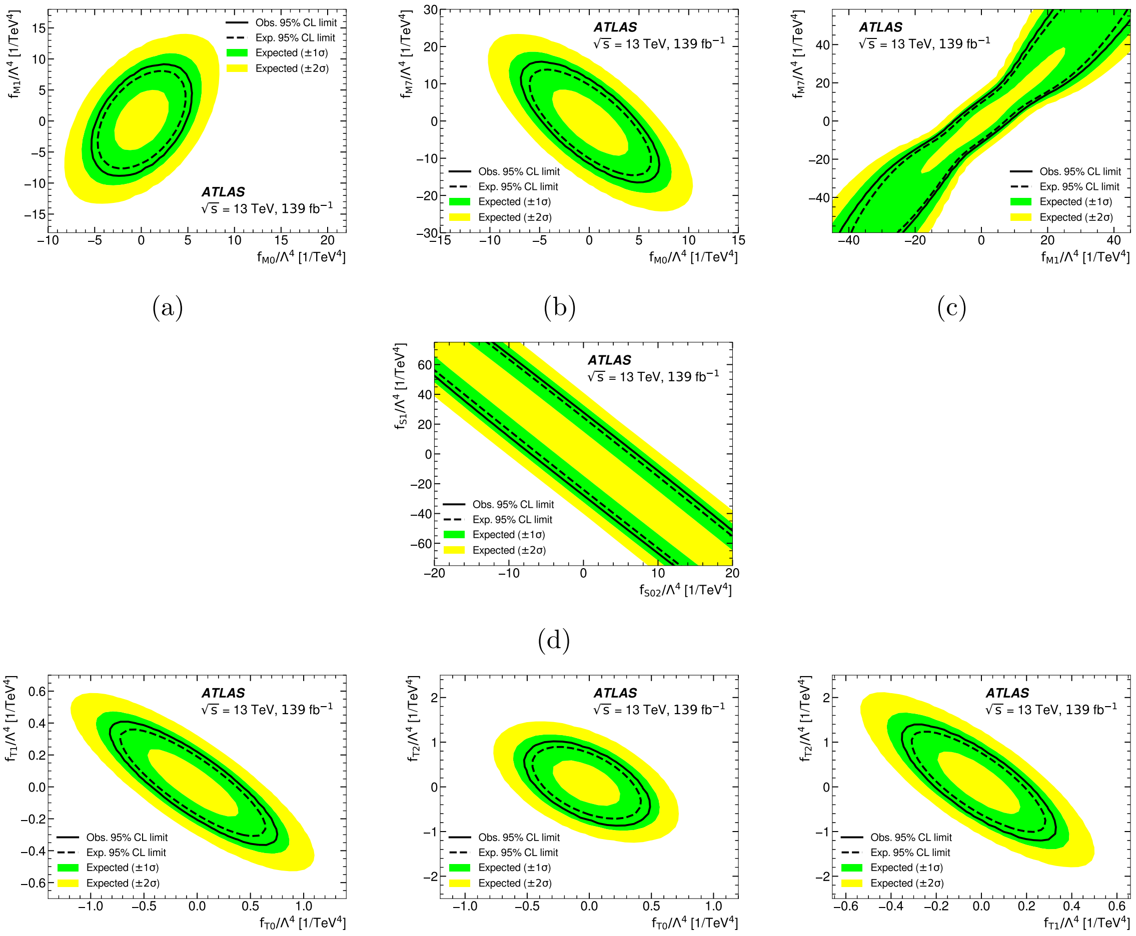

(a) (b) (c)

(d)

(e) (f) (g)

Figure 9. Two-dimensional median expected (dashed line) and observed (solid line) 95% CL intervals on parameters corresponding to the quartic operator combinations (a) M0-M1, (b) M0-M7, (c) M1-M7, (d) S1-S02, (e) T0-T1, (f) T0-T2 and (g) T1-T2 EFT parameters without any unitarisation procedure. The 1 (green) and 2 (yellow) sigma bands show the 68.3% and 95.4% CL regions for the expected limit curves, respectively. The limits on M7 are obtained without taking into account the SM-EFT interference term and EFT cross-term for the EW $W^{\pm}Zjj$ final state.

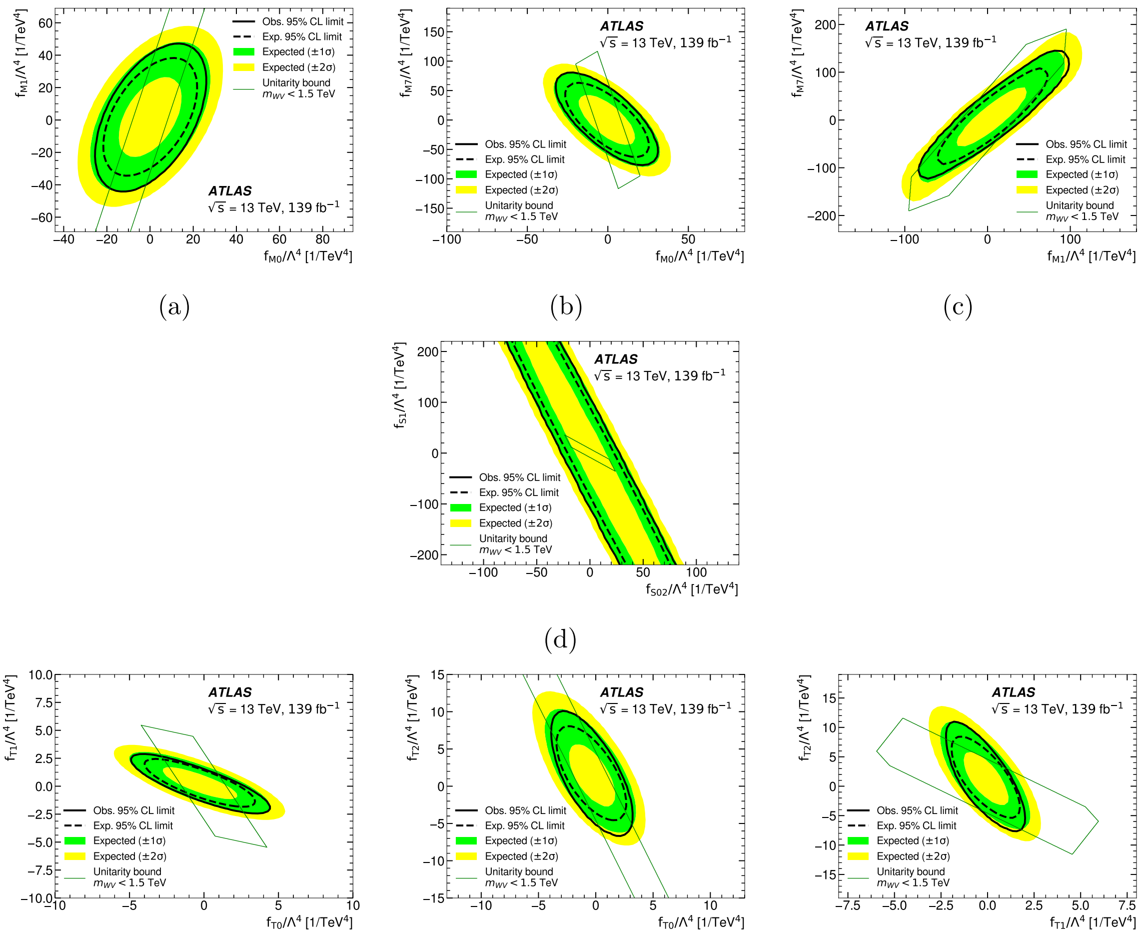

(a) (b) (c)

(d)

(e) (f) (g)

Figure 10. Two-dimensional median expected (dashed line) and observed (solid line) 95% CL intervals on parameters corresponding to the quartic operator combinations (a) M0-M1, (b) M0-M7, (c) M1-M7, (d) S1-S02, (e) T0-T1, (f) T0-T2 and (g) T1-T2 EFT parameters with a unitarisation cut-off scale of 1.5 TeV and unitarity bounds (green line). The two-dimensional unitarity bounds for pairs of operators are obtained for the two non-zero Wilson coefficients from the eigenvalues from ref. [99]. The 1 (green) and 2 (yellow) sigma bands show the 68.3% and 95.4% CL regions for the expected limit curves, respectively. The limits on M7 are obtained without taking into account the SM-EFT interference term and EFT cross-term for the EW $W^{\pm}Zjj$ final state.

9 Limits on doubly-charged Higgs boson production

In extended Higgs sectors with additional isotriplet scalar fields [100], charged Higgs bosons with couplings to W and Z bosons are present at tree level. The results from this measurement are interpreted to search for a doubly charged Higgs boson produced in VBF processes that decays into two same-sign W bosons. Specifically, the GM model [17] with both real and complex triplets is considered. The scalar potential consists of a custodial quintuplet of fermiophobic Higgs bosons ($\mathrm{H}_5^{\pm\pm}$, $\mathrm{H}_5^{\pm}$, and H_5^0) of common mass $m_{\mathrm{H}_5^{\pm\pm}}$ that couple to the W and Z bosons, and a custodial triplet of Higgs bosons ($\mathrm{H}_3^{\pm}$ and H_3^0) of common mass m_{H_3} with only fermionic couplings. In addition, there are two CP-even scalars, h and H with masses $m_\mathrm{h} \approx 125\,\mathrm{GeV}$ (identified as the SM-like Higgs boson) and m_H respectively, that are custodial singlets.

The VBF production and decays of the $\mathrm{H}_5^{\pm\pm}$ states depend on two parameters, $m_{\mathrm{H}_5^{\pm\pm}}$ and $\sin\theta_\mathrm{H}$, where $\sin\theta_\mathrm{H}$ characterises the contribution of the isotriplet scalar fields to the masses of the W and Z bosons. The `H5plane` benchmark is considered [60], where the triplet states are assumed to be heavier than the quintuplet states. Thus, in this benchmark the $\mathrm{H}_5^{\pm\pm}$ bosons decay to same-sign W boson pairs with a branching fraction of 100% [101].

The signal extraction follows an approach similar to the one presented in sections 7 and 8 to extract limits from the samples corresponding to 23 mass points between 200 GeV and 3 TeV (see section 3.4) using the transverse mass distribution m_T, which provides good discrimination between resonant signal and non-resonant background processes. The m_jj binning in the signal region is identical to the binning used in the SM fits while the m_T binning is modified to include an additional bin for the highest m_T range. The normalisations of the EW $W^\pm W^\pm jj$ and QCD $W^\pm Zjj$ background processes are freely floated in the fit. The $W^\pm W^\pm jj$ EW-QCD interference contribution is normalised to the square root of the EW $W^\pm W^\pm jj$ signal strength in the fit, similarly to the fits described in section 7.1. The $\mathrm{H}_5^{\pm\pm}$ signal contribution is proportional to $\sin^2\theta_\mathrm{H}$. In addition to the sources of systematic uncertainty described in section 6, theory uncertainties that affect the $\mathrm{H}_5^{\pm\pm}$ signal, namely variations of μ_R and μ_F, α_s, and PDFs, are considered. In addition, an uncertainty due to the missing NLO EW corrections is adopted, as recommended in ref. [101].

The post-fit inclusive distributions in the signal region for the SM background-only hypothesis are shown in figure 11 as a function of m_jj and m_T. The contributions from the $\mathrm{H}_5^{\pm\pm}$ signal simulation for the mass points at 300, 450, and 1000 GeV are shown for illustration purposes.

Upper limits at 95% CL on the product of the cross section and branching fraction $\sigma_\mathrm{VBF}(\mathrm{H}_5^{\pm\pm}) \times \mathcal{B}(\mathrm{H}_5^{\pm\pm} \to W^\pm W^\pm)$ for vector boson fusion production of doubly charged Higgs bosons as a function of mass from 200 to 3000 GeV are presented in figure 12. The corresponding limits on the $\sin\theta_\mathrm{H}$ parameter of the GM model as a function of $m_{\mathrm{H}_5^{\pm\pm}}$ are shown in figure 12. The black hatched region represents the parameter space for which the total width of the $\mathrm{H}_5^{\pm\pm}$ exceeds 10% of $m_{\mathrm{H}_5^{\pm\pm}}$, where the model is not applicable due to perturbativity and vacuum stability requirements [101]. The observed 95% CL limits exclude $\sin\theta_\mathrm{H}$ parameter values greater than 0.11–0.42 for the $m_{\mathrm{H}_5^{\pm\pm}}$ between 200 and 1500 GeV. These results show a local excess of events over the SM prediction at a resonance mass of

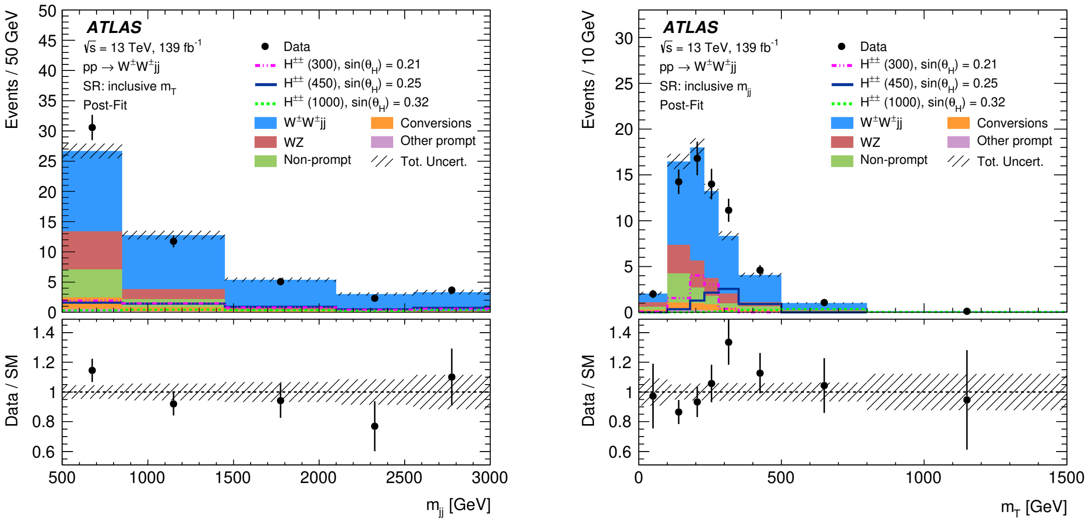

(a) (b)

Figure 11. Post-fit (a) m_{jj} and (b) m_{T} inclusive distributions in the signal region for the SM background-only hypothesis. Data are shown as black markers with vertical error bars representing the statistical uncertainty. Filled histograms show contributions of various SM processes, with the hatched band representing the total uncertainty of the model. The lines show the prediction of the $\mathrm{H}_5^{\pm\pm}$ model for values of $\sin\theta_{\mathrm{H}} = 0.21$ and $m_{\mathrm{H}_5^{\pm\pm}} = 300\,\mathrm{GeV}$, $\sin\theta_{\mathrm{H}} = 0.25$ and $m_{\mathrm{H}_5^{\pm\pm}} = 450\,\mathrm{GeV}$, and $\sin\theta_{\mathrm{H}} = 0.32$ and $m_{\mathrm{H}_5^{\pm\pm}} = 1000\,\mathrm{GeV}$, where the $\sin\theta_{\mathrm{H}}$ values correspond to the expected 95% CL limits for the respective mass points. The last bin of each distribution includes overflow events. The lower panel shows the ratio of the data to the SM prediction.

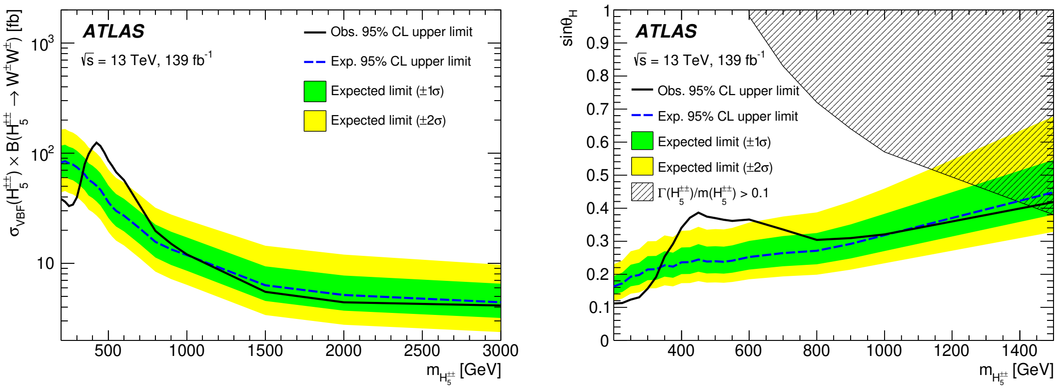

(a) (b)

Figure 12. Expected and observed exclusion limits at 95% CL for (a) $\sigma_{\mathrm{VBF}}(\mathrm{H}_5^{\pm\pm}) \times \mathcal{B}(\mathrm{H}_5^{\pm\pm} \to W^{\pm}W^{\pm})$ as a function of $m_{\mathrm{H}_5^{\pm\pm}}$, and for (b) $\sin\theta_{\mathrm{H}}$ as a function of $m_{\mathrm{H}_5^{\pm\pm}}$ in the GM model. The green (yellow) band is the 68% (95%) confidence interval around the median expected limit. The exclusion limits for $\sin\theta_{\mathrm{H}}$ are shown up to $m_{\mathrm{H}_5^{\pm\pm}} = 1500\,\mathrm{GeV}$ given the low sensitivity in the GM model above that mass. The hatched region covers the parameter space where the intrinsic width of the H++ boson would be larger than 10% of the mass and is disfavoured in the GM model [101].

around 450 GeV in figure 12(a), consistent with the results obtained in the SM part of the analysis. This excess is also observed in the m_{T} inclusive distribution shown in figure 11(b). The significance of the excess has been evaluated for the different mass points in terms of the local p-value. The excess is largest for the 450 GeV mass point, for which a p-value of 5.5×10^{-4} is obtained, corresponding to a local significance of 3.3 standard deviations. The fit of SM background plus $\mathrm{H}_5^{\pm\pm}$ signal to the data for this mass point yields the value of the normalisation factor for the EW $W^{\pm}W^{\pm}jj$ process $\mu^{\mathrm{EW}\,W^{\pm}W^{\pm}jj} = 0.79 \pm 0.15$. This value is much smaller than the one reported in section 7.3, since a better description of the m_{T} distribution in data is achieved here by compensating with a $\mathrm{H}_5^{\pm\pm}$ contribution. The excess for the 450 GeV mass point would correspond to $\sigma_{\mathrm{VBF}}(\mathrm{H}_5^{\pm\pm}) \times \mathcal{B}(\mathrm{H}_5^{\pm\pm} \to W^{\pm}W^{\pm}) = 72 \pm 25$ fb. The global significance of the excess was also evaluated [102]; it yields a global p-value of 5.4×10^{-3}, corresponding to a global significance of 2.5 standard deviations. In a similar, though less sensitive, search performed by the CMS Collaboration [103], no significant excess was observed in this mass region with respect to the SM background.

10 Conclusion

Measurements of the fiducial and differential $W^{\pm}W^{\pm}jj$ production cross sections at $\sqrt{s} = 13$ TeV using 139 fb^{-1} of data recorded by the ATLAS detector at the LHC are presented. The measured fiducial cross section of the electroweak production of $W^{\pm}W^{\pm}jj$ in the leptonic (muon and electron) decay modes is $\sigma_{\mathrm{fid}}^{\mathrm{EW}} = 2.92 \pm 0.22\,(\mathrm{stat.}) \pm 0.13\,(\mathrm{mod.\ syst.}) \pm 0.12\,(\mathrm{exp.\ syst.}) \pm 0.06\,(\mathrm{lumi.})$ fb, and for inclusive production is $\sigma_{\mathrm{fid}}^{\mathrm{EW+Int+QCD}} = 3.38 \pm 0.22\,(\mathrm{stat.}) \pm 0.11\,(\mathrm{mod.\ syst.}) \pm 0.14\,(\mathrm{exp.\ syst.}) \pm 0.06\,(\mathrm{lumi.})$ fb. These are the most precise fiducial cross section measurements of $W^{\pm}W^{\pm}jj$ production to date. The corresponding theoretical predictions obtained from MadGraph5_aMC@NLO +Herwig, $2.53 \pm 0.04\,(\mathrm{PDF})\ ^{+0.22}_{-0.19}\,(\mathrm{scale})$ fb and $2.92 \pm 0.05\,(\mathrm{PDF})\ ^{+0.34}_{-0.27}\,(\mathrm{scale})$ fb, are consistent with the measurement. Differential cross sections of the electroweak and inclusive $W^{\pm}W^{\pm}jj$ production as a function of $m_{\ell\ell}$, m_{T}, m_{jj}, $N_{\mathrm{gap\ jets}}$, and ξ_{j3} are obtained. These distributions are well described by theoretical predictions except for the m_{T} distribution, where for the electroweak (inclusive) production a p-value of 0.043 (0.012) is found, characterising the agreement between the measurement and nominal prediction from MadGraph5_aMC@NLO +Herwig.

The data are used to set upper and lower limits at 95% CL on anomalous quartic gauge couplings. The limits are set on individual EFT dimension-8 operator coefficients $f_{\mathrm{S02}}/\Lambda^4$, $f_{\mathrm{S1}}/\Lambda^4$, $f_{\mathrm{M0}}/\Lambda^4$, $f_{\mathrm{M1}}/\Lambda^4$, $f_{\mathrm{M7}}/\Lambda^4$, $f_{\mathrm{T0}}/\Lambda^4$, $f_{\mathrm{T1}}/\Lambda^4$, and $f_{\mathrm{T2}}/\Lambda^4$, where f_{S02} denotes a simultaneous variation of the operators O_{S0} and O_{S2} by the same amount. These constraints are competitive with those obtained by the CMS Collaboration using the same final state, based on the 137 fb^{-1} dataset. In addition, two-dimensional limits are set on pairs of operators.

The results are also interpreted in the context of the Georgi-Machacek model, yielding upper limits at 95% CL on the $\sin\theta_{\mathrm{H}}$ parameter as a function of $m_{\mathrm{H}_5^{\pm\pm}}$. These limits exclude $\sin\theta_{\mathrm{H}}$ parameter values greater than 0.11–0.42 for $m_{\mathrm{H}_5^{\pm\pm}}$ values from 200 to 1500 GeV. Upper limits at 95% CL on $\sigma_{\mathrm{VBF}}(\mathrm{H}_5^{\pm\pm}) \times \mathcal{B}(\mathrm{H}_5^{\pm\pm} \to W^{\pm}W^{\pm})$ are extracted for $m_{\mathrm{H}_5^{\pm\pm}}$ ranging from 200 to 3000 GeV. There is a local excess of events over the SM prediction at a resonance mass of around 450 GeV. The global significance of this excess is 2.5 standard deviations.

Acknowledgments

We thank CERN for the very successful operation of the LHC, as well as the support staff from our institutions without whom ATLAS could not be operated efficiently.

We acknowledge the support of ANPCyT, Argentina; YerPhI, Armenia; ARC, Australia; BMWFW and FWF, Austria; ANAS, Azerbaijan; CNPq and FAPESP, Brazil; NSERC, NRC and CFI, Canada; CERN; ANID, Chile; CAS, MOST and NSFC, China; Minciencias, Colombia; MEYS CR, Czech Republic; DNRF and DNSRC, Denmark; IN2P3-CNRS and CEA-DRF/IRFU, France; SRNSFG, Georgia; BMBF, HGF and MPG, Germany; GSRI, Greece; RGC and Hong Kong SAR, China; ISF and Benoziyo Center, Israel; INFN, Italy; MEXT and JSPS, Japan; CNRST, Morocco; NWO, Netherlands; RCN, Norway; MEiN, Poland; FCT, Portugal; MNE/IFA, Romania; MESTD, Serbia; MSSR, Slovakia; ARRS and MIZŠ, Slovenia; DSI/NRF, South Africa; MICINN, Spain; SRC and Wallenberg Foundation, Sweden; SERI, SNSF and Cantons of Bern and Geneva, Switzerland; MOST, Taipei; TENMAK, Türkiye; STFC, United Kingdom; DOE and NSF, United States of America. In addition, individual groups and members have received support from BCKDF, CANARIE, CRC and DRAC, Canada; PRIMUS 21/SCI/017 and UNCE SCI/013, Czech Republic; COST, ERC, ERDF, Horizon 2020, ICSC-NextGenerationEU and Marie Skłodowska-Curie Actions, European Union; Investissements d'Avenir Labex, Investissements d'Avenir Idex and ANR, France; DFG and AvH Foundation, Germany; Herakleitos, Thales and Aristeia programmes co-financed by EU-ESF and the Greek NSRF, Greece; BSF-NSF and MINERVA, Israel; Norwegian Financial Mechanism 2014-2021, Norway; NCN and NAWA, Poland; La Caixa Banking Foundation, CERCA Programme Generalitat de Catalunya and PROMETEO and GenT Programmes Generalitat Valenciana, Spain; Göran Gustafssons Stiftelse, Sweden; The Royal Society and Leverhulme Trust, United Kingdom.

The crucial computing support from all WLCG partners is acknowledged gratefully, in particular from CERN, the ATLAS Tier-1 facilities at TRIUMF/SFU (Canada), NDGF (Denmark, Norway, Sweden), CC-IN2P3 (France), KIT/GridKA (Germany), INFN-CNAF (Italy), NL-T1 (Netherlands), PIC (Spain), RAL (U.K.) and BNL (U.S.A.), the Tier-2 facilities worldwide and large non-WLCG resource providers. Major contributors of computing resources are listed in ref. [104].

References

[1] M.S. Chanowitz and M. Golden, *Like Charged Gauge Boson Pairs as a Probe of Electroweak Symmetry Breaking*, *Phys. Rev. Lett.* **61** (1988) 1053 [*Erratum ibid.* **63** (1989) 466] [INSPIRE].

[2] J. Bagger et al., *The strongly interacting W W system: Gold plated modes*, *Phys. Rev. D* **49** (1994) 1246 [`hep-ph/9306256`] [INSPIRE].

[3] J. Bagger et al., *CERN LHC analysis of the strongly interacting W W system: Gold plated modes*, *Phys. Rev. D* **52** (1995) 3878 [`hep-ph/9504426`] [INSPIRE].

[4] B.W. Lee, C. Quigg and H.B. Thacker, *Strength of Weak Interactions at Very High Energies and the Higgs Boson Mass*, *Phys. Rev. Lett.* **38** (1977) 883 [INSPIRE].

[5] B.W. Lee, C. Quigg and H.B. Thacker, *Weak Interactions at Very High-Energies: The role of the Higgs Boson Mass*, *Phys. Rev. D* **16** (1977) 1519 [INSPIRE].

[6] A. Alboteanu, W. Kilian and J. Reuter, *Resonances and unitarity in weak boson scattering at the LHC*, *JHEP* **11** (2008) 010 [`arXiv:0806.4145`] [INSPIRE].

[7] S.D. Rindani, *Strong gauge boson scattering at the LHC*, *Physics at the Large Hadron Collider* (2009) 145 [`arXiv:0910.5068`] [INSPIRE].

[8] A. Ballestrero et al., *Precise predictions for same-sign W-boson scattering at the LHC*, *Eur. Phys. J. C* **78** (2018) 671 [`arXiv:1803.07943`] [INSPIRE].

[9] M. Szleper, *The Higgs boson and the physics of WW scattering before and after Higgs discovery*, `arXiv:1412.8367` [INSPIRE].

[10] ATLAS collaboration, *Evidence for Electroweak Production of $W^{\pm}W^{\pm}jj$ in pp Collisions at $\sqrt{s} = 8$ TeV with the ATLAS Detector*, *Phys. Rev. Lett.* **113** (2014) 141803 [`arXiv:1405.6241`] [INSPIRE].

[11] ATLAS collaboration, *Measurement of $W^{\pm}W^{\pm}$ vector-boson scattering and limits on anomalous quartic gauge couplings with the ATLAS detector*, *Phys. Rev. D* **96** (2017) 012007 [`arXiv:1611.02428`] [INSPIRE].

[12] CMS collaboration, *Study of vector boson scattering and search for new physics in events with two same-sign leptons and two jets*, *Phys. Rev. Lett.* **114** (2015) 051801 [`arXiv:1410.6315`] [INSPIRE].

[13] CMS collaboration, *Observation of electroweak production of same-sign W boson pairs in the two jet and two same-sign lepton final state in proton-proton collisions at $\sqrt{s} = 13$ TeV*, *Phys. Rev. Lett.* **120** (2018) 081801 [`arXiv:1709.05822`] [INSPIRE].

[14] ATLAS collaboration, *Observation of electroweak production of a same-sign W boson pair in association with two jets in pp collisions at $\sqrt{s} = 13$ TeV with the ATLAS detector*, *Phys. Rev. Lett.* **123** (2019) 161801 [`arXiv:1906.03203`] [INSPIRE].

[15] CMS collaboration, *Measurements of production cross sections of WZ and same-sign WW boson pairs in association with two jets in proton-proton collisions at $\sqrt{s} = 13$ TeV*, *Phys. Lett. B* **809** (2020) 135710 [`arXiv:2005.01173`] [INSPIRE].

[16] O.J.P. Éboli, M.C. Gonzalez-Garcia and J.K. Mizukoshi, *$pp \to jje^{\pm}\mu^{\pm}\nu\nu$ and $jje^{\pm}\mu^{\mp}\nu\nu$ at $\mathcal{O}(\alpha_{\rm em}^6)$ and $\mathcal{O}(\alpha_{\rm em}^4\alpha_s^2)$ for the study of the quartic electroweak gauge boson vertex at CERN LHC*, *Phys. Rev. D* **74** (2006) 073005 [`hep-ph/0606118`] [INSPIRE].

[17] H. Georgi and M. Machacek, *Doubly charged Higgs bosons*, *Nucl. Phys. B* **262** (1985) 463 [INSPIRE].

[18] C. Bierlich et al., *Robust Independent Validation of Experiment and Theory: Rivet version 3*, *SciPost Phys.* **8** (2020) 026 [`arXiv:1912.05451`] [INSPIRE].

[19] E. Maguire, L. Heinrich and G. Watt, *HEPData: a repository for high energy physics data*, *J. Phys. Conf. Ser.* **898** (2017) 102006 [`arXiv:1704.05473`] [INSPIRE].

[20] ATLAS collaboration, *The ATLAS Experiment at the CERN Large Hadron Collider*, 2008 *JINST* **3** S08003 [INSPIRE].

[21] ATLAS Collaboration, *ATLAS Insertable B-Layer: Technical Design Report*, ATLAS-TDR-19, CERN-LHCC-2010-013, [Addendum: ATLAS-TDR-19-ADD-1, CERN-LHCC-2012-009].

[22] ATLAS IBL collaboration, *Production and Integration of the ATLAS Insertable B-Layer*, 2018 *JINST* **13** T05008 [`arXiv:1803.00844`] [INSPIRE].

[23] ATLAS collaboration, *Performance of the ATLAS Trigger System in 2015*, *Eur. Phys. J. C* **77** (2017) 317 [`arXiv:1611.09661`] [INSPIRE].

[24] ATLAS collaboration, *The ATLAS Collaboration Software and Firmware*, ATL-SOFT-PUB-2021-001, CERN, Geneva (2021).

[25] ATLAS collaboration, *Luminosity determination in pp collisions at* $\sqrt{s} = 13$ *TeV using the ATLAS detector at the LHC*, ATLAS-CONF-2019-021, CERN, Geneva (2019).

[26] G. Avoni et al., *The new LUCID-2 detector for luminosity measurement and monitoring in ATLAS*, 2018 *JINST* **13** P07017 [INSPIRE].

[27] ATLAS collaboration, *Performance of electron and photon triggers in ATLAS during LHC Run 2*, *Eur. Phys. J. C* **80** (2020) 47 [`arXiv:1909.00761`] [INSPIRE].

[28] ATLAS collaboration, *Performance of the ATLAS muon triggers in Run 2*, 2020 *JINST* **15** P09015 [`arXiv:2004.13447`] [INSPIRE].

[29] ATLAS collaboration, *ATLAS data quality operations and performance for 2015–2018 data-taking*, 2020 *JINST* **15** P04003 [`arXiv:1911.04632`] [INSPIRE].

[30] ATLAS collaboration, *The ATLAS Simulation Infrastructure*, *Eur. Phys. J. C* **70** (2010) 823 [`arXiv:1005.4568`] [INSPIRE].

[31] GEANT4 collaboration, *GEANT4—a simulation toolkit*, *Nucl. Instrum. Meth. A* **506** (2003) 250 [INSPIRE].

[32] T. Sjostrand, S. Mrenna and P.Z. Skands, *A Brief Introduction to PYTHIA 8.1*, *Comput. Phys. Commun.* **178** (2008) 852 [`arXiv:0710.3820`] [INSPIRE].

[33] NNPDF collaboration, R.D. Ball et al., *Parton distributions with LHC data*, *Nucl. Phys. B* **867** (2013) 244 [`arXiv:1207.1303`] [INSPIRE].

[34] ATLAS collaboration, *The Pythia 8 A3 tune description of ATLAS minimum bias and inelastic measurements incorporating the Donnachie-Landshoff diffractive model*, ATL-PHYS-PUB-2016-017, CERN, Geneva (2016).

[35] D.J. Lange, *The EvtGen particle decay simulation package*, *Nucl. Instrum. Meth. A* **462** (2001) 152 [INSPIRE].

[36] J. Alwall et al., *The automated computation of tree-level and next-to-leading order differential cross sections, and their matching to parton shower simulations*, *JHEP* **07** (2014) 079 [`arXiv:1405.0301`] [INSPIRE].

[37] M. Bähr et al., *Herwig++ Physics and Manual*, *Eur. Phys. J. C* **58** (2008) 639 [`arXiv:0803.0883`] [INSPIRE].

[38] J. Bellm et al., *Herwig 7.0/Herwig++ 3.0 release note*, *Eur. Phys. J. C* **76** (2016) 196 [`arXiv:1512.01178`] [INSPIRE].

[39] T. Sjöstrand et al., *An introduction to PYTHIA 8.2*, *Comput. Phys. Commun.* **191** (2015) 159 [`arXiv:1410.3012`] [INSPIRE].

[40] NNPDF collaboration, R.D. Ball et al., *Parton distributions for the LHC Run II*, *JHEP* **04** (2015) 040 [`arXiv:1410.8849`] [INSPIRE].

[41] S. Platzer and S. Gieseke, *Coherent Parton Showers with Local Recoils*, *JHEP* **01** (2011) 024 [`arXiv:0909.5593`] [INSPIRE].

[42] B. Cabouat and T. Sjöstrand, *Some Dipole Shower Studies*, *Eur. Phys. J. C* **78** (2018) 226 [`arXiv:1710.00391`] [INSPIRE].

[43] ATLAS collaboration, *Modelling of the vector boson scattering process $pp \to W^{\pm}W^{\pm}jj$ in Monte Carlo generators in ATLAS*, ATL-PHYS-PUB-2019-004, CERN, Geneva (2019).

[44] S. Alioli, P. Nason, C. Oleari and E. Re, *A general framework for implementing NLO calculations in shower Monte Carlo programs: the POWHEG BOX*, *JHEP* **06** (2010) 043 [`arXiv:1002.2581`] [INSPIRE].

[45] Sherpa collaboration, *Event Generation with Sherpa 2.2*, *SciPost Phys.* **7** (2019) 034 [`arXiv:1905.09127`] [INSPIRE].

[46] B. Jager and G. Zanderighi, *NLO corrections to electroweak and QCD production of W+W+ plus two jets in the POWHEGBOX*, *JHEP* **11** (2011) 055 [`arXiv:1108.0864`] [INSPIRE].

[47] ATLAS collaboration, *Measurement of the Z/γ^* boson transverse momentum distribution in pp collisions at $\sqrt{s} = 7$ TeV with the ATLAS detector*, *JHEP* **09** (2014) 145 [`arXiv:1406.3660`] [INSPIRE].

[48] J. Pumplin et al., *New generation of parton distributions with uncertainties from global QCD analysis*, *JHEP* **07** (2002) 012 [`hep-ph/0201195`] [INSPIRE].

[49] P. Golonka and Z. Was, *PHOTOS Monte Carlo: A precision tool for QED corrections in Z and W decays*, *Eur. Phys. J. C* **45** (2006) 97 [`hep-ph/0506026`] [INSPIRE].

[50] N. Davidson, T. Przedzinski and Z. Was, *PHOTOS interface in C++: Technical and Physics Documentation*, *Comput. Phys. Commun.* **199** (2016) 86 [`arXiv:1011.0937`] [INSPIRE].

[51] T. Gleisberg et al., *Event generation with SHERPA 1.1*, *JHEP* **02** (2009) 007 [`arXiv:0811.4622`] [INSPIRE].

[52] T. Gleisberg and S. Hoeche, *Comix, a new matrix element generator*, *JHEP* **12** (2008) 039 [`arXiv:0808.3674`] [INSPIRE].

[53] F. Cascioli, P. Maierhofer and S. Pozzorini, *Scattering Amplitudes with Open Loops*, *Phys. Rev. Lett.* **108** (2012) 111601 [`arXiv:1111.5206`] [INSPIRE].

[54] S. Schumann and F. Krauss, *A Parton shower algorithm based on Catani-Seymour dipole factorisation*, *JHEP* **03** (2008) 038 [`arXiv:0709.1027`] [INSPIRE].

[55] S. Höeche, F. Krauss, M. Schönherr and F. Siegert, *A critical appraisal of NLO+PS matching methods*, *JHEP* **09** (2012) 049 [`arXiv:1111.1220`] [INSPIRE].

[56] S. Höeche, F. Krauss, M. Schönherr and F. Siegert, *QCD matrix elements + parton showers: The NLO case*, *JHEP* **04** (2013) 027 [`arXiv:1207.5030`] [INSPIRE].

[57] S. Catani, F. Krauss, R. Kuhn and B.R. Webber, *QCD matrix elements + parton showers*, *JHEP* **11** (2001) 063 [`hep-ph/0109231`] [INSPIRE].

[58] S. Höeche, F. Krauss, S. Schumann and F. Siegert, *QCD matrix elements and truncated showers*, *JHEP* **05** (2009) 053 [`arXiv:0903.1219`] [INSPIRE].

[59] S. Frixione, *Isolated photons in perturbative QCD*, *Phys. Lett. B* **429** (1998) 369 [`hep-ph/9801442`] [INSPIRE].

[60] LHC Higgs Cross Section Working Group collaboration, D. de Florian et al. eds., *Handbook of LHC Higgs Cross Sections: 4. Deciphering the Nature of the Higgs Sector*, `arXiv:1610.07922` [`DOI:10.23731/CYRM-2017-002`] [INSPIRE].

[61] R. Hamberg, W.L. van Neerven and T. Matsuura, *A complete calculation of the order α_S^2 correction to the Drell-Yan K factor*, *Nucl. Phys. B* **359** (1991) 343 [*Erratum ibid.* **644** (2002) 403] [INSPIRE].

[62] R. Gavin, Y. Li, F. Petriello and S. Quackenbush, *W Physics at the LHC with FEWZ 2.1*, *Comput. Phys. Commun.* **184** (2013) 208 [`arXiv:1201.5896`] [INSPIRE].

[63] ATLAS collaboration, *ATLAS Pythia 8 tunes to 7 TeV data*, ATL-PHYS-PUB-2014-021, CERN, Geneva (2014).

[64] P. Artoisenet, R. Frederix, O. Mattelaer and R. Rietkerk, *Automatic spin-entangled decays of heavy resonances in Monte Carlo simulations*, *JHEP* **03** (2013) 015 [`arXiv:1212.3460`] [INSPIRE].

[65] M. Beneke, P. Falgari, S. Klein and C. Schwinn, *Hadronic top-quark pair production with NNLL threshold resummation*, *Nucl. Phys. B* **855** (2012) 695 [`arXiv:1109.1536`] [INSPIRE].

[66] M. Cacciari et al., *Top-pair production at hadron colliders with next-to-next-to-leading logarithmic soft-gluon resummation*, *Phys. Lett. B* **710** (2012) 612 [`arXiv:1111.5869`] [INSPIRE].

[67] P. Bärnreuther, M. Czakon and A. Mitov, *Percent Level Precision Physics at the Tevatron: First Genuine NNLO QCD Corrections to $q\bar{q} \to t\bar{t} + X$*, *Phys. Rev. Lett.* **109** (2012) 132001 [`arXiv:1204.5201`] [INSPIRE].

[68] M. Czakon and A. Mitov, *NNLO corrections to top-pair production at hadron colliders: the all-fermionic scattering channels*, *JHEP* **12** (2012) 054 [`arXiv:1207.0236`] [INSPIRE].

[69] M. Czakon and A. Mitov, *NNLO corrections to top pair production at hadron colliders: the quark-gluon reaction*, *JHEP* **01** (2013) 080 [`arXiv:1210.6832`] [INSPIRE].

[70] M. Czakon, P. Fiedler and A. Mitov, *Total Top-Quark Pair-Production Cross Section at Hadron Colliders Through $O(\alpha_S^4)$*, *Phys. Rev. Lett.* **110** (2013) 252004 [`arXiv:1303.6254`] [INSPIRE].

[71] M. Czakon and A. Mitov, *Top++: A program for the Calculation of the Top-Pair Cross-Section at Hadron Colliders*, *Comput. Phys. Commun.* **185** (2014) 2930 [`arXiv:1112.5675`] [INSPIRE].

[72] N. Kidonakis, *Theoretical results for electroweak-boson and single-top production*, *PoS* **DIS2015** (2015) 170 [`arXiv:1506.04072`] [INSPIRE].

[73] ATLAS collaboration, *Combined effective field theory interpretation of $W^\pm Zjj$ and $W^\pm W^\pm jj$ measurements using ATLAS 13 TeV data*, ATL-PHYS-PUB-2023-002, CERN, Geneva (2023).

[74] V. Hirschi and O. Mattelaer, *Automated event generation for loop-induced processes*, *JHEP* **10** (2015) 146 [`arXiv:1507.00020`] [INSPIRE].

[75] H.E. Logan and M.B. Reimer, *Characterizing a benchmark scenario for heavy Higgs boson searches in the Georgi-Machacek model*, *Phys. Rev. D* **96** (2017) 095029 [`arXiv:1709.01883`] [INSPIRE].

[76] ATLAS collaboration, *Electron and photon performance measurements with the ATLAS detector using the 2015–2017 LHC proton-proton collision data*, 2019 *JINST* **14** P12006 [`arXiv:1908.00005`] [INSPIRE].

[77] ATLAS collaboration, *Muon reconstruction and identification efficiency in ATLAS using the full Run 2 pp collision data set at $\sqrt{s} = 13$ TeV*, *Eur. Phys. J. C* **81** (2021) 578 [`arXiv:2012.00578`] [INSPIRE].

[78] M. Cacciari, G.P. Salam and G. Soyez, *The anti-k_t jet clustering algorithm*, *JHEP* **04** (2008) 063 [`arXiv:0802.1189`] [INSPIRE].

[79] ATLAS collaboration, *Jet reconstruction and performance using particle flow with the ATLAS Detector*, Eur. Phys. J. C **77** (2017) 466 [arXiv:1703.10485] [INSPIRE].

[80] ATLAS collaboration, *Performance of pile-up mitigation techniques for jets in pp collisions at $\sqrt{s} = 8$ TeV using the ATLAS detector*, Eur. Phys. J. C **76** (2016) 581 [arXiv:1510.03823] [INSPIRE].

[81] ATLAS collaboration, *Optimisation and performance studies of the ATLAS b-tagging algorithms for the 2017-18 LHC run*, ATL-PHYS-PUB-2017-013, CERN, Geneva (2017).

[82] ATLAS collaboration, *Electron reconstruction and identification in the ATLAS experiment using the 2015 and 2016 LHC proton-proton collision data at $\sqrt{s} = 13$ TeV*, Eur. Phys. J. C **79** (2019) 639 [arXiv:1902.04655] [INSPIRE].

[83] ATLAS collaboration, *Performance of missing transverse momentum reconstruction with the ATLAS detector using proton-proton collisions at $\sqrt{s} = 13$ TeV*, Eur. Phys. J. C **78** (2018) 903 [arXiv:1802.08168] [INSPIRE].

[84] ATLAS collaboration, *Measurement of the cross-section for electroweak production of dijets in association with a Z boson in pp collisions at $\sqrt{s} = 13$ TeV with the ATLAS detector*, Phys. Lett. B **775** (2017) 206 [arXiv:1709.10264] [INSPIRE].

[85] ATLAS collaboration, *Multi-Boson Simulation for 13 TeV ATLAS Analyses*, ATL-PHYS-PUB-2017-005, CERN, Geneva (2017).

[86] ATLAS collaboration, *Measurements of the inclusive and differential production cross sections of a top-quark–antiquark pair in association with a Z boson at $\sqrt{s} = 13$ TeV with the ATLAS detector*, Eur. Phys. J. C **81** (2021) 737 [arXiv:2103.12603] [INSPIRE].

[87] ATLAS collaboration, *Multi-Boson Simulation for 13 TeV ATLAS Analyses*, ATL-PHYS-PUB-2016-002, CERN, Geneva (2016).

[88] B. Biedermann, A. Denner and M. Pellen, *Complete NLO corrections to W^+W^+ scattering and its irreducible background at the LHC*, JHEP **10** (2017) 124 [arXiv:1708.00268] [INSPIRE].

[89] J. Butterworth et al., *PDF4LHC recommendations for LHC Run II*, J. Phys. G **43** (2016) 023001 [arXiv:1510.03865] [INSPIRE].

[90] ATLAS collaboration, *Search for leptonic charge asymmetry in $t\bar{t}W$ production in final states with three leptons at $\sqrt{s} = 13$ TeV*, JHEP **07** (2023) 033 [arXiv:2301.04245] [INSPIRE].

[91] ATLAS collaboration, *Observation of electroweak $W^{\pm}Z$ boson pair production in association with two jets in pp collisions at $\sqrt{s} =$ 13 TeV with the ATLAS detector*, Phys. Lett. B **793** (2019) 469 [arXiv:1812.09740] [INSPIRE].

[92] ATLAS collaboration, *Measurement of $W^{\pm}Z$ production cross sections and gauge boson polarisation in pp collisions at $\sqrt{s} = 13$ TeV with the ATLAS detector*, Eur. Phys. J. C **79** (2019) 535 [arXiv:1902.05759] [INSPIRE].

[93] O.J.P. Éboli and M.C. Gonzalez-Garcia, *Classifying the bosonic quartic couplings*, Phys. Rev. D **93** (2016) 093013 [arXiv:1604.03555] [INSPIRE].

[94] J. Kalinowski et al., *Same-sign WW scattering at the LHC: can we discover BSM effects before discovering new states?*, Eur. Phys. J. C **78** (2018) 403 [arXiv:1802.02366] [INSPIRE].

[95] A. Dedes, P. Kozów and M. Szleper, *Standard model EFT effects in vector-boson scattering at the LHC*, Phys. Rev. D **104** (2021) 013003 [arXiv:2011.07367] [INSPIRE].

[96] R. Bellan et al., *A sensitivity study of VBS and diboson WW to dimension-6 EFT operators at the LHC*, JHEP **05** (2022) 039 [arXiv:2108.03199] [INSPIRE].

[97] S.S. Wilks, *The Large-Sample Distribution of the Likelihood Ratio for Testing Composite Hypotheses*, *Annals Math. Statist.* **9** (1938) 60 [INSPIRE].

[98] G. Cowan, K. Cranmer, E. Gross and O. Vitells, *Asymptotic formulae for likelihood-based tests of new physics*, *Eur. Phys. J. C* **71** (2011) 1554 [*Erratum ibid.* **73** (2013) 2501] [`arXiv:1007.1727`] [INSPIRE].

[99] E.S. Almeida, O.J.P. Éboli and M.C. Gonzalez–Garcia, *Unitarity constraints on anomalous quartic couplings*, *Phys. Rev. D* **101** (2020) 113003 [`arXiv:2004.05174`] [INSPIRE].

[100] C. Englert, E. Re and M. Spannowsky, *Pinning down Higgs triplets at the LHC*, *Phys. Rev. D* **88** (2013) 035024 [`arXiv:1306.6228`] [INSPIRE].

[101] M. Zaro and H. Logan, *Recommendations for the interpretation of LHC searches for* H_5^0, $H_5^\pm$, *and* $H_5^{\pm\pm}$ *in vector boson fusion with decays to vector boson pairs*, LHCHXSWG-2015-001 [INSPIRE].

[102] E. Gross and O. Vitells, *Trial factors for the look elsewhere effect in high energy physics*, *Eur. Phys. J. C* **70** (2010) 525 [`arXiv:1005.1891`] [INSPIRE].

[103] CMS collaboration, *Search for charged Higgs bosons produced in vector boson fusion processes and decaying into vector boson pairs in proton–proton collisions at* $\sqrt{s} = 13$ *TeV*, *Eur. Phys. J. C* **81** (2021) 723 [`arXiv:2104.04762`] [INSPIRE].

[104] ATLAS collaboration, *ATLAS Computing Acknowledgements*, ATL-SOFT-PUB-2023-001, CERN, Geneva (2023).

The ATLAS collaboration

G. Aad[102], B. Abbott[120], K. Abeling[55], N.J. Abicht[49], S.H. Abidi[29], A. Aboulhorma[35e], H. Abramowicz[151], H. Abreu[150], Y. Abulaiti[117], A.C. Abusleme Hoffman[137a], B.S. Acharya[69a,69b,n], C. Adam Bourdarios[4], L. Adamczyk[86a], L. Adamek[155], S.V. Addepalli[26], M.J. Addison[101], J. Adelman[115], A. Adiguzel[21c], T. Adye[134], A.A. Affolder[136], Y. Afik[36], M.N. Agaras[13], J. Agarwala[73a,73b], A. Aggarwal[100], C. Agheorghiesei[27c], A. Ahmad[36], F. Ahmadov[38,z], W.S. Ahmed[104], S. Ahuja[95], X. Ai[62a], G. Aielli[76a,76b], A. Aikot[163], M. Ait Tamlihat[35e], B. Aitbenchikh[35a], I. Aizenberg[169], M. Akbiyik[100], T.P.A. Åkesson[98], A.V. Akimov[37], D. Akiyama[168], N.N. Akolkar[24], K. Al Khoury[41], G.L. Alberghi[23b], J. Albert[165], P. Albicocco[53], G.L. Albouy[60], S. Alderweireldt[52], M. Aleksa[36], I.N. Aleksandrov[38], C. Alexa[27b], T. Alexopoulos[10], F. Alfonsi[23b], M. Algren[56], M. Alhroob[120], B. Ali[132], H.M.J. Ali[91], S. Ali[148], S.W. Alibocus[92], M. Aliev[145], G. Alimonti[71a], W. Alkakhi[55], C. Allaire[66], B.M.M. Allbrooke[146], J.F. Allen[52], C.A. Allendes Flores[137f], P.P. Allport[20], A. Aloisio[72a,72b], F. Alonso[90], C. Alpigiani[138], M. Alvarez Estevez[99], A. Alvarez Fernandez[100], M. Alves Cardoso[56], M.G. Alviggi[72a,72b], M. Aly[101], Y. Amaral Coutinho[83b], A. Ambler[104], C. Amelung[36], M. Amerl[101], C.G. Ames[109], D. Amidei[106], S.P. Amor Dos Santos[130a], K.R. Amos[163], V. Ananiev[125], C. Anastopoulos[139], T. Andeen[11], J.K. Anders[36], S.Y. Andrean[47a,47b], A. Andreazza[71a,71b], S. Angelidakis[9], A. Angerami[41,ac], A.V. Anisenkov[37], A. Annovi[74a], C. Antel[56], M.T. Anthony[139], E. Antipov[145], M. Antonelli[53], F. Anulli[75a], M. Aoki[84], T. Aoki[153], J.A. Aparisi Pozo[163], M.A. Aparo[146], L. Aperio Bella[48], C. Appelt[18], A. Apyan[26], N. Aranzabal[36], C. Arcangeletti[53], A.T.H. Arce[51], E. Arena[92], J-F. Arguin[108], S. Argyropoulos[54], J.-H. Arling[48], O. Arnaez[4], H. Arnold[114], G. Artoni[75a,75b], H. Asada[111], K. Asai[118], S. Asai[153], N.A. Asbah[61], K. Assamagan[29], R. Astalos[28a], S. Atashi[160], R.J. Atkin[33a], M. Atkinson[162], H. Atmani[35f], P.A. Atmasiddha[106], K. Augsten[132], S. Auricchio[72a,72b], A.D. Auriol[20], V.A. Austrup[101], G. Avolio[36], K. Axiotis[56], G. Azuelos[108,ai], D. Babal[28b], H. Bachacou[135], K. Bachas[152,q], A. Bachiu[34], F. Backman[47a,47b], A. Badea[61], P. Bagnaia[75a,75b], M. Bahmani[18], A.J. Bailey[163], V.R. Bailey[162], J.T. Baines[134], L. Baines[94], C. Bakalis[10], O.K. Baker[172], E. Bakos[15], D. Bakshi Gupta[8], V. Balakrishnan[120], R. Balasubramanian[114], E.M. Baldin[37], P. Balek[86a], E. Ballabene[23b,23a], F. Balli[135], L.M. Baltes[63a], W.K. Balunas[32], J. Balz[100], E. Banas[87], M. Bandieramonte[129], A. Bandyopadhyay[24], S. Bansal[24], L. Barak[151], M. Barakat[48], E.L. Barberio[105], D. Barberis[57b,57a], M. Barbero[102], M.Z. Barel[114], K.N. Barends[33a], T. Barillari[110], M-S. Barisits[36], T. Barklow[143], P. Baron[122], D.A. Baron Moreno[101], A. Baroncelli[62a], G. Barone[29], A.J. Barr[126], J.D. Barr[96], L. Barranco Navarro[47a,47b], F. Barreiro[99], J. Barreiro Guimarães da Costa[14a], U. Barron[151], M.G. Barros Teixeira[130a], S. Barsov[37], F. Bartels[63a], R. Bartoldus[143], A.E. Barton[91], P. Bartos[28a], A. Basan[100], M. Baselga[49], A. Bassalat[66,b], M.J. Basso[156a], C.R. Basson[101], R.L. Bates[59], S. Batlamous[35e], J.R. Batley[32], B. Batool[141], M. Battaglia[136], D. Battulga[18], M. Bauce[75a,75b], M. Bauer[36], P. Bauer[24], L.T. Bazzano Hurrell[30], J.B. Beacham[51], T. Beau[127], P.H. Beauchemin[158], F. Becherer[54], P. Bechtle[24], H.P. Beck[19,p], K. Becker[167], C. Becot[48], A.J. Beddall[82], V.A. Bednyakov[38], C.P. Bee[145], L.J. Beemster[15], T.A. Beermann[36], M. Begalli[83d], M. Begel[29], A. Behera[145], J.K. Behr[48], J.F. Beirer[55], F. Beisiegel[24], M. Belfkir[159], G. Bella[151], L. Bellagamba[23b], A. Bellerive[34], P. Bellos[20], K. Beloborodov[37], N.L. Belyaev[37], D. Benchekroun[35a], F. Bendebba[35a], Y. Benhammou[151], M. Benoit[29], J.R. Bensinger[26], S. Bentvelsen[114], L. Beresford[48], M. Beretta[53], E. Bergeaas Kuutmann[161], N. Berger[4], B. Bergmann[132], J. Beringer[17a], G. Bernardi[5], C. Bernius[143], F.U. Bernlochner[24], F. Bernon[36,102], T. Berry[95], P. Berta[133], A. Berthold[50], I.A. Bertram[91], S. Bethke[110], A. Betti[75a,75b], A.J. Bevan[94], M. Bhamjee[33c], S. Bhatta[145], D.S. Bhattacharya[166], P. Bhattarai[143], V.S. Bhopatkar[121], R. Bi[29,ak], R.M. Bianchi[129], G. Bianco[23b,23a], O. Biebel[109], R. Bielski[123], M. Biglietti[77a], T.R.V. Billoud[132], M. Bindi[55], A. Bingul[21b], C. Bini[75a,75b], A. Biondini[92], C.J. Birch-sykes[101], G.A. Bird[20,134], M. Birman[169], M. Biros[133], S. Biryukov[146], T. Bisanz[49], E. Bisceglie[43b,43a], J.P. Biswal[134], D. Biswas[141], A. Bitadze[101], K. Bjørke[125], I. Bloch[48], C. Blocker[26], A. Blue[59], U. Blumenschein[94], J. Blumenthal[100], G.J. Bobbink[114], V.S. Bobrovnikov[37], M. Boehler[54], B. Boehm[166], D. Bogavac[36], A.G. Bogdanchikov[37], C. Bohm[47a], V. Boisvert[95], P. Bokan[48], T. Bold[86a], M. Bomben[5], M. Bona[94], M. Boonekamp[135], C.D. Booth[95], A.G. Borbély[59], I.S. Bordulev[37], H.M. Borecka-Bielska[108], L.S. Borgna[96], G. Borissov[91], D. Bortoletto[126], D. Boscherini[23b], M. Bosman[13], J.D. Bossio Sola[36], K. Bouaouda[35a], N. Bouchhar[163], J. Boudreau[129], E.V. Bouhova-Thacker[91], D. Boumediene[40], R. Bouquet[5], A. Boveia[119], J. Boyd[36], D. Boye[29], I.R. Boyko[38], J. Bracinik[20], N. Brahimi[62d], G. Brandt[171], O. Brandt[32], F. Braren[48], B. Brau[103], J.E. Brau[123], R. Brener[169], L. Brenner[114], R. Brenner[161], S. Bressler[169], D. Britton[59], D. Britzger[110], I. Brock[24], G. Brooijmans[41], W.K. Brooks[137f], E. Brost[29], L.M. Brown[165], L.E. Bruce[61], T.L. Bruckler[126], P.A. Bruckman de Renstrom[87], B. Brüers[48], A. Bruni[23b], G. Bruni[23b], M. Bruschi[23b], N. Bruscino[75a,75b], T. Buanes[16], Q. Buat[138], D. Buchin[110], A.G. Buckley[59], O. Bulekov[37], B.A. Bullard[143], S. Burdin[92], C.D. Burgard[49], A.M. Burger[40], B. Burghgrave[8], O. Burlayenko[54], J.T.P. Burr[32], C.D. Burton[11], J.C. Burzynski[142], E.L. Busch[41], V. Büscher[100], P.J. Bussey[59], J.M. Butler[25], C.M. Buttar[59], J.M. Butterworth[96], W. Buttinger[134], C.J. Buxo Vazquez[107], A.R. Buzykaev[37], S. Cabrera Urbán[163], L. Cadamuro[66], D. Caforio[58], H. Cai[129], Y. Cai[14a,14e], V.M.M. Cairo[36], O. Cakir[3a], N. Calace[36], P. Calafiura[17a], G. Calderini[127], P. Calfayan[68], G. Callea[59], L.P. Caloba[83b], D. Calvet[40], S. Calvet[40], T.P. Calvet[102], M. Calvetti[74a,74b], R. Camacho Toro[127], S. Camarda[36], D. Camarero Munoz[26], P. Camarri[76a,76b], M.T. Camerlingo[72a,72b], D. Cameron[36], C. Camincher[165], M. Campanelli[96], A. Camplani[42], V. Canale[72a,72b], A. Canesse[104], J. Cantero[163], Y. Cao[162], F. Capocasa[26], M. Capua[43b,43a], A. Carbone[71a,71b], R. Cardarelli[76a], J.C.J. Cardenas[8], F. Cardillo[163], T. Carli[36], G. Carlino[72a], J.I. Carlotto[13], B.T. Carlson[129,r], E.M. Carlson[165,156a], L. Carminati[71a,71b], A. Carnelli[135], M. Carnesale[75a,75b], S. Caron[113], E. Carquin[137f], S. Carrá[71a], G. Carratta[23b,23a], F. Carrio Argos[33g], J.W.S. Carter[155], T.M. Carter[52], M.P. Casado[13,i], M. Caspar[48], E.G. Castiglia[172], F.L. Castillo[4], L. Castillo Garcia[13], V. Castillo Gimenez[163], N.F. Castro[130a,130e], A. Catinaccio[36], J.R. Catmore[125], V. Cavaliere[29], N. Cavalli[23b,23a], V. Cavasinni[74a,74b], Y.C. Cekmecelioglu[48], E. Celebi[21a], F. Celli[126], M.S. Centonze[70a,70b],

V. Cepaitis[56], K. Cerny[122], A.S. Cerqueira[83a], A. Cerri[146], L. Cerrito[76a,76b], F. Cerutti[17a], B. Cervato[141], A. Cervelli[23b], G. Cesarini[53], S.A. Cetin[82], Z. Chadi[35a], D. Chakraborty[115], J. Chan[170], W.Y. Chan[153], J.D. Chapman[32], E. Chapon[135], B. Chargeishvili[149b], D.G. Charlton[20], T.P. Charman[94], M. Chatterjee[19], C. Chauhan[133], S. Chekanov[6], S.V. Chekulaev[156a], G.A. Chelkov[38,a], A. Chen[106], B. Chen[151], B. Chen[165], H. Chen[14c], H. Chen[29], J. Chen[62c], J. Chen[142], M. Chen[126], S. Chen[153], S.J. Chen[14c], X. Chen[62c,135], X. Chen[14b,ah], Y. Chen[62a], C.L. Cheng[170], H.C. Cheng[64a], S. Cheong[143], A. Cheplakov[38], E. Cheremushkina[48], E. Cherepanova[114], R. Cherkaoui El Moursli[35e], E. Cheu[7], K. Cheung[65], L. Chevalier[135], V. Chiarella[53], G. Chiarelli[74a], N. Chiedde[102], G. Chiodini[70a], A.S. Chisholm[20], A. Chitan[27b], M. Chitishvili[163], M.V. Chizhov[38], K. Choi[11], A.R. Chomont[75a,75b], Y. Chou[103], E.Y.S. Chow[114], T. Chowdhury[33g], K.L. Chu[169], M.C. Chu[64a], X. Chu[14a,14e], J. Chudoba[131], J.J. Chwastowski[87], D. Cieri[110], K.M. Ciesla[86a], V. Cindro[93], A. Ciocio[17a], F. Cirotto[72a,72b], Z.H. Citron[169,l], M. Citterio[71a], D.A. Ciubotaru[27b], B.M. Ciungu[155], A. Clark[56], P.J. Clark[52], J.M. Clavijo Columbie[48], S.E. Clawson[48], C. Clement[47a,47b], J. Clercx[48], Y. Coadou[102], M. Cobal[69a,69c], A. Coccaro[57b], R.F. Coelho Barrue[130a], R. Coelho Lopes De Sa[103], S. Coelli[71a], H. Cohen[151], A.E.C. Coimbra[71a,71b], B. Cole[41], J. Collot[60], P. Conde Muiño[130a,130g], M.P. Connell[33c], S.H. Connell[33c], I.A. Connelly[59], E.I. Conroy[126], F. Conventi[72a,aj], H.G. Cooke[20], A.M. Cooper-Sarkar[126], A. Cordeiro Oudot Choi[127], F. Cormier[164], L.D. Corpe[40], M. Corradi[75a,75b], F. Corriveau[104,x], A. Cortes-Gonzalez[18], M.J. Costa[163], F. Costanza[4], D. Costanzo[139], B.M. Cote[119], G. Cowan[95], K. Cranmer[170], D. Cremonini[23b,23a], S. Crépé-Renaudin[60], F. Crescioli[127], M. Cristinziani[141], M. Cristoforetti[78a,78b], V. Croft[114], J.E. Crosby[121], G. Crosetti[43b,43a], A. Cueto[99], T. Cuhadar Donszelmann[160], H. Cui[14a,14e], Z. Cui[7], W.R. Cunningham[59], F. Curcio[43b,43a], P. Czodrowski[36], M.M. Czurylo[63b], M.J. Da Cunha Sargedas De Sousa[57b,57a], J.V. Da Fonseca Pinto[83b], C. Da Via[101], W. Dabrowski[86a], T. Dado[49], S. Dahbi[33g], T. Dai[106], D. Dal Santo[19], C. Dallapiccola[103], M. Dam[42], G. D'amen[29], V. D'Amico[109], J. Damp[100], J.R. Dandoy[128], M.F. Daneri[30], M. Danninger[142], V. Dao[36], G. Darbo[57b], S. Darmora[6], S.J. Das[29,ak], S. D'Auria[71a,71b], C. David[156b], T. Davidek[133], B. Davis-Purcell[34], I. Dawson[94], H.A. Day-hall[132], K. De[8], R. De Asmundis[72a], N. De Biase[48], S. De Castro[23b,23a], N. De Groot[113], P. de Jong[114], H. De la Torre[115], A. De Maria[14c], A. De Salvo[75a], U. De Sanctis[76a,76b], A. De Santo[146], J.B. De Vivie De Regie[60], D.V. Dedovich[38], J. Degens[114], A.M. Deiana[44], F. Del Corso[23b,23a], J. Del Peso[99], F. Del Rio[63a], F. Deliot[135], C.M. Delitzsch[49], M. Della Pietra[72a,72b], D. Della Volpe[56], A. Dell'Acqua[36], L. Dell'Asta[71a,71b], M. Delmastro[4], P.A. Delsart[60], S. Demers[172], M. Demichev[38], S.P. Denisov[37], L. D'Eramo[40], D. Derendarz[87], F. Derue[127], P. Dervan[92], K. Desch[24], C. Deutsch[24], F.A. Di Bello[57b,57a], A. Di Ciaccio[76a,76b], L. Di Ciaccio[4], A. Di Domenico[75a,75b], C. Di Donato[72a,72b], A. Di Girolamo[36], G. Di Gregorio[5], A. Di Luca[78a,78b], B. Di Micco[77a,77b], R. Di Nardo[77a,77b], C. Diaconu[102], M. Diamantopoulou[34], F.A. Dias[114], T. Dias Do Vale[142], M.A. Diaz[137a,137b], F.G. Diaz Capriles[24], M. Didenko[163], E.B. Diehl[106], L. Diehl[54], S. Díez Cornell[48], C. Diez Pardos[141], C. Dimitriadi[161,24,161], A. Dimitrievska[17a], J. Dingfelder[24], I-M. Dinu[27b], S.J. Dittmeier[63b], F. Dittus[36], F. Djama[102], T. Djobava[149b], J.I. Djuvsland[16], C. Doglioni[101,98], A. Dohnalova[28a], J. Dolejsi[133], Z. Dolezal[133], K.M. Dona[39], M. Donadelli[83c], B. Dong[107], J. Donini[40], A. D'Onofrio[77a,77b], M. D'Onofrio[92], J. Dopke[134], A. Doria[72a], N. Dos Santos Fernandes[130a], P. Dougan[101], M.T. Dova[90], A.T. Doyle[59], M.A. Draguet[126], E. Dreyer[169], I. Drivas-koulouris[10], A.S. Drobac[158], M. Drozdova[56], D. Du[62a], T.A. du Pree[114], F. Dubinin[37], M. Dubovsky[28a], E. Duchovni[169], G. Duckeck[109], O.A. Ducu[27b], D. Duda[52], A. Dudarev[36], E.R. Duden[26], M. D'uffizi[101], L. Duflot[66], M. Dührssen[36], C. Dülsen[171], A.E. Dumitriu[27b], M. Dunford[63a], S. Dungs[49], K. Dunne[47a,47b], A. Duperrin[102], H. Duran Yildiz[3a], M. Düren[58], A. Durglishvili[149b], B.L. Dwyer[115], G.I. Dyckes[17a], M. Dyndal[86a], S. Dysch[101], B.S. Dziedzic[87], Z.O. Earnshaw[146], G.H. Eberwein[126], B. Eckerova[28a], S. Eggebrecht[55], E. Egidio Purcino De Souza[127], L.F. Ehrke[56], G. Eigen[16], K. Einsweiler[17a], T. Ekelof[161], P.A. Ekman[98], S. El Farkh[35b], Y. El Ghazali[35b], H. El Jarrari[35e,148], A. El Moussaouy[35a], V. Ellajosyula[161], M. Ellert[161], F. Ellinghaus[171], A.A. Elliot[94], N. Ellis[36], J. Elmsheuser[29], M. Elsing[36], D. Emeliyanov[134], Y. Enari[153], I. Ene[17a], S. Epari[13], J. Erdmann[49], P.A. Erland[87], M. Errenst[171], M. Escalier[66], C. Escobar[163], E. Etzion[151], G. Evans[130a], H. Evans[68], L.S. Evans[95], M.O. Evans[146], A. Ezhilov[37], S. Ezzarqtouni[35a], F. Fabbri[59], L. Fabbri[23b,23a], G. Facini[96], V. Fadeyev[136], R.M. Fakhrutdinov[37], S. Falciano[75a], L.F. Falda Ulhoa Coelho[36], P.J. Falke[24], J. Faltova[133], C. Fan[162], Y. Fan[14a], Y. Fang[14a,14e], M. Fanti[71a,71b], M. Faraj[69a,69b], Z. Farazpay[97], A. Farbin[8], A. Farilla[77a], T. Farooque[107], S.M. Farrington[52], F. Fassi[35e], D. Fassouliotis[9], M. Faucci Giannelli[76a,76b], W.J. Fawcett[32], L. Fayard[66], P. Federic[133], P. Federicova[131], O.L. Fedin[37,a], G. Fedotov[37], M. Feickert[170], L. Feligioni[102], D.E. Fellers[123], C. Feng[62b], M. Feng[14b], Z. Feng[114], M.J. Fenton[160], A.B. Fenyuk[37], L. Ferencz[48], R.A.M. Ferguson[91], S.I. Fernandez Luengo[137f], M.J.V. Fernoux[102], J. Ferrando[48], A. Ferrari[161], P. Ferrari[114,113], R. Ferrari[73a], D. Ferrere[56], C. Ferretti[106], F. Fiedler[100], A. Filipčič[93], E.K. Filmer[1], F. Filthaut[113], M.C.N. Fiolhais[130a,130c,c], L. Fiorini[163], W.C. Fisher[107], T. Fitschen[101], P.M. Fitzhugh[135], I. Fleck[141], P. Fleischmann[106], T. Flick[171], M. Flores[33d,ad], L.R. Flores Castillo[64a], L. Flores Sanz De Acedo[36], F.M. Follega[78a,78b], N. Fomin[16], J.H. Foo[155], B.C. Forland[68], A. Formica[135], A.C. Forti[101], E. Fortin[36], A.W. Fortman[61], M.G. Foti[17a], L. Fountas[9,j], D. Fournier[66], H. Fox[91], P. Francavilla[74a,74b], S. Francescato[61], S. Franchellucci[56], M. Franchini[23b,23a], S. Franchino[63a], D. Francis[36], L. Franco[113], L. Franconi[48], M. Franklin[61], G. Frattari[26], A.C. Freegard[94], W.S. Freund[83b], Y.Y. Frid[151], J. Friend[59], N. Fritzsche[50], A. Froch[54], D. Froidevaux[36], J.A. Frost[126], Y. Fu[62a], M. Fujimoto[118,ae], E. Fullana Torregrosa[163,*], K.Y. Fung[64a], E. Furtado De Simas Filho[83b], M. Furukawa[153], J. Fuster[163], A. Gabrielli[23b,23a], A. Gabrielli[155], P. Gadow[36], G. Gagliardi[57b,57a], L.G. Gagnon[17a], E.J. Gallas[126], B.J. Gallop[134], K.K. Gan[119], S. Ganguly[153], J. Gao[62a], Y. Gao[52], F.M. Garay Walls[137a,137b], B. Garcia[29], C. García[163], A. Garcia Alonso[114], A.G. Garcia Caffaro[172], J.E. García Navarro[163], M. Garcia-Sciveres[17a], G.L. Gardner[128], R.W. Gardner[39], N. Garelli[158], D. Garg[80], R.B. Garg[143,o], J.M. Gargan[52], C.A. Garner[155], S.J. Gasiorowski[138], P. Gaspar[83b], G. Gaudio[73a], V. Gautam[13], P. Gauzzi[75a,75b], I.L. Gavrilenko[37], A. Gavrilyuk[37], C. Gay[164], G. Gaycken[48], E.N. Gazis[10], A.A. Geanta[27b], C.M. Gee[136], C. Gemme[57b], M.H. Genest[60], S. Gentile[75a,75b], A.D. Gentry[112], S. George[95], W.F. George[20], T. Geralis[46], P. Gessinger-Befurt[36], M.E. Geyik[171], M. Ghani[167], M. Ghneimat[141], K. Ghorbanian[94], A. Ghosal[141], A. Ghosh[160], A. Ghosh[7], B. Giacobbe[23b], S. Giagu[75a,75b], T. Giani[114], P. Giannetti[74a], A. Giannini[62a], S.M. Gibson[95], M. Gignac[136], D.T. Gil[86b], A.K. Gilbert[86a], B.J. Gilbert[41], D. Gillberg[34], G. Gilles[114], N.E.K. Gillwald[48], L. Ginabat[127], D.M. Gingrich[2,ai], M.P. Giordani[69a,69c], P.F. Giraud[135], G. Giugliarelli[69a,69c], D. Giugni[71a], F. Giuli[36], I. Gkialas[9,j], L.K. Gladilin[37], C. Glasman[99], G.R. Gledhill[123], G. Glemža[48], M. Glisic[123], I. Gnesi[43b,f], Y. Go[29,ak], M. Goblirsch-Kolb[36], B. Gocke[49], D. Godin[108], B. Gokturk[21a], S. Goldfarb[105], T. Golling[56], M.G.D. Gololo[33g], D. Golubkov[37], J.P. Gombas[107], A. Gomes[130a,130b], G. Gomes Da Silva[141], A.J. Gomez Delegido[163], R. Gonçalo[130a,130c], G. Gonella[123], L. Gonella[20], A. Gongadze[149c], F. Gonnella[20], J.L. Gonski[41], R.Y. González Andana[52], S. González de la Hoz[163], S. Gonzalez Fernandez[13], R. Gonzalez Lopez[92], C. Gonzalez Renteria[17a], M.V. Gonzalez Rodrigues[48], R. Gonzalez Suarez[161], S. Gonzalez-Sevilla[56], G.R. Gonzalvo Rodriguez[163], L. Goossens[36], B. Gorini[36], E. Gorini[70a,70b], A. Gorišek[93], T.C. Gosart[128], A.T. Goshaw[51], M.I. Gostkin[38], S. Goswami[121], C.A. Gottardo[36], S.A. Gotz[109], M. Gouighri[35b], V. Goumarre[48], A.G. Goussiou[138], N. Govender[33c], I. Grabowska-Bold[86a], K. Graham[34], E. Gramstad[125], S. Grancagnolo[70a,70b], M. Grandi[146], C.M. Grant[1,135], P.M. Gravila[27f], F.G. Gravili[70a,70b], H.M. Gray[17a], M. Greco[70a,70b], C. Grefe[24], I.M. Gregor[48], P. Grenier[143], C. Grieco[13], A.A. Grillo[136], K. Grimm[31], S. Grinstein[13,t], J.-F. Grivaz[66], E. Gross[169], J. Grosse-Knetter[55], C. Grud[106], J.C. Grundy[126], L. Guan[106], W. Guan[29], C. Gubbels[164], J.G.R. Guerrero Rojas[163], G. Guerrieri[69a,69c], F. Guescini[110], R. Gugel[100], J.A.M. Guhit[106], A. Guida[18], T. Guillemin[4], E. Guilloton[167,134], S. Guindon[36], F. Guo[14a,14e], J. Guo[62c], L. Guo[48], Y. Guo[106], R. Gupta[48], S. Gurbuz[24], S.S. Gurdasani[54], G. Gustavino[36], M. Guth[56], P. Gutierrez[120], L.F. Gutierrez Zagazeta[128], C. Gutschow[96], C. Gwenlan[126], C.B. Gwilliam[92], E.S. Haaland[125], A. Haas[117], M. Habedank[48], C. Haber[17a], H.K. Hadavand[8], A. Hadef[100], S. Hadzic[110], J.J. Hahn[141], E.H. Haines[96], M. Haleem[166], J. Haley[121], J.J. Hall[139], G.D. Hallewell[102], L. Halser[19], K. Hamano[165], M. Hamer[24], G.N. Hamity[52], E.J. Hampshire[95], J. Han[62b], K. Han[62a], L. Han[14c], L. Han[62a], S. Han[17a], Y.F. Han[155], K. Hanagaki[84], M. Hance[136], D.A. Hangal[41,ac], H. Hanif[142], M.D. Hank[128], R. Hankache[101], J.B. Hansen[42], J.D. Hansen[42], P.H. Hansen[42], K. Hara[157], D. Harada[56], T. Harenberg[171], S. Harkusha[37], M.L. Harris[103], Y.T. Harris[126], J. Harrison[13], N.M. Harrison[119], P.F. Harrison[167], N.M. Hartman[110], N.M. Hartmann[109], Y. Hasegawa[140], A. Hasib[52], S. Haug[19], R. Hauser[107], C.M. Hawkes[20], R.J. Hawkings[36], Y. Hayashi[153], S. Hayashida[111], D. Hayden[107], C. Hayes[106], R.L. Hayes[114], C.P. Hays[126], J.M. Hays[94], H.S. Hayward[92], F. He[62a], M. He[14a,14e], Y. He[154], Y. He[48], N.B. Heatley[94], V. Hedberg[98], A.L. Heggelund[125], N.D. Hehir[94,*], C. Heidegger[54], K.K. Heidegger[54], W.D. Heidorn[81], J. Heilman[34], S. Heim[48], T. Heim[17a], B. Heinemann[48,af], J.G. Heinlein[128], J.J. Heinrich[123], L. Heinrich[110,ag], J. Hejbal[131], L. Helary[48], A. Held[170], S. Hellesund[16], C.M. Helling[164], S. Hellman[47a,47b], R.C.W. Henderson[91],

L. Henkelmann[32], A.M. Henriques Correia[36], H. Herde[98], Y. Hernández Jiménez[145],
L.M. Herrmann[24], T. Herrmann[50], G. Herten[54], R. Hertenberger[109], L. Hervas[36],
M.E. Hesping[100], N.P. Hessey[156a], H. Hibi[85], S.J. Hillier[20], J.R. Hinds[107],
F. Hinterkeuser[24], M. Hirose[124], S. Hirose[157], D. Hirschbuehl[171], T.G. Hitchings[101],
B. Hiti[93], J. Hobbs[145], R. Hobincu[27e], N. Hod[169], M.C. Hodgkinson[139],
B.H. Hodkinson[32], A. Hoecker[36], J. Hofer[48], T. Holm[24], M. Holzbock[110],
L.B.A.H. Hommels[32], B.P. Honan[101], J. Hong[62c], T.M. Hong[129], B.H. Hooberman[162],
W.H. Hopkins[6], Y. Horii[111], S. Hou[148], A.S. Howard[93], J. Howarth[59], J. Hoya[6],
M. Hrabovsky[122], A. Hrynevich[48], T. Hryn'ova[4], P.J. Hsu[65], S.-C. Hsu[138], Q. Hu[62a],
Y.F. Hu[14a,14e], S. Huang[64b], X. Huang[14c], Y. Huang[139], Y. Huang[14a], Z. Huang[101],
Z. Hubacek[132], M. Huebner[24], F. Huegging[24], T.B. Huffman[126], C.A. Hugli[48],
M. Huhtinen[36], S.K. Huiberts[16], R. Hulsken[104], N. Huseynov[12,a], J. Huston[107],
J. Huth[61], R. Hyneman[143], G. Iacobucci[56], G. Iakovidis[29], I. Ibragimov[141],
L. Iconomidou-Fayard[66], P. Iengo[72a,72b], R. Iguchi[153], T. Iizawa[126], Y. Ikegami[84],
N. Ilic[155], H. Imam[35a], M. Ince Lezki[56], T. Ingebretsen Carlson[47a,47b], G. Introzzi[73a,73b],
M. Iodice[77a], V. Ippolito[75a,75b], R.K. Irwin[92], M. Ishino[153], W. Islam[170], C. Issever[18,48],
S. Istin[21a,am], H. Ito[168], J.M. Iturbe Ponce[64a], R. Iuppa[78a,78b], A. Ivina[169], J.M. Izen[45],
V. Izzo[72a], P. Jacka[131,132], P. Jackson[1], R.M. Jacobs[48], B.P. Jaeger[142], C.S. Jagfeld[109],
G. Jain[156a], P. Jain[54], G. Jäkel[171], K. Jakobs[54], T. Jakoubek[169], J. Jamieson[59],
K.W. Janas[86a], M. Javurkova[103], F. Jeanneau[135], L. Jeanty[123], J. Jejelava[149a,aa],
P. Jenni[54,g], C.E. Jessiman[34], S. Jézéquel[4], C. Jia[62b], J. Jia[145], X. Jia[61], X. Jia[14a,14e],
Z. Jia[14c], Y. Jiang[62a], S. Jiggins[48], J. Jimenez Pena[13], S. Jin[14c], A. Jinaru[27b],
O. Jinnouchi[154], P. Johansson[139], K.A. Johns[7], J.W. Johnson[136], D.M. Jones[32],
E. Jones[48], P. Jones[32], R.W.L. Jones[91], T.J. Jones[92], H.L. Joos[55,36], R. Joshi[119],
J. Jovicevic[15], X. Ju[17a], J.J. Junggeburth[103], T. Junkermann[63a], A. Juste Rozas[13,t],
M.K. Juzek[87], S. Kabana[137e], A. Kaczmarska[87], M. Kado[110], H. Kagan[119], M. Kagan[143],
A. Kahn[41], A. Kahn[128], C. Kahra[100], T. Kaji[153], E. Kajomovitz[150], N. Kakati[169],
I. Kalaitzidou[54], C.W. Kalderon[29], A. Kamenshchikov[155], N.J. Kang[136], D. Kar[33g],
K. Karava[126], M.J. Kareem[156b], E. Karentzos[54], I. Karkanias[152], O. Karkout[114],
S.N. Karpov[38], Z.M. Karpova[38], V. Kartvelishvili[91], A.N. Karyukhin[37], E. Kasimi[152],
J. Katzy[48], S. Kaur[34], K. Kawade[140], M.P. Kawale[120], T. Kawamoto[135], E.F. Kay[36],
F.I. Kaya[158], S. Kazakos[107], V.F. Kazanin[37], Y. Ke[145], J.M. Keaveney[33a], R. Keeler[165],
G.V. Kehris[61], J.S. Keller[34], A.S. Kelly[96], J.J. Kempster[146], K.E. Kennedy[41],
P.D. Kennedy[100], O. Kepka[131], B.P. Kerridge[167], S. Kersten[171], B.P. Kerševan[93],
S. Keshri[66], L. Keszeghova[28a], S. Ketabchi Haghighat[155], M. Khandoga[127], A. Khanov[121],
A.G. Kharlamov[37], T. Kharlamova[37], E.E. Khoda[138], T.J. Khoo[18], G. Khoriauli[166],
J. Khubua[149b], Y.A.R. Khwaira[66], A. Kilgallon[123], D.W. Kim[47a,47b], Y.K. Kim[39],
N. Kimura[96], M.K. Kingston[55], A. Kirchhoff[55], C. Kirfel[24], F. Kirfel[24], J. Kirk[134],
A.E. Kiryunin[110], C. Kitsaki[10], O. Kivernyk[24], M. Klassen[63a], C. Klein[34], L. Klein[166],
M.H. Klein[106], M. Klein[92], S.B. Klein[56], U. Klein[92], P. Klimek[36], A. Klimentov[29],
T. Klioutchnikova[36], P. Kluit[114], S. Kluth[110], E. Kneringer[79], T.M. Knight[155],
A. Knue[49], R. Kobayashi[88], M. Kobel[50], D. Kobylianskii[169], S.F. Koch[126], M. Kocian[143],
P. Kodyš[133], D.M. Koeck[123], P.T. Koenig[24], T. Koffas[34], M. Kolb[135], I. Koletsou[4],

T. Komarek[122], K. Köneke[54], A.X.Y. Kong[1], T. Kono[118], N. Konstantinidis[96], B. Konya[98], R. Kopeliansky[68], S. Koperny[86a], K. Korcyl[87], K. Kordas[152,e], G. Koren[151], A. Korn[96], S. Korn[55], I. Korolkov[13], N. Korotkova[37], B. Kortman[114], O. Kortner[110], S. Kortner[110], W.H. Kostecka[115], V.V. Kostyukhin[141], A. Kotsokechagia[135], A. Kotwal[51], A. Koulouris[36], A. Kourkoumeli-Charalampidi[73a,73b], C. Kourkoumelis[9], E. Kourlitis[110,ag], O. Kovanda[146], R. Kowalewski[165], W. Kozanecki[135], A.S. Kozhin[37], V.A. Kramarenko[37], G. Kramberger[93], P. Kramer[100], M.W. Krasny[127], A. Krasznahorkay[36], J.W. Kraus[171], J.A. Kremer[100], T. Kresse[50], J. Kretzschmar[92], K. Kreul[18], P. Krieger[155], S. Krishnamurthy[103], M. Krivos[133], K. Krizka[20], K. Kroeninger[49], H. Kroha[110], J. Kroll[131], J. Kroll[128], K.S. Krowpman[107], U. Kruchonak[38], H. Krüger[24], N. Krumnack[81], M.C. Kruse[51], J.A. Krzysiak[87], O. Kuchinskaia[37], S. Kuday[3a], S. Kuehn[36], R. Kuesters[54], T. Kuhl[48], V. Kukhtin[38], Y. Kulchitsky[37,a], S. Kuleshov[137d,137b], M. Kumar[33g], N. Kumari[48], A. Kupco[131], T. Kupfer[49], A. Kupich[37], O. Kuprash[54], H. Kurashige[85], L.L. Kurchaninov[156a], O. Kurdysh[66], Y.A. Kurochkin[37], A. Kurova[37], M. Kuze[154], A.K. Kvam[103], J. Kvita[122], T. Kwan[104], N.G. Kyriacou[106], L.A.O. Laatu[102], C. Lacasta[163], F. Lacava[75a,75b], H. Lacker[18], D. Lacour[127], N.N. Lad[96], E. Ladygin[38], B. Laforge[127], T. Lagouri[137e], F.Z. Lahbabi[35a], S. Lai[55], I.K. Lakomiec[86a], N. Lalloue[60], J.E. Lambert[165], S. Lammers[68], W. Lampl[7], C. Lampoudis[152,e], A.N. Lancaster[115], E. Lançon[29], U. Landgraf[54], M.P.J. Landon[94], V.S. Lang[54], R.J. Langenberg[103], O.K.B. Langrekken[125], A.J. Lankford[160], F. Lanni[36], K. Lantzsch[24], A. Lanza[73a], A. Lapertosa[57b,57a], J.F. Laporte[135], T. Lari[71a], F. Lasagni Manghi[23b], M. Lassnig[36], V. Latonova[131], A. Laudrain[100], A. Laurier[150], S.D. Lawlor[95], Z. Lawrence[101], M. Lazzaroni[71a,71b], B. Le[101], E.M. Le Boulicaut[51], B. Leban[93], A. Lebedev[81], M. LeBlanc[101], F. Ledroit-Guillon[60], A.C.A. Lee[96], S.C. Lee[148], S. Lee[47a,47b], T.F. Lee[92], L.L. Leeuw[33c], H.P. Lefebvre[95], M. Lefebvre[165], C. Leggett[17a], G. Lehmann Miotto[36], M. Leigh[56], W.A. Leight[103], W. Leinonen[113], A. Leisos[152,s], M.A.L. Leite[83c], C.E. Leitgeb[48], R. Leitner[133], K.J.C. Leney[44], T. Lenz[24], S. Leone[74a], C. Leonidopoulos[52], A. Leopold[144], C. Leroy[108], R. Les[107], C.G. Lester[32], M. Levchenko[37], J. Levêque[4], D. Levin[106], L.J. Levinson[169], M.P. Lewicki[87], D.J. Lewis[4], A. Li[5], B. Li[62b], C. Li[62a], C-Q. Li[62c], H. Li[62a], H. Li[62b], H. Li[14c], H. Li[14b], H. Li[62b], K. Li[138], L. Li[62c], M. Li[14a,14e], Q.Y. Li[62a], S. Li[14a,14e], S. Li[62d,62c,d], T. Li[5], X. Li[104], Z. Li[126], Z. Li[104], Z. Li[92], Z. Li[14a,14e], S. Liang[14a,14e], Z. Liang[14a], M. Liberatore[135], B. Liberti[76a], K. Lie[64c], J. Lieber Marin[83b], H. Lien[68], K. Lin[107], R.E. Lindley[7], J.H. Lindon[2], E. Lipeles[128], A. Lipniacka[16], A. Lister[164], J.D. Little[4], B. Liu[14a], B.X. Liu[142], D. Liu[62d,62c], J.B. Liu[62a], J.K.K. Liu[32], K. Liu[62d,62c], M. Liu[62a], M.Y. Liu[62a], P. Liu[14a], Q. Liu[62d,138,62c], X. Liu[62a], Y. Liu[14d,14e], Y.L. Liu[62b], Y.W. Liu[62a], J. Llorente Merino[142], S.L. Lloyd[94], E.M. Lobodzinska[48], P. Loch[7], S. Loffredo[76a,76b], T. Lohse[18], K. Lohwasser[139], E. Loiacono[48], M. Lokajicek[131,*], J.D. Lomas[20], J.D. Long[162], I. Longarini[160], L. Longo[70a,70b], R. Longo[162], I. Lopez Paz[67], A. Lopez Solis[48], J. Lorenz[109], N. Lorenzo Martinez[4], A.M. Lory[109], G. Löschcke Centeno[146], O. Loseva[37], X. Lou[47a,47b], X. Lou[14a,14e], A. Lounis[66], J. Love[6], P.A. Love[91], G. Lu[14a,14e], M. Lu[80], S. Lu[128], Y.J. Lu[65], H.J. Lubatti[138], C. Luci[75a,75b], F.L. Lucio Alves[14c], A. Lucotte[60],

F. Luehring[68], I. Luise[145], O. Lukianchuk[66], O. Lundberg[144], B. Lund-Jensen[144], N.A. Luongo[123], M.S. Lutz[151], D. Lynn[29], H. Lyons[92], R. Lysak[131], E. Lytken[98], V. Lyubushkin[38], T. Lyubushkina[38], M.M. Lyukova[145], H. Ma[29], K. Ma[62a], L.L. Ma[62b], Y. Ma[121], D.M. Mac Donell[165], G. Maccarrone[53], J.C. MacDonald[100], P.C. Machado De Abreu Farias[83b], R. Madar[40], W.F. Mader[50], T. Madula[96], J. Maeda[85], T. Maeno[29], M. Maerker[50], H. Maguire[139], V. Maiboroda[135], A. Maio[130a,130b,130d], K. Maj[86a], O. Majersky[48], S. Majewski[123], N. Makovec[66], V. Maksimovic[15], B. Malaescu[127], Pa. Malecki[87], V.P. Maleev[37], F. Malek[60], M. Mali[93], D. Malito[95], U. Mallik[80], S. Maltezos[10], S. Malyukov[38], J. Mamuzic[13], G. Mancini[53], G. Manco[73a,73b], J.P. Mandalia[94], I. Mandić[93], L. Manhaes de Andrade Filho[83a], I.M. Maniatis[169], J. Manjarres Ramos[102,ab], D.C. Mankad[169], A. Mann[109], B. Mansoulie[135], S. Manzoni[36], A. Marantis[152,s], G. Marchiori[5], M. Marcisovsky[131], C. Marcon[71a], M. Marinescu[20], M. Marjanovic[120], E.J. Marshall[91], Z. Marshall[17a], S. Marti-Garcia[163], T.A. Martin[167], V.J. Martin[52], B. Martin dit Latour[16], L. Martinelli[75a,75b], M. Martinez[13,t], P. Martinez Agullo[163], V.I. Martinez Outschoorn[103], P. Martinez Suarez[13], S. Martin-Haugh[134], V.S. Martoiu[27b], A.C. Martyniuk[96], A. Marzin[36], D. Mascione[78a,78b], L. Masetti[100], T. Mashimo[153], J. Masik[101], A.L. Maslennikov[37], L. Massa[23b], P. Massarotti[72a,72b], P. Mastrandrea[74a,74b], A. Mastroberardino[43b,43a], T. Masubuchi[153], T. Mathisen[161], J. Matousek[133], N. Matsuzawa[153], J. Maurer[27b], B. Maček[93], D.A. Maximov[37], R. Mazini[148], I. Maznas[152], M. Mazza[107], S.M. Mazza[136], E. Mazzeo[71a,71b], C. Mc Ginn[29], J.P. Mc Gowan[104], S.P. Mc Kee[106], E.F. McDonald[105], A.E. McDougall[114], J.A. Mcfayden[146], R.P. McGovern[128], G. Mchedlidze[149b], R.P. Mckenzie[33g], T.C. Mclachlan[48], D.J. Mclaughlin[96], K.D. McLean[165], S.J. McMahon[134], P.C. McNamara[105], C.M. Mcpartland[92], R.A. McPherson[165,x], S. Mehlhase[109], A. Mehta[92], D. Melini[150], B.R. Mellado Garcia[33g], A.H. Melo[55], F. Meloni[48], A.M. Mendes Jacques Da Costa[101], H.Y. Meng[155], L. Meng[91], S. Menke[110], M. Mentink[36], E. Meoni[43b,43a], C. Merlassino[126], L. Merola[72a,72b], C. Meroni[71a,71b], G. Merz[106], O. Meshkov[37], J. Metcalfe[6], A.S. Mete[6], C. Meyer[68], J-P. Meyer[135], R.P. Middleton[134], L. Mijović[52], G. Mikenberg[169], M. Mikestikova[131], M. Mikuž[93], H. Mildner[100], A. Milic[36], C.D. Milke[44], D.W. Miller[39], L.S. Miller[34], A. Milov[169], D.A. Milstead[47a,47b], T. Min[14c], A.A. Minaenko[37], I.A. Minashvili[149b], L. Mince[59], A.I. Mincer[117], B. Mindur[86a], M. Mineev[38], Y. Mino[88], L.M. Mir[13], M. Miralles Lopez[163], M. Mironova[17a], A. Mishima[153], M.C. Missio[113], A. Mitra[167], V.A. Mitsou[163], Y. Mitsumori[111], O. Miu[155], P.S. Miyagawa[94], T. Mkrtchyan[63a], M. Mlinarevic[96], T. Mlinarevic[96], M. Mlynarikova[36], S. Mobius[19], P. Moder[48], P. Mogg[109], A.F. Mohammed[14a,14e], S. Mohapatra[41], G. Mokgatitswane[33g], L. Moleri[169], B. Mondal[141], S. Mondal[132], K. Mönig[48], E. Monnier[102], L. Monsonis Romero[163], J. Montejo Berlingen[13], M. Montella[119], F. Montereali[77a,77b], F. Monticelli[90], S. Monzani[69a,69c], N. Morange[66], A.L. Moreira De Carvalho[130a], M. Moreno Llácer[163], C. Moreno Martinez[56], P. Morettini[57b], S. Morgenstern[36], M. Morii[61], M. Morinaga[153], A.K. Morley[36], F. Morodei[75a,75b], L. Morvaj[36], P. Moschovakos[36], B. Moser[36], M. Mosidze[149b], T. Moskalets[54], P. Moskvitina[113], J. Moss[31,m], E.J.W. Moyse[103], O. Mtintsilana[33g], S. Muanza[102], J. Mueller[129], D. Muenstermann[91], R. Müller[19], G.A. Mullier[161], A.J. Mullin[32], J.J. Mullin[128], D.P. Mungo[155], D. Munoz Perez[163], F.J. Munoz Sanchez[101], M. Murin[101], W.J. Murray[167,134], A. Murrone[71a,71b], J.M. Muse[120], M. Muškinja[17a], C. Mwewa[29], A.G. Myagkov[37,a], A.J. Myers[8], A.A. Myers[129], G. Myers[68], M. Myska[132], B.P. Nachman[17a], O. Nackenhorst[49], A. Nag[50], K. Nagai[126], K. Nagano[84], J.L. Nagle[29,ak], E. Nagy[102], A.M. Nairz[36], Y. Nakahama[84], K. Nakamura[84], K. Nakkalil[5], H. Nanjo[124], R. Narayan[44], E.A. Narayanan[112], I. Naryshkin[37], M. Naseri[34], S. Nasri[159], C. Nass[24], G. Navarro[22a], J. Navarro-Gonzalez[163], R. Nayak[151], A. Nayaz[18], P.Y. Nechaeva[37], F. Nechansky[48], L. Nedic[126], T.J. Neep[20], A. Negri[73a,73b], M. Negrini[23b], C. Nellist[114], C. Nelson[104], K. Nelson[106], S. Nemecek[131], M. Nessi[36,h], M.S. Neubauer[162], F. Neuhaus[100], J. Neundorf[48], R. Newhouse[164], P.R. Newman[20], C.W. Ng[129], Y.W.Y. Ng[48], B. Ngair[35e], H.D.N. Nguyen[108], R.B. Nickerson[126], R. Nicolaidou[135], J. Nielsen[136], M. Niemeyer[55], J. Niermann[55,36], N. Nikiforou[36], V. Nikolaenko[37,a], I. Nikolic-Audit[127], K. Nikolopoulos[20], P. Nilsson[29], I. Ninca[48], H.R. Nindhito[56], G. Ninio[151], A. Nisati[75a], N. Nishu[2], R. Nisius[110], J-E. Nitschke[50], E.K. Nkadimeng[33g], T. Nobe[153], D.L. Noel[32], T. Nommensen[147], M.B. Norfolk[139], R.R.B. Norisam[96], B.J. Norman[34], J. Novak[93], T. Novak[48], L. Novotny[132], R. Novotny[112], L. Nozka[122], K. Ntekas[160], N.M.J. Nunes De Moura Junior[83b], E. Nurse[96], J. Ocariz[127], A. Ochi[85], I. Ochoa[130a], S. Oerdek[48,u], J.T. Offermann[39], A. Ogrodnik[133], A. Oh[101], C.C. Ohm[144], H. Oide[84], R. Oishi[153], M.L. Ojeda[48], M.W. O'Keefe[92], Y. Okumura[153], L.F. Oleiro Seabra[130a], S.A. Olivares Pino[137d], D. Oliveira Damazio[29], D. Oliveira Goncalves[83a], J.L. Oliver[160], A. Olszewski[87], Ö.O. Öncel[54], A.P. O'Neill[19], A. Onofre[130a,130e], P.U.E. Onyisi[11], M.J. Oreglia[39], G.E. Orellana[90], D. Orestano[77a,77b], N. Orlando[13], R.S. Orr[155], V. O'Shea[59], L.M. Osojnak[128], R. Ospanov[62a], G. Otero y Garzon[30], H. Otono[89], P.S. Ott[63a], G.J. Ottino[17a], M. Ouchrif[35d], J. Ouellette[29], F. Ould-Saada[125], M. Owen[59], R.E. Owen[134], K.Y. Oyulmaz[21a], V.E. Ozcan[21a], N. Ozturk[8], S. Ozturk[82], H.A. Pacey[126], A. Pacheco Pages[13], C. Padilla Aranda[13], G. Padovano[75a,75b], S. Pagan Griso[17a], G. Palacino[68], A. Palazzo[70a,70b], S. Palestini[36], J. Pan[172], T. Pan[64a], D.K. Panchal[11], C.E. Pandini[114], J.G. Panduro Vazquez[95], H.D. Pandya[1], H. Pang[14b], P. Pani[48], G. Panizzo[69a,69c], L. Paolozzi[56], C. Papadatos[108], S. Parajuli[44], A. Paramonov[6], C. Paraskevopoulos[10], D. Paredes Hernandez[64b], T.H. Park[155], M.A. Parker[32], F. Parodi[57b,57a], E.W. Parrish[115], V.A. Parrish[52], J.A. Parsons[41], U. Parzefall[54], B. Pascual Dias[108], L. Pascual Dominguez[151], E. Pasqualucci[75a], S. Passaggio[57b], F. Pastore[95], P. Pasuwan[47a,47b], P. Patel[87], U.M. Patel[51], J.R. Pater[101], T. Pauly[36], J. Pearkes[143], M. Pedersen[125], R. Pedro[130a], S.V. Peleganchuk[37], O. Penc[36], E.A. Pender[52], H. Peng[62a], K.E. Penski[109], M. Penzin[37], B.S. Peralva[83d], A.P. Pereira Peixoto[60], L. Pereira Sanchez[47a,47b], D.V. Perepelitsa[29,ak], E. Perez Codina[156a], M. Perganti[10], L. Perini[71a,71b,*], H. Pernegger[36], O. Perrin[40], K. Peters[48], R.F.Y. Peters[101], B.A. Petersen[36], T.C. Petersen[42], E. Petit[102], V. Petousis[132], C. Petridou[152,e], A. Petrukhin[141], M. Pettee[17a], N.E. Pettersson[36], A. Petukhov[37], K. Petukhova[133], R. Pezoa[137f], L. Pezzotti[36], G. Pezzullo[172], T.M. Pham[170], T. Pham[105], P.W. Phillips[134], G. Piacquadio[145], E. Pianori[17a], F. Piazza[71a,71b], R. Piegaia[30], D. Pietreanu[27b], A.D. Pilkington[101], M. Pinamonti[69a,69c], J.L. Pinfold[2],

JHEP04(2024)026

B.C. Pinheiro Pereira[130a], A.E. Pinto Pinoargote[100,135], L. Pintucci[69a,69c], K.M. Piper[146], A. Pirttikoski[56], D.A. Pizzi[34], L. Pizzimento[64b], A. Pizzini[114], M.-A. Pleier[29], V. Plesanovs[54], V. Pleskot[133], E. Plotnikova[38], G. Poddar[4], R. Poettgen[98], L. Poggioli[127], I. Pokharel[55], S. Polacek[133], G. Polesello[73a], A. Poley[142,156a], R. Polifka[132], A. Polini[23b], C.S. Pollard[167], Z.B. Pollock[119], V. Polychronakos[29], E. Pompa Pacchi[75a,75b], D. Ponomarenko[113], L. Pontecorvo[36], S. Popa[27a], G.A. Popeneciu[27d], A. Poreba[36], D.M. Portillo Quintero[156a], S. Pospisil[132], M.A. Postill[139], P. Postolache[27c], K. Potamianos[167], P.A. Potepa[86a], I.N. Potrap[38], C.J. Potter[32], H. Potti[1], T. Poulsen[48], J. Poveda[163], M.E. Pozo Astigarraga[36], A. Prades Ibanez[163], J. Pretel[54], D. Price[101], M. Primavera[70a], M.A. Principe Martin[99], R. Privara[122], T. Procter[59], M.L. Proffitt[138], N. Proklova[128], K. Prokofiev[64c], G. Proto[110], S. Protopopescu[29], J. Proudfoot[6], M. Przybycien[86a], W.W. Przygoda[86b], J.E. Puddefoot[139], D. Pudzha[37], D. Pyatiizbyantseva[37], J. Qian[106], D. Qichen[101], Y. Qin[101], T. Qiu[52], A. Quadt[55], M. Queitsch-Maitland[101], G. Quetant[56], R.P. Quinn[164], G. Rabanal Bolanos[61], D. Rafanoharana[54], F. Ragusa[71a,71b], J.L. Rainbolt[39], J.A. Raine[56], S. Rajagopalan[29], E. Ramakoti[37], K. Ran[48,14e], N.P. Rapheeha[33g], H. Rasheed[27b], V. Raskina[127], D.F. Rassloff[63a], S. Rave[100], B. Ravina[55], I. Ravinovich[169], M. Raymond[36], A.L. Read[125], N.P. Readioff[139], D.M. Rebuzzi[73a,73b], G. Redlinger[29], A.S. Reed[110], K. Reeves[26], J.A. Reidelsturz[171], D. Reikher[151], A. Rej[141], C. Rembser[36], A. Renardi[48], M. Renda[27b], M.B. Rendel[110], F. Renner[48], A.G. Rennie[160], A.L. Rescia[48], S. Resconi[71a], M. Ressegotti[57b,57a], S. Rettie[36], J.G. Reyes Rivera[107], E. Reynolds[17a], O.L. Rezanova[37], P. Reznicek[133], N. Ribaric[91], E. Ricci[78a,78b], R. Richter[110], S. Richter[47a,47b], E. Richter-Was[86b], M. Ridel[127], S. Ridouani[35d], P. Rieck[117], P. Riedler[36], E.M. Riefel[47a,47b], M. Rijssenbeek[145], A. Rimoldi[73a,73b], M. Rimoldi[48], L. Rinaldi[23b,23a], T.T. Rinn[29], M.P. Rinnagel[109], G. Ripellino[161], I. Riu[13], P. Rivadeneira[48], J.C. Rivera Vergara[165], F. Rizatdinova[121], E. Rizvi[94], B.A. Roberts[167], B.R. Roberts[17a], S.H. Robertson[104,x], D. Robinson[32], C.M. Robles Gajardo[137f], M. Robles Manzano[100], A. Robson[59], A. Rocchi[76a,76b], C. Roda[74a,74b], S. Rodriguez Bosca[63a], Y. Rodriguez Garcia[22a], A. Rodriguez Rodriguez[54], A.M. Rodríguez Vera[156b], S. Roe[36], J.T. Roemer[160], A.R. Roepe-Gier[136], J. Roggel[171], O. Røhne[125], R.A. Rojas[103], C.P.A. Roland[68], J. Roloff[29], A. Romaniouk[37], E. Romano[73a,73b], M. Romano[23b], A.C. Romero Hernandez[162], N. Rompotis[92], L. Roos[127], S. Rosati[75a], B.J. Rosser[39], E. Rossi[126], E. Rossi[72a,72b], L.P. Rossi[57b], L. Rossini[54], R. Rosten[119], M. Rotaru[27b], B. Rottler[54], C. Rougier[102,ab], D. Rousseau[66], D. Rousso[32], A. Roy[162], S. Roy-Garand[155], A. Rozanov[102], Y. Rozen[150], X. Ruan[33g], A. Rubio Jimenez[163], A.J. Ruby[92], V.H. Ruelas Rivera[18], T.A. Ruggeri[1], A. Ruggiero[126], A. Ruiz-Martinez[163], A. Rummler[36], Z. Rurikova[54], N.A. Rusakovich[38], H.L. Russell[165], G. Russo[75a,75b], J.P. Rutherfoord[7], S. Rutherford Colmenares[32], K. Rybacki[91], M. Rybar[133], E.B. Rye[125], A. Ryzhov[44], J.A. Sabater Iglesias[56], P. Sabatini[163], L. Sabetta[75a,75b], H.F-W. Sadrozinski[136], F. Safai Tehrani[75a], B. Safarzadeh Samani[146], M. Safdari[143], S. Saha[165], M. Sahinsoy[110], M. Saimpert[135], M. Saito[153], T. Saito[153], D. Salamani[36], A. Salnikov[143], J. Salt[163], A. Salvador Salas[13], D. Salvatore[43b,43a], F. Salvatore[146], A. Salzburger[36], D. Sammel[54], D. Sampsonidis[152,e], D. Sampsonidou[123], J. Sánchez[163],

A. Sanchez Pineda[4], V. Sanchez Sebastian[163], H. Sandaker[125], C.O. Sander[48],
J.A. Sandesara[103], M. Sandhoff[171], C. Sandoval[22b], D.P.C. Sankey[134], T. Sano[88],
A. Sansoni[53], L. Santi[75a,75b], C. Santoni[40], H. Santos[130a,130b], S.N. Santpur[17a],
A. Santra[169], K.A. Saoucha[116b], J.G. Saraiva[130a,130d], J. Sardain[7], O. Sasaki[84],
K. Sato[157], C. Sauer[63b], F. Sauerburger[54], E. Sauvan[4], P. Savard[155,ai], R. Sawada[153],
C. Sawyer[134], L. Sawyer[97], I. Sayago Galvan[163], C. Sbarra[23b], A. Sbrizzi[23b,23a],
T. Scanlon[96], J. Schaarschmidt[138], P. Schacht[110], D. Schaefer[39], U. Schäfer[100],
A.C. Schaffer[66,44], D. Schaile[109], R.D. Schamberger[145], C. Scharf[18], M.M. Schefer[19],
V.A. Schegelsky[37], D. Scheirich[133], F. Schenck[18], M. Schernau[160], C. Scheulen[55],
C. Schiavi[57b,57a], E.J. Schioppa[70a,70b], M. Schioppa[43b,43a], B. Schlag[143,o],
K.E. Schleicher[54], S. Schlenker[36], J. Schmeing[171], M.A. Schmidt[171], K. Schmieden[100],
C. Schmitt[100], S. Schmitt[48], L. Schoeffel[135], A. Schoening[63b], P.G. Scholer[54],
E. Schopf[126], M. Schott[100], J. Schovancova[36], S. Schramm[56], F. Schroeder[171],
T. Schroer[56], H-C. Schultz-Coulon[63a], M. Schumacher[54], B.A. Schumm[136], Ph. Schune[135],
A.J. Schuy[138], H.R. Schwartz[136], A. Schwartzman[143], T.A. Schwarz[106], Ph. Schwemling[135],
R. Schwienhorst[107], A. Sciandra[136], G. Sciolla[26], F. Scuri[74a], C.D. Sebastiani[92],
K. Sedlaczek[115], P. Seema[18], S.C. Seidel[112], A. Seiden[136], B.D. Seidlitz[41], C. Seitz[48],
J.M. Seixas[83b], G. Sekhniaidze[72a], S.J. Sekula[44], L. Selem[60], N. Semprini-Cesari[23b,23a],
D. Sengupta[56], V. Senthilkumar[163], L. Serin[66], L. Serkin[69a,69b], M. Sessa[76a,76b],
H. Severini[120], F. Sforza[57b,57a], A. Sfyrla[56], E. Shabalina[55], R. Shaheen[144],
J.D. Shahinian[128], D. Shaked Renous[169], L.Y. Shan[14a], M. Shapiro[17a], A. Sharma[36],
A.S. Sharma[164], P. Sharma[80], S. Sharma[48], P.B. Shatalov[37], K. Shaw[146], S.M. Shaw[101],
A. Shcherbakova[37], Q. Shen[62c,5], P. Sherwood[96], L. Shi[96], X. Shi[14a], C.O. Shimmin[172],
J.D. Shinner[95], I.P.J. Shipsey[126], S. Shirabe[56,h], M. Shiyakova[38,v], J. Shlomi[169],
M.J. Shochet[39], J. Shojaii[105], D.R. Shope[125], B. Shrestha[120], S. Shrestha[119,al],
E.M. Shrif[33g], M.J. Shroff[165], P. Sicho[131], A.M. Sickles[162], E. Sideras Haddad[33g],
A. Sidoti[23b], F. Siegert[50], Dj. Sijacki[15], R. Sikora[86a], F. Sili[90], J.M. Silva[20],
M.V. Silva Oliveira[29], S.B. Silverstein[47a], S. Simion[66], R. Simoniello[36], E.L. Simpson[59],
H. Simpson[146], L.R. Simpson[106], N.D. Simpson[98], S. Simsek[82], S. Sindhu[55], P. Sinervo[155],
S. Singh[155], S. Sinha[48], S. Sinha[101], M. Sioli[23b,23a], I. Siral[36], E. Sitnikova[48],
S.Yu. Sivoklokov[37,*], J. Sjölin[47a,47b], A. Skaf[55], E. Skorda[20], P. Skubic[120],
M. Slawinska[87], V. Smakhtin[169], B.H. Smart[134], J. Smiesko[36], S.Yu. Smirnov[37],
Y. Smirnov[37], L.N. Smirnova[37,a], O. Smirnova[98], A.C. Smith[41], E.A. Smith[39],
H.A. Smith[126], J.L. Smith[92], R. Smith[143], M. Smizanska[91], K. Smolek[132],
A.A. Snesarev[37], S.R. Snider[155], H.L. Snoek[114], S. Snyder[29], R. Sobie[165,x], A. Soffer[151],
C.A. Solans Sanchez[36], E.Yu. Soldatov[37], U. Soldevila[163], A.A. Solodkov[37], S. Solomon[26],
A. Soloshenko[38], K. Solovieva[54], O.V. Solovyanov[40], V. Solovyev[37], P. Sommer[36],
A. Sonay[13], W.Y. Song[156b], J.M. Sonneveld[114], A. Sopczak[132], A.L. Sopio[96],
F. Sopkova[28b], V. Sothilingam[63a], S. Sottocornola[68], R. Soualah[116b], Z. Soumaimi[35e],
D. South[48], N. Soybelman[169], S. Spagnolo[70a,70b], M. Spalla[110], D. Sperlich[54],
G. Spigo[36], S. Spinali[91], D.P. Spiteri[59], M. Spousta[133], E.J. Staats[34], A. Stabile[71a,71b],
R. Stamen[63a], A. Stampekis[20], M. Standke[24], E. Stanecka[87], M.V. Stange[50],
B. Stanislaus[17a], M.M. Stanitzki[48], B. Stapf[48], E.A. Starchenko[37], G.H. Stark[136],

J. Stark[102,ab], D.M. Starko[156b], P. Staroba[131], P. Starovoitov[63a], S. Stärz[104], R. Staszewski[87], G. Stavropoulos[46], J. Steentoft[161], P. Steinberg[29], B. Stelzer[142,156a], H.J. Stelzer[129], O. Stelzer-Chilton[156a], H. Stenzel[58], T.J. Stevenson[146], G.A. Stewart[36], J.R. Stewart[121], M.C. Stockton[36], G. Stoicea[27b], M. Stolarski[130a], S. Stonjek[110], A. Straessner[50], J. Strandberg[144], S. Strandberg[47a,47b], M. Stratmann[171], M. Strauss[120], T. Strebler[102], P. Strizenec[28b], R. Ströhmer[166], D.M. Strom[123], L.R. Strom[48], R. Stroynowski[44], A. Strubig[47a,47b], S.A. Stucci[29], B. Stugu[16], J. Stupak[120], N.A. Styles[48], D. Su[143], S. Su[62a], W. Su[62d], X. Su[62a,66], K. Sugizaki[153], V.V. Sulin[37], M.J. Sullivan[92], D.M.S. Sultan[78a,78b], L. Sultanaliyeva[37], S. Sultansoy[3b], T. Sumida[88], S. Sun[106], S. Sun[170], O. Sunneborn Gudnadottir[161], N. Sur[102], M.R. Sutton[146], H. Suzuki[157], M. Svatos[131], M. Swiatlowski[156a], T. Swirski[166], I. Sykora[28a], M. Sykora[133], T. Sykora[133], D. Ta[100], K. Tackmann[48,u], A. Taffard[160], R. Tafirout[156a], J.S. Tafoya Vargas[66], E.P. Takeva[52], Y. Takubo[84], M. Talby[102], A.A. Talyshev[37], K.C. Tam[64b], N.M. Tamir[151], A. Tanaka[153], J. Tanaka[153], R. Tanaka[66], M. Tanasini[57b,57a], Z. Tao[164], S. Tapia Araya[137f], S. Tapprogge[100], A. Tarek Abouelfadl Mohamed[107], S. Tarem[150], K. Tariq[14a], G. Tarna[102,27b], G.F. Tartarelli[71a], P. Tas[133], M. Tasevsky[131], E. Tassi[43b,43a], A.C. Tate[162], G. Tateno[153], Y. Tayalati[35e,w], G.N. Taylor[105], W. Taylor[156b], H. Teagle[92], A.S. Tee[170], R. Teixeira De Lima[143], P. Teixeira-Dias[95], J.J. Teoh[155], K. Terashi[153], J. Terron[99], S. Terzo[13], M. Testa[53], R.J. Teuscher[155,x], A. Thaler[79], O. Theiner[56], N. Themistokleous[52], T. Theveneaux-Pelzer[102], O. Thielmann[171], D.W. Thomas[95], J.P. Thomas[20], E.A. Thompson[17a], P.D. Thompson[20], E. Thomson[128], Y. Tian[55], V. Tikhomirov[37,a], Yu.A. Tikhonov[37], S. Timoshenko[37], D. Timoshyn[133], E.X.L. Ting[1], P. Tipton[172], S.H. Tlou[33g], A. Tnourji[40], K. Todome[154], S. Todorova-Nova[133], S. Todt[50], M. Togawa[84], J. Tojo[89], S. Tokár[28a], K. Tokushuku[84], O. Toldaiev[68], R. Tombs[32], M. Tomoto[84,111], L. Tompkins[143,o], K.W. Topolnicki[86b], E. Torrence[123], H. Torres[102,ab], E. Torró Pastor[163], M. Toscani[30], C. Tosciri[39], M. Tost[11], D.R. Tovey[139], A. Traeet[16], I.S. Trandafir[27b], T. Trefzger[166], A. Tricoli[29], I.M. Trigger[156a], S. Trincaz-Duvoid[127], D.A. Trischuk[26], B. Trocmé[60], C. Troncon[71a], L. Truong[33c], M. Trzebinski[87], A. Trzupek[87], F. Tsai[145], M. Tsai[106], A. Tsiamis[152,e], P.V. Tsiareshka[37], S. Tsigaridas[156a], A. Tsirigotis[152,s], V. Tsiskaridze[155], E.G. Tskhadadze[149a], M. Tsopoulou[152,e], Y. Tsujikawa[88], I.I. Tsukerman[37], V. Tsulaia[17a], S. Tsuno[84], O. Tsur[150], K. Tsuri[118], D. Tsybychev[145], Y. Tu[64b], A. Tudorache[27b], V. Tudorache[27b], A.N. Tuna[36], S. Turchikhin[57b,57a], I. Turk Cakir[3a], R. Turra[71a], T. Turtuvshin[38,y], P.M. Tuts[41], S. Tzamarias[152,e], P. Tzanis[10], E. Tzovara[100], F. Ukegawa[157], P.A. Ulloa Poblete[137c,137b], E.N. Umaka[29], G. Unal[36], M. Unal[11], A. Undrus[29], G. Unel[160], J. Urban[28b], P. Urquijo[105], G. Usai[8], R. Ushioda[154], M. Usman[108], Z. Uysal[21b], L. Vacavant[102], V. Vacek[132], B. Vachon[104], K.O.H. Vadla[125], T. Vafeiadis[36], A. Vaitkus[96], C. Valderanis[109], E. Valdes Santurio[47a,47b], M. Valente[156a], S. Valentinetti[23b,23a], A. Valero[163], E. Valiente Moreno[163], A. Vallier[102,ab], J.A. Valls Ferrer[163], D.R. Van Arneman[114], T.R. Van Daalen[138], A. Van Der Graaf[49], P. Van Gemmeren[6], M. Van Rijnbach[125,36], S. Van Stroud[96], I. Van Vulpen[114], M. Vanadia[76a,76b], W. Vandelli[36], M. Vandenbroucke[135], E.R. Vandewall[121], D. Vannicola[151],

L. Vannoli[57b,57a], R. Vari[75a], E.W. Varnes[7], C. Varni[17b], T. Varol[148], D. Varouchas[66], L. Varriale[163], K.E. Varvell[147], M.E. Vasile[27b], L. Vaslin[40], G.A. Vasquez[165], A. Vasyukov[38], F. Vazeille[40], T. Vazquez Schroeder[36], J. Veatch[31], V. Vecchio[101], M.J. Veen[103], I. Veliscek[126], L.M. Veloce[155], F. Veloso[130a,130c], S. Veneziano[75a], A. Ventura[70a,70b], S. Ventura Gonzalez[135], A. Verbytskyi[110], M. Verducci[74a,74b], C. Vergis[24], M. Verissimo De Araujo[83b], W. Verkerke[114], J.C. Vermeulen[114], C. Vernieri[143], M. Vessella[103], M.C. Vetterli[142,ai], A. Vgenopoulos[152,e], N. Viaux Maira[137f], T. Vickey[139], O.E. Vickey Boeriu[139], G.H.A. Viehhauser[126], L. Vigani[63b], M. Villa[23b,23a], M. Villaplana Perez[163], E.M. Villhauer[52], E. Vilucchi[53], M.G. Vincter[34], G.S. Virdee[20], A. Vishwakarma[52], A. Visibile[114], C. Vittori[36], I. Vivarelli[146], V. Vladimirov[167], E. Voevodina[110], F. Vogel[109], P. Vokac[132], Yu. Volkotrub[86a], J. Von Ahnen[48], E. Von Toerne[24], B. Vormwald[36], V. Vorobel[133], K. Vorobev[37], M. Vos[163], K. Voss[141], J.H. Vossebeld[92], M. Vozak[114], L. Vozdecky[94], N. Vranjes[15], M. Vranjes Milosavljevic[15], M. Vreeswijk[114], R. Vuillermet[36], O. Vujinovic[100], I. Vukotic[39], S. Wada[157], C. Wagner[103], J.M. Wagner[17a], W. Wagner[171], S. Wahdan[171], H. Wahlberg[90], M. Wakida[111], J. Walder[134], R. Walker[109], W. Walkowiak[141], A. Wall[128], T. Wamorkar[6], A.Z. Wang[170], C. Wang[100], C. Wang[62c], H. Wang[17a], J. Wang[64a], R.-J. Wang[100], R. Wang[61], R. Wang[6], S.M. Wang[148], S. Wang[62b], T. Wang[62a], W.T. Wang[80], W. Wang[14a], X. Wang[14c], X. Wang[162], X. Wang[62c], Y. Wang[62d], Y. Wang[14c], Z. Wang[106], Z. Wang[62d,51,62c], Z. Wang[106], A. Warburton[104], R.J. Ward[20], N. Warrack[59], A.T. Watson[20], H. Watson[59], M.F. Watson[20], E. Watton[59,134], G. Watts[138], B.M. Waugh[96], C. Weber[29], H.A. Weber[18], M.S. Weber[19], S.M. Weber[63a], C. Wei[62a], Y. Wei[126], A.R. Weidberg[126], E.J. Weik[117], J. Weingarten[49], M. Weirich[100], C. Weiser[54], C.J. Wells[48], T. Wenaus[29], B. Wendland[49], T. Wengler[36], N.S. Wenke[110], N. Wermes[24], M. Wessels[63a], A.M. Wharton[91], A.S. White[61], A. White[8], M.J. White[1], D. Whiteson[160], L. Wickremasinghe[124], W. Wiedenmann[170], C. Wiel[50], M. Wielers[134], C. Wiglesworth[42], D.J. Wilbern[120], H.G. Wilkens[36], D.M. Williams[41], H.H. Williams[128], S. Williams[32], S. Willocq[103], B.J. Wilson[101], P.J. Windischhofer[39], F.I. Winkel[30], F. Winklmeier[123], B.T. Winter[54], J.K. Winter[101], M. Wittgen[143], M. Wobisch[97], Z. Wolffs[114], J. Wollrath[160], M.W. Wolter[87], H. Wolters[130a,130c], A.F. Wongel[48], S.D. Worm[48], B.K. Wosiek[87], K.W. Woźniak[87], S. Wozniewski[55], K. Wraight[59], C. Wu[20], J. Wu[14a,14e], M. Wu[64a], M. Wu[113], S.L. Wu[170], X. Wu[56], Y. Wu[62a], Z. Wu[135], J. Wuerzinger[110,ag], T.R. Wyatt[101], B.M. Wynne[52], S. Xella[42], L. Xia[14c], M. Xia[14b], J. Xiang[64c], M. Xie[62a], X. Xie[62a], S. Xin[14a,14e], J. Xiong[17a], D. Xu[14a], H. Xu[62a], L. Xu[62a], R. Xu[128], T. Xu[106], Y. Xu[14b], Z. Xu[52], Z. Xu[14a], B. Yabsley[147], S. Yacoob[33a], Y. Yamaguchi[154], E. Yamashita[153], H. Yamauchi[157], T. Yamazaki[17a], Y. Yamazaki[85], J. Yan[62c], S. Yan[126], Z. Yan[25], H.J. Yang[62c,62d], H.T. Yang[62a], S. Yang[62a], T. Yang[64c], X. Yang[62a], X. Yang[14a], Y. Yang[44], Y. Yang[62a], Z. Yang[62a], W-M. Yao[17a], Y.C. Yap[48], H. Ye[14c], H. Ye[55], J. Ye[14a], S. Ye[29], X. Ye[62a], Y. Yeh[96], I. Yeletskikh[38], B.K. Yeo[17b], M.R. Yexley[96], P. Yin[41], K. Yorita[168], S. Younas[27b], C.J.S. Young[36], C. Young[143], C. Yu[14a,14e], Y. Yu[62a], M. Yuan[106], R. Yuan[62b,k], L. Yue[96], M. Zaazoua[62a], B. Zabinski[87], E. Zaid[52], T. Zakareishvili[149b], N. Zakharchuk[34], S. Zambito[56], J.A. Zamora Saa[137d,137b], J. Zang[153], D. Zanzi[54], O. Zaplatilek[132],

C. Zeitnitz[171], H. Zeng[14a], J.C. Zeng[162], D.T. Zenger Jr[26], O. Zenin[37], T. Ženiš[28a], S. Zenz[94], S. Zerradi[35a], D. Zerwas[66], M. Zhai[14a,14e], B. Zhang[14c], D.F. Zhang[139], J. Zhang[62b], J. Zhang[6], K. Zhang[14a,14e], L. Zhang[14c], P. Zhang[14a,14e], R. Zhang[170], S. Zhang[106], T. Zhang[153], X. Zhang[62c], X. Zhang[62b], Y. Zhang[62c,5], Y. Zhang[96], Z. Zhang[17a], Z. Zhang[66], H. Zhao[138], P. Zhao[51], T. Zhao[62b], Y. Zhao[136], Z. Zhao[62a], A. Zhemchugov[38], J. Zheng[14c], K. Zheng[162], X. Zheng[62a], Z. Zheng[143], D. Zhong[162], B. Zhou[106], H. Zhou[7], N. Zhou[62c], Y. Zhou[7], C.G. Zhu[62b], J. Zhu[106], Y. Zhu[62c], Y. Zhu[62a], X. Zhuang[14a], K. Zhukov[37], V. Zhulanov[37], N.I. Zimine[38], J. Zinsser[63b], M. Ziolkowski[141], L. Živković[15], A. Zoccoli[23b,23a], K. Zoch[56], T.G. Zorbas[139], O. Zormpa[46], W. Zou[41], L. Zwalinski[36]

[1] *Department of Physics, University of Adelaide, Adelaide; Australia*

[2] *Department of Physics, University of Alberta, Edmonton AB; Canada*

[3] (a) *Department of Physics, Ankara University, Ankara;* (b) *Division of Physics, TOBB University of Economics and Technology, Ankara; Türkiye*

[4] *LAPP, Université Savoie Mont Blanc, CNRS/IN2P3, Annecy; France*

[5] *APC, Université Paris Cité, CNRS/IN2P3, Paris; France*

[6] *High Energy Physics Division, Argonne National Laboratory, Argonne IL; United States of America*

[7] *Department of Physics, University of Arizona, Tucson AZ; United States of America*

[8] *Department of Physics, University of Texas at Arlington, Arlington TX; United States of America*

[9] *Physics Department, National and Kapodistrian University of Athens, Athens; Greece*

[10] *Physics Department, National Technical University of Athens, Zografou; Greece*

[11] *Department of Physics, University of Texas at Austin, Austin TX; United States of America*

[12] *Institute of Physics, Azerbaijan Academy of Sciences, Baku; Azerbaijan*

[13] *Institut de Física d'Altes Energies (IFAE), Barcelona Institute of Science and Technology, Barcelona; Spain*

[14] (a) *Institute of High Energy Physics, Chinese Academy of Sciences, Beijing;* (b) *Physics Department, Tsinghua University, Beijing;* (c) *Department of Physics, Nanjing University, Nanjing;* (d) *School of Science, Shenzhen Campus of Sun Yat-sen University;* (e) *University of Chinese Academy of Science (UCAS), Beijing; China*

[15] *Institute of Physics, University of Belgrade, Belgrade; Serbia*

[16] *Department for Physics and Technology, University of Bergen, Bergen; Norway*

[17] (a) *Physics Division, Lawrence Berkeley National Laboratory, Berkeley CA;* (b) *University of California, Berkeley CA; United States of America*

[18] *Institut für Physik, Humboldt Universität zu Berlin, Berlin; Germany*

[19] *Albert Einstein Center for Fundamental Physics and Laboratory for High Energy Physics, University of Bern, Bern; Switzerland*

[20] *School of Physics and Astronomy, University of Birmingham, Birmingham; United Kingdom*

[21] (a) *Department of Physics, Bogazici University, Istanbul;* (b) *Department of Physics Engineering, Gaziantep University, Gaziantep;* (c) *Department of Physics, Istanbul University, Istanbul; Türkiye*

[22] (a) *Facultad de Ciencias y Centro de Investigaciónes, Universidad Antonio Nariño, Bogotá;* (b) *Departamento de Física, Universidad Nacional de Colombia, Bogotá; Colombia*

[23] (a) *Dipartimento di Fisica e Astronomia A. Righi, Università di Bologna, Bologna;* (b) *INFN Sezione di Bologna; Italy*

[24] *Physikalisches Institut, Universität Bonn, Bonn; Germany*

[25] *Department of Physics, Boston University, Boston MA; United States of America*

[26] *Department of Physics, Brandeis University, Waltham MA; United States of America*

[27] (a) *Transilvania University of Brasov, Brasov;* (b) *Horia Hulubei National Institute of Physics and Nuclear Engineering, Bucharest;* (c) *Department of Physics, Alexandru Ioan Cuza University of Iasi, Iasi;* (d) *National Institute for Research and Development of Isotopic and Molecular Technologies, Physics Department, Cluj-Napoca;* (e) *National University of Science and Technology Politechnica, Bucharest;* (f) *West University*

in Timisoara, Timisoara;(g) Faculty of Physics, University of Bucharest, Bucharest; Romania

[28] *(a) Faculty of Mathematics, Physics and Informatics, Comenius University, Bratislava;(b) Department of Subnuclear Physics, Institute of Experimental Physics of the Slovak Academy of Sciences, Kosice; Slovak Republic*

[29] *Physics Department, Brookhaven National Laboratory, Upton NY; United States of America*

[30] *Universidad de Buenos Aires, Facultad de Ciencias Exactas y Naturales, Departamento de Física, y CONICET, Instituto de Física de Buenos Aires (IFIBA), Buenos Aires; Argentina*

[31] *California State University, CA; United States of America*

[32] *Cavendish Laboratory, University of Cambridge, Cambridge; United Kingdom*

[33] *(a) Department of Physics, University of Cape Town, Cape Town;(b) iThemba Labs, Western Cape;(c) Department of Mechanical Engineering Science, University of Johannesburg, Johannesburg;(d) National Institute of Physics, University of the Philippines Diliman (Philippines);(e) University of South Africa, Department of Physics, Pretoria;(f) University of Zululand, KwaDlangezwa;(g) School of Physics, University of the Witwatersrand, Johannesburg; South Africa*

[34] *Department of Physics, Carleton University, Ottawa ON; Canada*

[35] *(a) Faculté des Sciences Ain Chock, Réseau Universitaire de Physique des Hautes Energies - Université Hassan II, Casablanca;(b) Faculté des Sciences, Université Ibn-Tofail, Kénitra;(c) Faculté des Sciences Semlalia, Université Cadi Ayyad, LPHEA-Marrakech;(d) LPMR, Faculté des Sciences, Université Mohamed Premier, Oujda;(e) Faculté des sciences, Université Mohammed V, Rabat;(f) Institute of Applied Physics, Mohammed VI Polytechnic University, Ben Guerir; Morocco*

[36] *CERN, Geneva; Switzerland*

[37] *Affiliated with an institute covered by a cooperation agreement with CERN*

[38] *Affiliated with an international laboratory covered by a cooperation agreement with CERN*

[39] *Enrico Fermi Institute, University of Chicago, Chicago IL; United States of America*

[40] *LPC, Université Clermont Auvergne, CNRS/IN2P3, Clermont-Ferrand; France*

[41] *Nevis Laboratory, Columbia University, Irvington NY; United States of America*

[42] *Niels Bohr Institute, University of Copenhagen, Copenhagen; Denmark*

[43] *(a) Dipartimento di Fisica, Università della Calabria, Rende;(b) INFN Gruppo Collegato di Cosenza, Laboratori Nazionali di Frascati; Italy*

[44] *Physics Department, Southern Methodist University, Dallas TX; United States of America*

[45] *Physics Department, University of Texas at Dallas, Richardson TX; United States of America*

[46] *National Centre for Scientific Research "Demokritos", Agia Paraskevi; Greece*

[47] *(a) Department of Physics, Stockholm University;(b) Oskar Klein Centre, Stockholm; Sweden*

[48] *Deutsches Elektronen-Synchrotron DESY, Hamburg and Zeuthen; Germany*

[49] *Fakultät Physik , Technische Universität Dortmund, Dortmund; Germany*

[50] *Institut für Kern- und Teilchenphysik, Technische Universität Dresden, Dresden; Germany*

[51] *Department of Physics, Duke University, Durham NC; United States of America*

[52] *SUPA - School of Physics and Astronomy, University of Edinburgh, Edinburgh; United Kingdom*

[53] *INFN e Laboratori Nazionali di Frascati, Frascati; Italy*

[54] *Physikalisches Institut, Albert-Ludwigs-Universität Freiburg, Freiburg; Germany*

[55] *II. Physikalisches Institut, Georg-August-Universität Göttingen, Göttingen; Germany*

[56] *Département de Physique Nucléaire et Corpusculaire, Université de Genève, Genève; Switzerland*

[57] *(a) Dipartimento di Fisica, Università di Genova, Genova;(b) INFN Sezione di Genova; Italy*

[58] *II. Physikalisches Institut, Justus-Liebig-Universität Giessen, Giessen; Germany*

[59] *SUPA - School of Physics and Astronomy, University of Glasgow, Glasgow; United Kingdom*

[60] *LPSC, Université Grenoble Alpes, CNRS/IN2P3, Grenoble INP, Grenoble; France*

[61] *Laboratory for Particle Physics and Cosmology, Harvard University, Cambridge MA; United States of America*

[62] *(a) Department of Modern Physics and State Key Laboratory of Particle Detection and Electronics, University of Science and Technology of China, Hefei;(b) Institute of Frontier and Interdisciplinary Science and Key Laboratory of Particle Physics and Particle Irradiation (MOE), Shandong University, Qingdao;(c) School of Physics and Astronomy, Shanghai Jiao Tong University, Key Laboratory for Particle Astrophysics and Cosmology (MOE), SKLPPC, Shanghai;(d) Tsung-Dao Lee Institute, Shanghai; China*

[63] (a) Kirchhoff-Institut für Physik, Ruprecht-Karls-Universität Heidelberg, Heidelberg;(b) Physikalisches Institut, Ruprecht-Karls-Universität Heidelberg, Heidelberg; Germany
[64] (a) Department of Physics, Chinese University of Hong Kong, Shatin, N.T., Hong Kong;(b) Department of Physics, University of Hong Kong, Hong Kong;(c) Department of Physics and Institute for Advanced Study, Hong Kong University of Science and Technology, Clear Water Bay, Kowloon, Hong Kong; China
[65] Department of Physics, National Tsing Hua University, Hsinchu; Taiwan
[66] IJCLab, Université Paris-Saclay, CNRS/IN2P3, 91405, Orsay; France
[67] Centro Nacional de Microelectrónica (IMB-CNM-CSIC), Barcelona; Spain
[68] Department of Physics, Indiana University, Bloomington IN; United States of America
[69] (a) INFN Gruppo Collegato di Udine, Sezione di Trieste, Udine;(b) ICTP, Trieste;(c) Dipartimento Politecnico di Ingegneria e Architettura, Università di Udine, Udine; Italy
[70] (a) INFN Sezione di Lecce;(b) Dipartimento di Matematica e Fisica, Università del Salento, Lecce; Italy
[71] (a) INFN Sezione di Milano;(b) Dipartimento di Fisica, Università di Milano, Milano; Italy
[72] (a) INFN Sezione di Napoli;(b) Dipartimento di Fisica, Università di Napoli, Napoli; Italy
[73] (a) INFN Sezione di Pavia;(b) Dipartimento di Fisica, Università di Pavia, Pavia; Italy
[74] (a) INFN Sezione di Pisa;(b) Dipartimento di Fisica E. Fermi, Università di Pisa, Pisa; Italy
[75] (a) INFN Sezione di Roma;(b) Dipartimento di Fisica, Sapienza Università di Roma, Roma; Italy
[76] (a) INFN Sezione di Roma Tor Vergata;(b) Dipartimento di Fisica, Università di Roma Tor Vergata, Roma; Italy
[77] (a) INFN Sezione di Roma Tre;(b) Dipartimento di Matematica e Fisica, Università Roma Tre, Roma; Italy
[78] (a) INFN-TIFPA;(b) Università degli Studi di Trento, Trento; Italy
[79] Universität Innsbruck, Department of Astro and Particle Physics, Innsbruck; Austria
[80] University of Iowa, Iowa City IA; United States of America
[81] Department of Physics and Astronomy, Iowa State University, Ames IA; United States of America
[82] Istinye University, Sariyer, Istanbul; Türkiye
[83] (a) Departamento de Engenharia Elétrica, Universidade Federal de Juiz de Fora (UFJF), Juiz de Fora;(b) Universidade Federal do Rio De Janeiro COPPE/EE/IF, Rio de Janeiro;(c) Instituto de Física, Universidade de São Paulo, São Paulo;(d) Rio de Janeiro State University, Rio de Janeiro; Brazil
[84] KEK, High Energy Accelerator Research Organization, Tsukuba; Japan
[85] Graduate School of Science, Kobe University, Kobe; Japan
[86] (a) AGH University of Krakow, Faculty of Physics and Applied Computer Science, Krakow;(b) Marian Smoluchowski Institute of Physics, Jagiellonian University, Krakow; Poland
[87] Institute of Nuclear Physics Polish Academy of Sciences, Krakow; Poland
[88] Faculty of Science, Kyoto University, Kyoto; Japan
[89] Research Center for Advanced Particle Physics and Department of Physics, Kyushu University, Fukuoka; Japan
[90] Instituto de Física La Plata, Universidad Nacional de La Plata and CONICET, La Plata; Argentina
[91] Physics Department, Lancaster University, Lancaster; United Kingdom
[92] Oliver Lodge Laboratory, University of Liverpool, Liverpool; United Kingdom
[93] Department of Experimental Particle Physics, Jožef Stefan Institute and Department of Physics, University of Ljubljana, Ljubljana; Slovenia
[94] School of Physics and Astronomy, Queen Mary University of London, London; United Kingdom
[95] Department of Physics, Royal Holloway University of London, Egham; United Kingdom
[96] Department of Physics and Astronomy, University College London, London; United Kingdom
[97] Louisiana Tech University, Ruston LA; United States of America
[98] Fysiska institutionen, Lunds universitet, Lund; Sweden
[99] Departamento de Física Teorica C-15 and CIAFF, Universidad Autónoma de Madrid, Madrid; Spain
[100] Institut für Physik, Universität Mainz, Mainz; Germany
[101] School of Physics and Astronomy, University of Manchester, Manchester; United Kingdom
[102] CPPM, Aix-Marseille Université, CNRS/IN2P3, Marseille; France
[103] Department of Physics, University of Massachusetts, Amherst MA; United States of America
[104] Department of Physics, McGill University, Montreal QC; Canada
[105] School of Physics, University of Melbourne, Victoria; Australia

[106] *Department of Physics, University of Michigan, Ann Arbor MI; United States of America*
[107] *Department of Physics and Astronomy, Michigan State University, East Lansing MI; United States of America*
[108] *Group of Particle Physics, University of Montreal, Montreal QC; Canada*
[109] *Fakultät für Physik, Ludwig-Maximilians-Universität München, München; Germany*
[110] *Max-Planck-Institut für Physik (Werner-Heisenberg-Institut), München; Germany*
[111] *Graduate School of Science and Kobayashi-Maskawa Institute, Nagoya University, Nagoya; Japan*
[112] *Department of Physics and Astronomy, University of New Mexico, Albuquerque NM; United States of America*
[113] *Institute for Mathematics, Astrophysics and Particle Physics, Radboud University/Nikhef, Nijmegen; Netherlands*
[114] *Nikhef National Institute for Subatomic Physics and University of Amsterdam, Amsterdam; Netherlands*
[115] *Department of Physics, Northern Illinois University, DeKalb IL; United States of America*
[116] (a) *New York University Abu Dhabi, Abu Dhabi;* (b) *University of Sharjah, Sharjah; United Arab Emirates*
[117] *Department of Physics, New York University, New York NY; United States of America*
[118] *Ochanomizu University, Otsuka, Bunkyo-ku, Tokyo; Japan*
[119] *Ohio State University, Columbus OH; United States of America*
[120] *Homer L. Dodge Department of Physics and Astronomy, University of Oklahoma, Norman OK; United States of America*
[121] *Department of Physics, Oklahoma State University, Stillwater OK; United States of America*
[122] *Palacký University, Joint Laboratory of Optics, Olomouc; Czech Republic*
[123] *Institute for Fundamental Science, University of Oregon, Eugene, OR; United States of America*
[124] *Graduate School of Science, Osaka University, Osaka; Japan*
[125] *Department of Physics, University of Oslo, Oslo; Norway*
[126] *Department of Physics, Oxford University, Oxford; United Kingdom*
[127] *LPNHE, Sorbonne Université, Université Paris Cité, CNRS/IN2P3, Paris; France*
[128] *Department of Physics, University of Pennsylvania, Philadelphia PA; United States of America*
[129] *Department of Physics and Astronomy, University of Pittsburgh, Pittsburgh PA; United States of America*
[130] (a) *Laboratório de Instrumentação e Física Experimental de Partículas - LIP, Lisboa;* (b) *Departamento de Física, Faculdade de Ciências, Universidade de Lisboa, Lisboa;* (c) *Departamento de Física, Universidade de Coimbra, Coimbra;* (d) *Centro de Física Nuclear da Universidade de Lisboa, Lisboa;* (e) *Departamento de Física, Universidade do Minho, Braga;* (f) *Departamento de Física Teórica y del Cosmos, Universidad de Granada, Granada (Spain);* (g) *Departamento de Física, Instituto Superior Técnico, Universidade de Lisboa, Lisboa; Portugal*
[131] *Institute of Physics of the Czech Academy of Sciences, Prague; Czech Republic*
[132] *Czech Technical University in Prague, Prague; Czech Republic*
[133] *Charles University, Faculty of Mathematics and Physics, Prague; Czech Republic*
[134] *Particle Physics Department, Rutherford Appleton Laboratory, Didcot; United Kingdom*
[135] *IRFU, CEA, Université Paris-Saclay, Gif-sur-Yvette; France*
[136] *Santa Cruz Institute for Particle Physics, University of California Santa Cruz, Santa Cruz CA; United States of America*
[137] (a) *Departamento de Física, Pontificia Universidad Católica de Chile, Santiago;* (b) *Millennium Institute for Subatomic physics at high energy frontier (SAPHIR), Santiago;* (c) *Instituto de Investigación Multidisciplinario en Ciencia y Tecnología, y Departamento de Física, Universidad de La Serena;* (d) *Universidad Andres Bello, Department of Physics, Santiago;* (e) *Instituto de Alta Investigación, Universidad de Tarapacá, Arica;* (f) *Departamento de Física, Universidad Técnica Federico Santa María, Valparaíso; Chile*
[138] *Department of Physics, University of Washington, Seattle WA; United States of America*
[139] *Department of Physics and Astronomy, University of Sheffield, Sheffield; United Kingdom*
[140] *Department of Physics, Shinshu University, Nagano; Japan*
[141] *Department Physik, Universität Siegen, Siegen; Germany*
[142] *Department of Physics, Simon Fraser University, Burnaby BC; Canada*
[143] *SLAC National Accelerator Laboratory, Stanford CA; United States of America*

[144] *Department of Physics, Royal Institute of Technology, Stockholm; Sweden*
[145] *Departments of Physics and Astronomy, Stony Brook University, Stony Brook NY; United States of America*
[146] *Department of Physics and Astronomy, University of Sussex, Brighton; United Kingdom*
[147] *School of Physics, University of Sydney, Sydney; Australia*
[148] *Institute of Physics, Academia Sinica, Taipei; Taiwan*
[149] *(a) E. Andronikashvili Institute of Physics, Iv. Javakhishvili Tbilisi State University, Tbilisi; (b) High Energy Physics Institute, Tbilisi State University, Tbilisi; (c) University of Georgia, Tbilisi; Georgia*
[150] *Department of Physics, Technion, Israel Institute of Technology, Haifa; Israel*
[151] *Raymond and Beverly Sackler School of Physics and Astronomy, Tel Aviv University, Tel Aviv; Israel*
[152] *Department of Physics, Aristotle University of Thessaloniki, Thessaloniki; Greece*
[153] *International Center for Elementary Particle Physics and Department of Physics, University of Tokyo, Tokyo; Japan*
[154] *Department of Physics, Tokyo Institute of Technology, Tokyo; Japan*
[155] *Department of Physics, University of Toronto, Toronto ON; Canada*
[156] *(a) TRIUMF, Vancouver BC; (b) Department of Physics and Astronomy, York University, Toronto ON; Canada*
[157] *Division of Physics and Tomonaga Center for the History of the Universe, Faculty of Pure and Applied Sciences, University of Tsukuba, Tsukuba; Japan*
[158] *Department of Physics and Astronomy, Tufts University, Medford MA; United States of America*
[159] *United Arab Emirates University, Al Ain; United Arab Emirates*
[160] *Department of Physics and Astronomy, University of California Irvine, Irvine CA; United States of America*
[161] *Department of Physics and Astronomy, University of Uppsala, Uppsala; Sweden*
[162] *Department of Physics, University of Illinois, Urbana IL; United States of America*
[163] *Instituto de Física Corpuscular (IFIC), Centro Mixto Universidad de Valencia - CSIC, Valencia; Spain*
[164] *Department of Physics, University of British Columbia, Vancouver BC; Canada*
[165] *Department of Physics and Astronomy, University of Victoria, Victoria BC; Canada*
[166] *Fakultät für Physik und Astronomie, Julius-Maximilians-Universität Würzburg, Würzburg; Germany*
[167] *Department of Physics, University of Warwick, Coventry; United Kingdom*
[168] *Waseda University, Tokyo; Japan*
[169] *Department of Particle Physics and Astrophysics, Weizmann Institute of Science, Rehovot; Israel*
[170] *Department of Physics, University of Wisconsin, Madison WI; United States of America*
[171] *Fakultät für Mathematik und Naturwissenschaften, Fachgruppe Physik, Bergische Universität Wuppertal, Wuppertal; Germany*
[172] *Department of Physics, Yale University, New Haven CT; United States of America*

[a] *Also Affiliated with an institute covered by a cooperation agreement with CERN*
[b] *Also at An-Najah National University, Nablus; Palestine*
[c] *Also at Borough of Manhattan Community College, City University of New York, New York NY; United States of America*
[d] *Also at Center for High Energy Physics, Peking University; China*
[e] *Also at Center for Interdisciplinary Research and Innovation (CIRI-AUTH), Thessaloniki; Greece*
[f] *Also at Centro Studi e Ricerche Enrico Fermi; Italy*
[g] *Also at CERN, Geneva; Switzerland*
[h] *Also at Département de Physique Nucléaire et Corpusculaire, Université de Genève, Genève; Switzerland*
[i] *Also at Departament de Fisica de la Universitat Autonoma de Barcelona, Barcelona; Spain*
[j] *Also at Department of Financial and Management Engineering, University of the Aegean, Chios; Greece*
[k] *Also at Department of Physics and Astronomy, Michigan State University, East Lansing MI; United States of America*
[l] *Also at Department of Physics, Ben Gurion University of the Negev, Beer Sheva; Israel*
[m] *Also at Department of Physics, California State University, Sacramento; United States of America*
[n] *Also at Department of Physics, King's College London, London; United Kingdom*
[o] *Also at Department of Physics, Stanford University, Stanford CA; United States of America*

[p] *Also at Department of Physics, University of Fribourg, Fribourg; Switzerland*
[q] *Also at Department of Physics, University of Thessaly; Greece*
[r] *Also at Department of Physics, Westmont College, Santa Barbara; United States of America*
[s] *Also at Hellenic Open University, Patras; Greece*
[t] *Also at Institucio Catalana de Recerca i Estudis Avancats, ICREA, Barcelona; Spain*
[u] *Also at Institut für Experimentalphysik, Universität Hamburg, Hamburg; Germany*
[v] *Also at Institute for Nuclear Research and Nuclear Energy (INRNE) of the Bulgarian Academy of Sciences, Sofia; Bulgaria*
[w] *Also at Institute of Applied Physics, Mohammed VI Polytechnic University, Ben Guerir; Morocco*
[x] *Also at Institute of Particle Physics (IPP); Canada*
[y] *Also at Institute of Physics and Technology, Mongolian Academy of Sciences, Ulaanbaatar; Mongolia*
[z] *Also at Institute of Physics, Azerbaijan Academy of Sciences, Baku; Azerbaijan*
[aa] *Also at Institute of Theoretical Physics, Ilia State University, Tbilisi; Georgia*
[ab] *Also at L2IT, Université de Toulouse, CNRS/IN2P3, UPS, Toulouse; France*
[ac] *Also at Lawrence Livermore National Laboratory, Livermore; United States of America*
[ad] *Also at National Institute of Physics, University of the Philippines Diliman (Philippines); Philippines*
[ae] *Also at Ochanomizu University, Otsuka, Bunkyo-ku, Tokyo; Japan*
[af] *Also at Physikalisches Institut, Albert-Ludwigs-Universität Freiburg, Freiburg; Germany*
[ag] *Also at Technical University of Munich, Munich; Germany*
[ah] *Also at The Collaborative Innovation Center of Quantum Matter (CICQM), Beijing; China*
[ai] *Also at TRIUMF, Vancouver BC; Canada*
[aj] *Also at Università di Napoli Parthenope, Napoli; Italy*
[ak] *Also at University of Colorado Boulder, Department of Physics, Colorado; United States of America*
[al] *Also at Washington College, Chestertown, MD; United States of America*
[am] *Also at Yeditepe University, Physics Department, Istanbul; Türkiye*
[*] *Deceased*